

AD-A015 140

A COMPUTER PROGRAM FOR THE PREDICTION OF SOLID
PROPELLANT ROCKET MOTOR PERFORMANCE. VOLUME I

D. E. Coats, et al

Ultrasystems, Incorporated

Prepared for:

Air Force Rocket Propulsion Laboratory

July 1975

DISTRIBUTED BY:

NTIS

National Technical Information Service
U. S. DEPARTMENT OF COMMERCE

280089

ADA015140

AFRPL-TR-75-36

A COMPUTER PROGRAM FOR THE PREDICTION OF SOLID PROPELLANT
ROCKET MOTOR PERFORMANCE, VOL. I

FINAL REPORT

Ultrasystems, Inc.
2400 Michelson Drive
Irvine, California 92664

Authors: D. E. Coats
J. N. Levine
G. R. Nickerson
T. J. Tyson

N. S. Cohen
D. P. Harry III
C. F. Price

JULY 1975

APPROVED FOR PUBLIC RELEASE;

DISTRIBUTION UNLIMITED

DDC
REGISTERED
SEP 24 1975
REPRODUCIBLE
C

Reproduced by
NATIONAL TECHNICAL
INFORMATION SERVICE
US Department of Commerce
Springfield, VA. 22151

AIR FORCE ROCKET PROPULSION LABORATORY
DIRECTOR OF SCIENCE AND TECHNOLOGY
AIR FORCE SYSTEMS COMMAND
EDWARDS, CALIFORNIA 93523

NOTICES

"When U. S. Government drawings, specifications, or other data are used for any purpose other than a definitely related government procurement operation, the Government thereby incurs no responsibility nor any obligation whatsoever, and the fact that the Government may have formulated, furnished, or in any way supplied the said drawings, specifications or other data, is not to be regarded by implication or otherwise, or in any manner licensing the holder or any other person or corporation, or conveying any rights or permission to manufacture use, or sell any patented invention that may in any way be related thereto."

FOREWORD

This report was submitted by Ultrasystems, Inc., Environmental and Applied Sciences Division, 2400 Michelson Drive, Irvine, California 92664, under Contract No. F04611-73-C-0038, Job Order No. 305909LZ with the Air Force Rocket Propulsion Laboratory, Edwards, CA 93523.

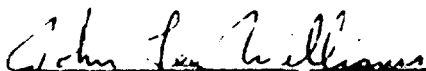
This report consists of three volumes. Volume I describes a computer program for the prediction of Solid Propellant Rocket Motor Performance. The computer program described herein will be referred to as the SPP program, and describes the engineering analysis which was used in developing this computer program and the results obtained to date.

Volume II of this report is a programming document of the computer program which was developed under this contract. It includes a subroutine-by-subroutine description of all of the elements of the SPP program.

Volume III of this report is a Program User's Manual which describes the input necessary to execute the SPP computer program and the information required to interpret the output. A sample case is also included.

This report has been reviewed by the Information Office/DOZ and is releasable to the National Technical Information Service (NTIS). At NTIS it will be available to the general public, including foreign nations.

This report is unclassified and suitable for public release.

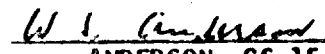


JOHN L. WILLIAMS, Lt., USAF
Project Engineer



W. C. ANDREPONT, GS-14, Chief
Combustion Group

FOR THE COMMANDER



W. S. ANDERSON, GS-15, Acting Chief
Technology Division

UNCLASSIFIED

SECURITY CLASSIFICATION OF THIS PAGE (When Data Entered)

REPORT DOCUMENTATION PAGE		READ INSTRUCTIONS BEFORE COMPLETING FORM
1. REPORT NUMBER AFRPL-TR-75-36	2. GOVT ACCESSION NO.	3. RECIPIENT'S CATALOG NUMBER
4. TITLE (and Subtitle) A Computer Program for the Prediction of Solid Propellant Rocket Motor Performance, Vol. I, II, and III		5. TYPE OF REPORT & PERIOD COVERED FINAL REPORT
7. AUTHOR(s) D. E. Coats N. S. Cohen J. N. Levine D. P. Harry III, et al (Ultrasystems, Inc.) (Lockheed Propulsion)		6. PERFORMING ORG. REPORT NUMBER
9. PERFORMING ORGANIZATION NAME AND ADDRESS Ultrasystems, Inc. 2400 Michelson Drive Irvine, California 92664		8. CONTRACT OR GRANT NUMBER(s) F04611-73-C-0038
11. CONTROLLING OFFICE NAME AND ADDRESS Air Force Rocket Propulsion Laboratory/DY Edwards, CA 93523		10. PROGRAM ELEMENT, PROJECT, TASK AREA & WORK UNIT NUMBERS JON 305909LZ
14. MONITORING AGENCY NAME & ADDRESS (if different from Controlling Office)		12. REPORT DATE July 1975
		13. NUMBER OF PAGES
		15. SECURITY CLASS. (of this report) UNCLASSIFIED
		15a. DECLASSIFICATION/DOWNGRADING SCHEDULE
16. DISTRIBUTION STATEMENT (of this Report) APPROVED FOR PUBLIC RELEASE; DISTRIBUTION UNLIMITED		
17. DISTRIBUTION STATEMENT (of the abstract entered in Block 20, if different from Report)		
18. SUPPLEMENTARY NOTES		
19. KEY WORDS (Continue on reverse side if necessary and identify by block number) Performance prediction Specific impulse losses Solid Rocket Motors Ballistic Analysis		
20. ABSTRACT (Continue on reverse side if necessary and identify by block number) A flexible, modular, fully automated, solid rocket motor performance prediction program has been developed. The program, which has been given the acronym SPP is based on six pre-existing computer codes. These codes have been integrated and modified, as required. To supplement the theory, where necessary, and to increase the flexibility of the program, a number of existing and newly developed semi-empirical correlations were incorporated into the program. The program has a general three-dimensional grain design capability, coupled to a one-dimensional ballistics analysis. The deviations from ideal performance are		

DD FORM 1 JAN 73 1473 EDITION OF 1 NOV 65 IS OBSOLETE

UNCLASSIFIED

SECURITY CLASSIFICATION OF THIS PAGE (When Data Entered)

UNCLASSIFIED

SECURITY CLASSIFICATION OF THIS PAGE(When Data Entered)

computed as a series of independent efficiencies. The program currently treats the following losses: two-dimensional/two-phase (coupled), nozzle erosion, kinetics, boundary layer, combustion efficiency, submergence. The program predicts average delivered performance, as well as mass flow, pressure, thrust, impulse, and specific impulse as functions of time and trajectory.

In order to assess the validity of the SPP program, calculated results were compared to firing data for four different types of motors. While conclusive statements regarding the accuracy and range of validity of the SPP program cannot be made until additional verification efforts are conducted, the results of these four test cases were encouraging. These calculations also served to demonstrate the desirability of eliminating some of the present limitations of the program.

UNCLASSIFIED

SECURITY CLASSIFICATION OF THIS PAGE(When Data Entered)

PREFACE

This is Volume I of a three-part report which describes a computer program for the prediction of Solid Propellant Rocket Motor Performance. The computer program described herein will be referred to as the SPP program.

Volume I of this report describes the engineering analysis which was used in developing this computer program and the results obtained to date.

Volume II of this report is a programming document of the computer program which was developed under this contract. It includes a subroutine-by-subroutine description of all of the elements of the SPP program.

Volume III of this report is a Program User's Manual which describes the input necessary to execute the SPP computer program and the information required to interpret the output. A sample case is also included.

TABLE OF CONTENTS

	<u>Page No.</u>
PREFACE	i
ABSTRACT	iii
NOMENCLATURE	iv
1. INTRODUCTION	1-1
2. METHOD OF APPROACH	2-1
2.1 General Description	2-1
2.2 Definition of Losses	2-4
2.3 Calculation of Delivered Performance	2-6
2.4 Loss Interactions and Reference Performance Values	2-8
3. ANALYTICAL METHODS	3-1
3.1 Master Control Module	3-1
3.2 Theoretical Performance Module	3-5
3.3 Grain Design and Ballistics Module	3-10
3.4 Kinetics Module	3-21
3.5 Two Dimensional Two Phase Module	3-29
3.6 Boundary Layer Loss Module	3-36
3.7 Inter-Module Interfaces	3-41
4. PERFORMANCE LOSS CORRELATIONS	4-1
4.1 Combustion Efficiency	4-1
4.2 Specific Impulse Efficiency	4-15
5. OTHER CONSIDERATIONS	5-1
5.1 Burning Rate	5-1
5.2 Nozzle Throat Erosion	5-5
5.3 Insulation Degradation	5-8
5.4 Aluminum Oxide Particle Size	5-9
6. COMPARISONS WITH MOTOR FIRING DATA	6-1
6.1 Extended Delta Motor	6-2
6.2 SRAM First Pulse	6-4
6.3 Aerojet 2.75 FFAR	6-6
6.4 Sealed Envelope Prediction: C4 Third Stage	6-12
6.5 Summary of Results	6-13
7. CONCLUSIONS AND RECOMMENDATIONS	7-1
7.1 Conclusions	7-1
7.2 Recommendations	7-2
8. REFERENCES	8-1
APPENDIX A - REACTION RATE SCREENING	A-1

ABSTRACT

A flexible, modular, fully automated, solid rocket motor performance prediction program has been developed. The program, which has been given the acronym SPP is based on six pre-existing computer codes. These codes have been integrated and modified, as required. To supplement the theory, where necessary, and to increase the flexibility of the program, a number of existing and newly developed semi-empirical correlations were incorporated into the program. The program has a general three-dimensional grain design capability, coupled to a one-dimensional ballistics analysis. The deviations from ideal performance are computed as a series of independent efficiencies. The program currently treats the following losses: two-dimensional/two-phase (coupled), nozzle erosion, kinetics, boundary layer, combustion efficiency, submergence. The program predicts average delivered performance, as well as mass flow, pressure, thrust, impulse, and specific impulse as functions of time and trajectory.

The theoretical models and empirical correlations upon which the program is based are described, together with the assumptions that are employed. The known limitations of the analysis are presented to aid the user in determining the range of applicability of the program.

In order to assess the validity of the SPP program, calculated results were compared to firing data for four different types of motors. While conclusive statements regarding the accuracy and range of validity of the SPP program cannot be made until additional verification efforts are conducted, the results of these four test cases were encouraging. These calculations also served to demonstrate the desirability of eliminating some of the present limitations of the program.

NOMENCLATURE

A	-	Nozzle area
A_b	-	Propellant burn area
A_p	-	Port area
C^*	-	Characteristic exhaust velocity
C_D	-	Nozzle discharge coefficient
C_H	-	Film coefficient
c_i	-	Mass fraction of i^{th} species
C_p	-	Specific heat of gas
C_s	-	Specific heat of propellant
D	-	Diameter
D_p	-	Particle diameter
F	-	Thrust
g	-	Gravitational constant
h	-	Enthalpy
ΔH_m	-	Heat of fusion
I	-	Impulse
I_{sp}	-	Specific impulse
K_N	-	Ratio of propellant burn area to nozzle throat area
L^*	-	Characteristic length of motor
\dot{m}	-	Nozzle mass flow rate
M	-	Molecular weight, also Mach No.
n	-	Burning rate pressure exponent
P	-	Pressure
\dot{P}	-	Rate of change of pressure
Pr	-	Prandtl number
r	-	Propellant burning rate, also throat radius
R	-	Gas constant
\bar{r}	-	Universal gas constant
\dot{r}_t	-	Nozzle erosion rate
t	-	Time
T	-	Temperature
u	-	Gas velocity
w	-	Propellant web
X_i	-	Mole fraction
x	-	Axial distance

NOMI NCLATURE (Cont'd)

Subscripts

a	-	Ambient
BL	-	Boundary Layer
c	-	Chamber
CE	-	Combustion efficiency
D	-	Delivered
D _a	-	Delivered to ambient
DIV	-	Divergence
e	-	Nozzle exit, or boundary layer edge
F	-	Flame temperature
i	-	Initial, t=0
I	-	Insulation
KIN	-	Kinetics
l	-	Liquid phase
ODK	-	Based on ODK program results
RE	-	Restricted equilibrium
s	-	Slot, or solid phase
SUB	-	Submergence
T	-	Total
t	-	Throat
TEL	-	Based on TEL program results
TD2P	-	Based on TD2P program results
th	-	Theoretical

Superscripts

($\bar{\quad}$)	-	Average
(\quad)*	-	At the nozzle throat

NOMENCLATURE (Cont'd)

Greek Symbols

α	-	Thermal diffusivity
R'_C	-	Nozzle erosion parameter
γ	-	Isentropic exponent
δ^*	-	Boundary layer displacement thickness
ϵ	-	Nozzle expansion ratio
η	-	Loss efficiency
θ	-	Boundary layer momentum thickness
κ	-	Thermal conductivity
λ	-	Emissivity
μ	-	Viscosity
f	-	Mole fraction of condensed phase
ρ	-	Density
σ	-	Stefan-Boltzman constant

1. INTRODUCTION

The physical phenomena which govern the overall efficiency of a solid rocket motor are quite numerous and complex. For this reason the prediction of solid rocket motor delivered performance has, historically, been empirically oriented. Total reliance on correlations of firing data is undesirable, however, as their ranges of applicability cannot usually be clearly defined, and a priori performance predictions for new motor designs or propellants cannot be made with confidence. In order to achieve the desired generality, performance predictions should, where possible, be based on physically realistic models of the controlling phenomena.

Over the past ten, to fifteen, years individual facets of the performance prediction problem in solid rocket motors have been the subject of considerable study. Reference 1 contains a survey of the state-of-the-art up to 1971. Some of the more recent developments in this field (including parts of the present investigation) are discussed in Reference 2. Terse description of rocket industry analytical performance prediction capabilities as of July 1974 may be found in Reference 3. Some recent analytical and experimental work is described in References 68 and 69.

When this effort was initiated, analytical models for most of the physical processes governing motor performance had been formulated, and computer programs based on these models were in existence. Unfortunately, these computer programs were developed independently; each program addressing a particular aspect of the overall problem. Few organizations possessed a large enough operational subset of these programs to make analytical performance predictions. This situation provided the primary motivation for the present effort.

It was believed that the existing technology was capable of yielding adequate performance predictions, but it was felt that a systematic and efficient procedure for implementing this technology was required in order to foster its use on an industry-wide basis. Thus, the primary goal of this program was to develop an automated, computerized, methodology, based on existing methods, which would be capable of predicting delivered specific impulse to within $\pm 2\%$ and delivered thrust and total impulse to within $\pm 5\%$. The method of approach utilized to achieve this goal is outlined in Section 2. Since we can expect continuing advances in

the state-of-the-art, the Solid Rocket Performance Program (SPP) was modularly structured so as to be able to easily accommodate them.

The theoretical techniques employed in the SPP program are succinctly described in Section 3. This report is not meant to be a detailed dissertation on solid rocket performance prediction methods. Its purpose is to indicate the methods selected to meet the objectives of this study, the reasons for their selection, their primary assumptions; and limitations. Detailed descriptions of the theoretical models and solution techniques may be found in the pre-existing source material referenced throughout the text. However, in cases where existing methods were significantly modified, or extended, details of the changes are provided herein.

Pre-existing and newly developed performance loss correlations are presented in Section 4. Certain of these correlations, e.g. combustion efficiency, are required since theoretical models for all of the pertinent phenomena have yet to be developed; the others have been incorporated into the program for the sake of increased flexibility.

No performance prediction methodology would be complete without considering such effects as burn rate, nozzle erosion and particle size. The manner in which these, and other items, were addressed is described in Section 5.

The limited comparisons of analytical predictions with test data that have been carried out to date are described in Section 6. Conclusions drawn from this study are presented in Section 7.1. Section 7.2 contains a list of the more significant limitations of the SPP program and our recommendations for future efforts directed towards alleviating them. This is followed by Section 8, which contains the references cited in the text.

As noted in the Preface this report is Volume 1 of a three volume set. Since this volume and Volume 3 (User's Manual) will often be used by different parties some of the descriptive material contained herein has also been incorporated into the User's Manual.

In accordance with the last two of the listed program characteristics the Solid Rocket Performance Program (SPP), was modularly structured; each module (with the exception of the control module) having been based on a pre-existing computer program. The following programs form the foundation of the SPP program:

- One Dimensional Equilibrium Program (ODE)⁽⁴⁾
- One Dimensional Kinetics Program (ODK)⁽⁵⁾
- Two Dimensional Two Phase Program (TD2P)⁽⁶⁾
- Turbulent Boundary Layer Program (TEL)⁽⁷⁾
- Three Dimensional Grain Design Program⁽⁸⁾
- Motor Ballistics Program⁽⁹⁾

Each of the first four of these programs is a separate module in the SPP program, while the last two programs have been combined in a single module. These programs have been combined with a control module which permits them to be run together automatically. The six modules that comprise the SPP program are schematically shown in Figure 2-1. The primary function, or functions, of each module is also indicated. All of the programs which were adopted for use in the SPP program have been modified to some degree to better suit the present purpose. These modifications are discussed in Section 3, as part of the module by module description of the program.

The SPP program has also been designed to provide the user of the code flexibility in selecting which of the modules are to be exercised in any one computer run. The control module allows all of the modules and programs to be exercised sequentially in a single run. Often, however, this is not the most efficient approach. Therefore, the program also allows the performance related modules to be exercised individually, or in any user determined combination. A complete performance prediction, utilizing all of the program modules can be carried out in parts as efficiently (from a computer time standpoint) as if only a single run were made. This is made possible by the nature of the linkage structure built into the program. All of the data which needs to be transferred from one module to another is written out on an external logical unit (in addition to being automatically transferred internally). At the completion of a run, this linkage data can then be punched, or stored in some other permanent manner. This data is then available for use in subsequent runs, thereby eliminating the need for redundantly exercising a module.

In accordance with the last two of the listed program characteristics the Solid Rocket Performance Program (SPP), was modularly structured; each module (with the exception of the control module) having been based on a pre-existing computer program. The following programs form the foundation of the SPP program:

- One Dimensional Equilibrium Program (ODE)⁽⁴⁾
- One Dimensional Kinetics Program (ODK)⁽⁵⁾
- Two Dimensional Two Phase Program (TD2P)⁽⁶⁾
- Turbulent Boundary Layer Program (TEL)⁽⁷⁾
- Three Dimensional Grain Design Program⁽⁸⁾
- Motor Ballistics Program⁽⁹⁾

Each of the first four of these programs is a separate module in the SPP program, while the last two programs have been combined in a single module. These programs have been combined with a control module which permits them to be run together automatically. The six modules that comprise the SPP program are schematically shown in Figure 2-1. The primary function, or functions, of each module is also indicated. All of the programs which were adopted for use in the SPP program have been modified to some degree to better suit the present purpose. These modifications are discussed in Section 3, as part of the module by module description of the program.

The SPP program has also been designed to provide the user of the code flexibility in selecting which of the modules are to be exercised in any one computer run. The control module allows all of the modules and programs to be exercised sequentially in a single run. Often, however, this is not the most efficient approach. Therefore, the program also allows the performance related modules to be exercised individually, or in any user determined combination. A complete performance prediction, utilizing all of the program modules can be carried out in parts as efficiently (from a computer time standpoint) as if only a single run were made. This is made possible by the nature of the linkage structure built into the program. All of the data which needs to be transferred from one module to another is written out on an external logical unit (in addition to being automatically transferred internally). At the completion of a run, this linkage data can then be punched, or stored in some other permanent manner. This data is then available for use in subsequent runs, thereby eliminating the need for redundantly exercising a module.

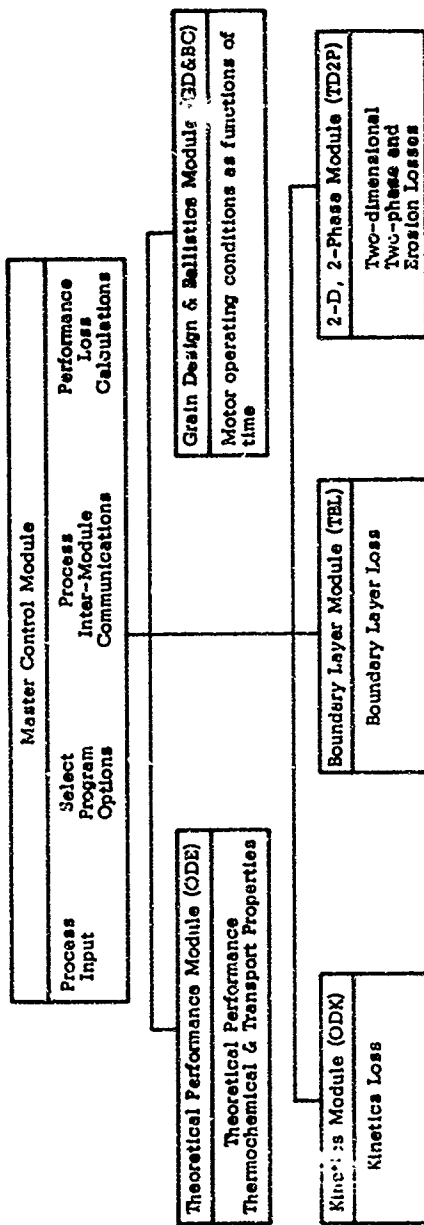


Figure 2-1. Modular Structure of the SPP Program

This type of linkage has two major advantages. The first is an obvious savings in computer run time for parametric studies in which the output from one or more modules is unchanged from case to case. The second is the ability to use other analyses (if appropriate) by "fooling" the SPP code into accepting them as an integral part of its own computational procedure. This allows the user to substitute the output from any other code or analysis into the SPP performance prediction procedure, provided it is able to conform to the proper format.

In conclusion, the SPP program may be described as a modular, flexible, code which combines theory and empiricism to provide accurate predictions of solid rocket motor delivered performance. The analytical techniques and correlations currently utilized in the SPP are summarized in Table 2-1. In many cases the program allows the user (an option) to directly input a performance related quantity. In these cases (indicated in the table) the pertinent analytical and/or empirical calculations are bypassed, in favor of the input quantity.

2.2 Definition of Losses

The basic method of approach used in the development of the SPP computer program is to calculate the maximum or ideal 'theoretical' performance of a rocket motor and to subtract from that maximum performance the losses or deviations from the "theoretical" performance which are known to occur in a real rocket motor. In implementing such an approach it is often assumed that the various losses can be treated independently. As noted in Section 2.3, all of the losses should not be treated independently. There are some interactions strong enough to warrant consideration. With these exceptions in mind, the concept of treating the losses independently appears to be valid, considering the success of this approach, and others of a similar nature.

A standardized performance nomenclature does not exist. Therefore, for the sake of clarity, the definitions used herein are listed below.

- Performance - unless otherwise specified, performance will be in terms of specific impulse I_{sp} , delivered to a vacuum.
- Theoretical I_{sp} - the maximum possible I_{sp} which can be delivered at the initial area ratio by a propellant at a given chamber pressure and total enthalpy. Referred to as $I_{sp,th}$.

Table 2-1
SUMMARY OF SPP PROGRAM CAPABILITIES

ITEM	ANALYTICAL COMPUTATION	CORRELATION	INPUT	SUB-SECTION REFERENCE
Theoretical Performance	ODE		X	3.2
Kinetics Loss	ODK	X	X	3.4, 4.2.3
Two Dimensional Loss	TD2P	X	X	3.1, 3.5, 4.2.2
Two Phase Loss		X	X	3.1, 3.5, 4.2.5
Fusion Loss				3.1, 3.5.3
Boundary Layer Loss	TBL	X	X	3.6, 4.2.4
Nozzle Erosion		X	X	5.2
Grain Geometry & Ballistics	BAL			3.3
Submergence Loss		X	X	4.2.6
Combustion Efficiency	Modification of Correlation	X	X	3.1, 4.1
Particle Size		X	TD2P(only)	5.4
Burning Rate	BAL (motor)		(Strand)	5.1
Insulation Dilution		(BAL only)		3.3, 2.3, 5.3

- Loss - the decrement from the theoretical I_{sp} which can be attributed to a physical phenomena not included in the calculation of $I_{sp_{th}}$.
- Two phase flow loss - the decrement in performance due to finite velocity and temperature differences between the gas and condensed phase.
- Two dimensional or divergence loss - the decrement in performance which is due to the momentum of the rocket exhaust not being totally aligned with the axis of the motor.
- Finite Rate Kinetics loss - the decrement in performance which is due to incomplete transfer of latent heat to sensible heat caused by the finite time required for gas phase chemical reactions to occur.
- Boundary Layer Loss - the decrement in performance due to viscous forces adjacent to the nozzle wall and heat transfer to the nozzle wall.
- Erosion Loss - the decrement in performance associated with erosion induced changes in the nozzle exit area ratio
- Submergence Loss - the decrement in performance that can only be attributed to the fact that a given nozzle is submerged.
- Combustion Efficiency - as used here, the term combustion efficiency will refer only to the degradation of I_{sp} due to a departure of chamber total temperature from the theoretically calculated total temperature.
- Delivered Performance - the calculated performance of the rocket motor which includes all of the losses considered herein.

2.3 Calculation of Delivered Performance

Within the framework already discussed (i.e., separation of individual losses), there are three basic methods which can be used to calculate delivered I_{sp} . The first method is to calculate discrete decrements in performance, ΔI_{sp} , and to subtract these losses from the theoretical specific impulse, $I_{sp_{th}}$. That is

$$I_{sp_D} = I_{sp_{th}} - \sum \Delta I_{sp_{loss}} \quad (2-1)$$

The second method is to calculate a series of efficiencies, η 's, to be applied multiplicatively, i.e.

$$I_{spD} = I_{spth} \pi \eta_{loss} \quad (2-2)$$

Both of the above methods are the same through first order, thus, if the losses are small they yield the same result.

The third method, selected by the JANNAF Committee on Performance Standardization for liquid rocket engines, is a combination of the first two methods. That is, all of the losses except the boundary layer loss are treated as efficiencies while the boundary layer loss is treated as a decrement. Hence,

$$I_{spD} = I_{spth} \pi \eta_{loss} - \Delta I_{spBL} \quad (2-3)$$

This latter method of approach was selected for incorporation in the SPP code for two reasons. The first reason being that there was no compelling reason to deviate from what has been established as a "standardized" method, and secondly, that any other combination of the above methods yields substantially the same end result.

Unless a grain design and ballistics solution is obtained, the only other performance related quantity that is calculated is the specific impulse delivered to average ambient pressure, I_{spD_a} , defined as follows:

$$I_{spD_a} = I_{spD} - \frac{\bar{P}_a}{\bar{P}_c} \frac{\bar{\epsilon} C_{th}^*}{C_D g} \quad (2-4)$$

where:

- \bar{P}_a = average ambient pressure (psi)
- \bar{P}_c = average chamber pressure (psi)
- $\bar{\epsilon}$ = average nozzle expansion ratio
- C_{th}^* = theoretical C^* (ft/sec)
- C_D = nozzle discharge coefficient (from (TD2P))

If a grain design and ballistics solution is obtained delivered thrust (vacuum and ambient), delivered specific impulse (vacuum and ambient) and mass flow are calculated as functions of time. The I_{sp} values are calculated by applying equation (2-3) and (2-4) at successive time increments. Delivered thrust values are then computed as follows*,

$$F_D(t) = \dot{m}(t) I_{spD}(t) \quad (2-5)$$

$$F_{D_a}(t) = F_D(t) - P_a(t) A_e \quad (2-6)$$

The total mass flow, m_T , total impulse I_T , time averaged specific impulse, \bar{I}_{spD} , and time averaged mass flow rate, \bar{m} are also calculated in the indicated manner,

$$m_T = \int_0^{t_{burn}} \dot{m}(t) dt \quad (2-7)$$

$$I_T = \int_0^{t_{burn}} F_{D_a}(t) dt \quad (2-8)$$

$$\bar{I}_{spD} = I_T/m_T \quad (2-9)$$

$$\bar{m} = m_T/t_{burn} \quad (2-10)$$

where t_{burn} denotes the total motor burn time.

2.4 Loss Interactions and Reference Performance Values

The concept of defining a theoretical I_{sp} and various individual losses is a convenient artifice that allows us to predict delivered performance. In addition to being artificial, this concept of treating individual losses is somewhat subjective. The number of "losses" that are defined, and what they are called, can, and does, vary from one performance prediction methodology to another. There is a constraint on this subjectivism, however, which unfortunately is sometimes violated. One way of expressing this constraint is as follows: any number of individual losses may be defined, as long as each physical source of non-ideal performance is accounted for once, and only once.

*If a grain design and ballistics solution is obtained, but a two phase flow solution is not, then thrust is calculated somewhat differently. See Section 3.3.2 for the related details.

2.4.1 Loss Interactions

In defining a set of losses one normally tries to arrange for each loss to be primarily determined by a single physical phenomenon or flow characteristic. Since the phenomena controlling motor performance are, in reality, a nonlinear mutually interacting set a one to one correspondance between phenomena and losses can be achieved only in a relative sense. Each of the "real", non-ideal, processes influences each of the losses, but to varying degrees. In order to satisfy the aforementioned constraint all of the significant influences of each phenomena should be accounted for, but only once. The losses listed in Section 2.2 were defined such that each is primarily the result of a single physical phenomenon, or effect. For example, the kinetics loss is chiefly a result of finite rate kinetic effects. Table 2-2 (from Ref. 10) represents an attempt to quantify the degree to which a given phenomenon influences the losses that are not directly related to it. Most, but not all of the losses and phenomena are listed in this table. The table should be read down and to the left. The number that appears in each square (except the diagonals, which represent the interaction of a loss with its chief determinant) indicates the relative degree of interaction between the indicated loss and phenomenon. The key to interpreting this number is given in the legend below the table. The importance of the various interactions is thus characterized in terms of their potential for influencing predicted delivered performance.

In developing the present methodology it was decided to directly incorporate only those interactions which were felt to be of primary importance. It can be seen from Table 2-2 that there are two such interactions. These are: the effect of non one-dimensional flow on the boundary layer loss; the effect of multiphase flow on the divergence loss.

Two dimensional effects have an important impact on the nozzle boundary layer because of the sensitivity of the boundary layer to free stream conditions. The wall streamline in a typical nozzle differs substantially from the one dimensional analysis streamline for the nozzle, particularly in the nozzle throat region where the heat transfer rates are the highest.

The effect of multiphase flow on divergence loss is important because of the manner in which heat is transferred from the particles to the gas. Because of their

Table 2-2 Interaction of Physical Phenomena with Performance Loss Calculations

PERFORMANCE LOSSES \ PHENOMENA	Divergence Loss	Boundary Layer Loss	Kinetic Loss	Two-Phase Flow Loss	Combustion Inefficiency
Non One-Dimensional Flow	X	1	2	2	3
Viscosity And Thermal Conductivity	3	X	3	2	3
Finite Rate Chemistry	3	2	X	3	3
Multiphase Flow	1	2	2	X	3
Incomplete Combustion	3	2	2	3	X

Legend:

1. Primary Importance (could be $> 0.2\%$ effect on I_{sp})
2. Secondary Importance (probably $< 0.2\%$ effect on I_{sp})
3. Generally Not Important

inertia, particle concentrations will be greater near the nozzle axis than the nozzle wall. Consequently, there will be greater heat addition to the axis streamline than to the wall streamline. This is demonstrated by the fact that two dimensional two phase flow calculations for a perfect gas show a greater maximum velocity for the axis streamline than for the wall streamline. Thus, two phase flow effects cause a reduction in the percentage of misaligned thrust (lower divergence loss).

It should be pointed out that the estimates given in Table 2-2 are based on typical motor configurations and operating conditions. The importance of the various interactions should be reexamined in extreme cases. For instance, in a motor operating at very low pressure, with a metalized propellant, the coupling between incomplete combustion and the kinetics loss could become significant.

2.4.2 Reference Performance Values

Some of the individual loss calculations directly yield a performance decrement or an efficiency, e.g., the boundary layer loss. The other performance loss calculations yield I_{sp} values, e.g. kinetics loss, 2-D, 2-phase loss. It is not desirable to directly utilize any of these I_{sp} values in the calculation of delivered performance. Rather, these calculated I_{sp} values should be related to a reference value of I_{sp} ; thereby producing either an efficiency, or a performance decrement.*

Properly defined reference values are one of the keys to successful implementation of a performance prediction methodology based on separation of losses. One must make sure that the reference computation includes all of the same physical phenomena and assumptions as the related loss calculation, except for the phenomenon, or phenomena, responsible for the loss, as defined. Ideally, this reference calculation should be made by the same computer code which is selected to make the loss calculation, since this would minimize deviations due to numerical techniques, truncation and roundoff errors. However, such an approach is not always practicable. For example, both the equations for the two phase flow and chemical kinetics losses become "stiff" in the equilibrium limit and result in unacceptably long and difficult calculational procedures. Even if sophisticated numerical tech-

*In the present methodology the use of efficiencies is preferred. It is felt that efficiencies better compensate for the omission of things like real gas effects.

niques are used to calculate the "near" equilibrium case, extrapolation to the full equilibrium solution introduces errors which can negate the advantage gained by using the same computer code.

In developing the reference performance calculations used in the present methodology the following criteria were used:

The conceptual differences between the reference and loss calculations should include only those mechanisms which cause the loss.

Computational efficiency should be considered, without sacrificing accuracy and consistency.

The modifications to existing computer codes should be kept to a minimum to minimize program development costs.

The adopted procedures are described in Section 3.

3. ANALYTICAL METHODS

The theoretical methods employed in the SPP program were all adapted from existing computer programs. Thus, the basic theories and computational techniques have all been previously documented. As a result of the number of analyses contained in the present methodology no attempt was made to combine these pre-existing documents into a single entity. The purpose of this section is to indicate the methods selected, the reasons for their selection, their primary assumptions and limitations. Wherever applicable, details of current modifications and/or extensions to the pre-existing analyses are included. This section is structured along the lines of the program, i.e. the methods are discussed in relation to the module in which they are utilized. The interfaces between the modules are also described. While it does not include analytical methods, in the usual sense of the word, the Master Control Module is described first, since it is a key element in the overall program structure.

3.1 Master Control Module

The master control module (MC) controls the execution of the SPP computer code. The MC module selects, via user input, which of the five basic calculation modules are to be executed, and whether calculated, input, or empirical, losses are to be selected for the calculation of delivered specific impulse, thrust, and total impulse. This module also controls all of the internal communication between modules.

In addition to its control functions the MC module stores selected results from each of the performance loss modules and then uses them to calculate delivered performance. Table 3-1 shows the variables used to calculate delivered performance, and indicates the module in which each is calculated.

The delivered performance calculation does not use all of the variables listed in Table 3-1 in their given form.

Where necessary the MC module combines, ratios, averages, etc., these variables, in order to generate the desired quantities. The empirical performance loss estimates are also computed in the MC module.

Table 3-1. Variables Used In Delivered Performance Calculation

Module	Variable
Theoretical Performance	$I_{sp_{th}}, I_{sp_{REQ}}$ at ϵ_1 .
Grain Design and Ballistics	$P_c, \dot{m}, r^*, L^*, \eta_{c^*}$ as functions of t .
Kinetics	$I_{sp_{KIN}}$ at ϵ_1 .
Two Dimensional Two Phase Flow	$I_{sp_{TD2P}}, \eta'_{TD2P}$ as functions of ϵ and C_D .
Turbulent Boundary Layer	$\Delta I_{sp_{TBL}}$

The equations used to calculate delivered performance have been given in Section 2.3. The equation for vacuum delivered specific impulse, previously written in symbolic form (equation 2-3), is written here in the manner used in the program.

$$I_{sp_D} = I_{sp_{th}} \eta_{KIN} \cdot \eta_{TD2P} \cdot \eta_{CL} \cdot \eta_{SUB} - \Delta I_{sp_{TBL}} \quad (3-1)$$

The theoretical specific impulse, $I_{sp_{th}}$ is based on the initial ($t=0$) nozzle exit area ratio.

The loss due to finite rate chemical kinetics is treated as an efficiency factor, η_{KIN} . The kinetic efficiency is calculated as the ratio of an I_{sp} calculated by the CDK module, to an I_{sp} calculated by a special option in the ODE module. This special ODE option, referred to as the "Restricted Equilibrium" option causes the ODE program to compute an I_{sp} based on the more restrictive physical assumptions employed in the ODK calculation. This procedure, which is further described in Section 3.4, is necessary if certain losses are not to be counted twice.

If a motor experiences throat erosion during the course of a firing the nozzle exit area ratio, and hence, the specific impulse, varies with time. The performance decrement associated with this phenomena is usually called the erosion loss. While this loss can be estimated based on one-dimensional calculations, it was felt that a two-dimensional estimate of this effect would be superior. Thus, for eroding nozzles, η_{TD2P} is calculated as follows:

$$\bar{\eta}_{TD2P} = \bar{\eta}_{TD2P} \frac{I_{spTD2P}(\bar{\epsilon})}{I_{spTD2P}(\epsilon_1)} \quad (3-2)$$

The quantity $\bar{\eta}_{TD2P}$ is the time averaged two dimensional two phase efficiency. The TD2P module calculates an efficiency as a function of the area ratio ϵ . Area ratio as a function of time is established from the input, or internally calculated, nozzle erosion rate. This allows $\bar{\eta}_{TD2P}$ to be calculated as

$$\bar{\eta}_{TD2P} = \frac{\int_{t_0}^{t_f} \eta_{TD2P}(\epsilon(t)) dt}{t_f - t_0} \quad (3-3)$$

As defined in equation (3-1) η_{TD2P} includes the "erosion" loss, in addition to the coupled two-phase and divergence losses. The erosion loss, as defined herein, is equal to the ratio of the 2-D, 2-phase I_{sp} at the time averaged expansion ratio, $I_{spTD2P}(\bar{\epsilon})$, to the specific impulse evaluated at the initial expansion ratio, $I_{spTD2P}(\epsilon_1)$. (Future modifications to the program should break the erosion loss out as a separate efficiency.)

The combustion efficiency, η_{CE} , is obtained from the average empirical c^* efficiency as follows:

$$\eta_{CE} = C_D \bar{\eta}_{c^*} \quad (3-4)$$

$$\eta_{CE} = 1.0, \text{ if the previous relation yields a value greater than unity}$$

The c^* efficiency is a correlation of experimentally measured c^* values (see Section 4.1) and, therefore, includes all of the physical effects which determine the nozzle mass flow rate. One of these effects, the combined two dimensional, two phase, effect on mass flow, is also included in the calculation of η_{TD2P} . The definition of η_{CE} in equation (3-4) prevents the mass flow effect related to the nozzle discharge coefficient, C_D , from being counted twice.

It is well known that the discharge coefficient for single phase, two dimensional, flow is less than unity. However, it is also well established that in non-equilibrium two phase flow more mass flows through a nozzle at a given chamber

pressure than would if the particles were in velocity and thermal equilibrium. By itself this effect would produce C_D values greater than unity. For most metalized solid propellant motors the net result of these two opposing effects is a discharge coefficient greater than unity. Since η_{c^*} is empirically obtained, and subject to scatter, the second part of equation (3-4) is added to prevent meaningless values of η_{CE} from being calculated (i.e. $\eta_{CE} > 1$).

If the combustion efficiency were 100% (complete combustion) the c^* efficiency of the motor, η_{c^*} , would be given by

$$\eta_{c^*} = \frac{1}{C_D} \quad (3-5)$$

Thus, in such cases, η_{c^*} would usually be less than unity for metalized propellants, and would always be greater than unity for non-metalized propellants.*

The submergence efficiency, η_{SUB} , is based on an empirical correlation and is a function of the throat radius, mass fraction of condensed phase, length of submergence to length of the internal motor, and chamber pressure. This correlation is discussed in more detail in Section 4.2.6.

The decrement in performance due to the formation of a turbulent boundary layer in the motor nozzle is transmitted directly to the MC module and is reported as a function of area ratio. The decrement in I_{sp} is taken to be the value corresponding to the initial nozzle exit area ratio. This decrement is assumed to be independent of erosion induced area ratio changes, and throat roughness.

Delivered performance (I_{sp} only) is calculated somewhat differently when based completely on the performance loss correlations presented in Section 4. Instead of equation (3-1), the following relation is employed,

$$I_{spD} = I_{spth} \eta_{KIN} \eta_{2D} \eta_{2P} \eta_{CE} \eta_{SUB} - \Delta I_{spBL} \quad (3-6)$$

Most solid rocket motors have normalized radii of curvature ≈ 2 and, in the absence of particles C_D tends to be $.99 \leq C_D < 1$, or, in other words, with perfect combustion η_{c^} would be bounded as follows, $1 < \eta_{c^*} \leq 1.01$. This small effect tends to be masked by measurement and data reduction errors, and many times test engineers are reluctant to report values of η_{c^*} greater than unity due to the mistaken assumption that such values are physically impossible to achieve.

In the simplified performance prediction methodology the two dimensional, η_{2D} , and two phase, η_{2P} , efficiencies are treated separately. The combustion efficiency, η_{CE} , is simply equated to the empirical c^* efficiency, η_{c^*} ; and the so-called "erosion loss" is not directly accounted for. If an estimate of the erosion loss is desired, and a TD2P solution has not been obtained, one can compute the ratio $I_{sp_{th}}(\bar{\epsilon})/I_{sp_{th}}(\epsilon(t=0))$, where $I_{sp_{th}}(\epsilon(t=0))$ is the specific impulse at the initial nozzle expansion ratio, usually denoted simply by $I_{sp_{th}}$. In order to compare the delivered specific impulses obtained theoretically (equation (3-1)), and empirically (equation (3-6)) an estimate of the erosion loss must be added to (3-6), or equivalently, $I_{sp_{th}}$ must be replaced by $I_{sp_{th}}(\bar{\epsilon})$.

The Master Control Module also calculates the other performance related quantities of interest $I_{sp_{D_2}}$, $F_{D_2}(t)$, I_T , etc., using equations (2-4) to (2-10).

3.2 Theoretical Performance Module

3.2.1 Approach

For a specified propellant combination the maximum specific impulse, $I_{sp_{th}}$, which can possibly be delivered can be predicted using any of a number of standard computer codes developed for this purpose. A survey conducted by the JANNAP Performance Standardization Working Group found sixteen such computer programs, each of which represented an independent development. All of these programs are, in principle, capable of calculating the quantities of interest, i.e. shifting and frozen I_{sp} and C_F , exhaust species etc. However, many of these programs, in practice, cannot adequately handle the solid phases required in solid rocket motor applications. Of the remaining applicable programs, two stand out by virtue of their excellent characteristics. These programs are:

The ODE Computer Program developed by NASA/LRC and described in NASA SP 273, Reference 4.

The Theoretical I_{sp} Program developed by the AFRPL and described in Reference 10 and 11.

with either computer program area ratio expansion calculations

yielding theoretical performance can be carried out for any rocket engine of current or projected use provided basic thermodynamic data exists for the propellant. Each computer program currently contains a vast library of thermodynamic data. A comparison of these two computer programs as applied to the proposed effort is presented in the paragraphs below.

The ODE Program

This computer program has been under continuous development at NASA/LRC since the mid 1950's. In 1968 it was adapted by the ICRPG (currently JANNAP) Performance Standardization Working Group as the standard computer program for theoretical performance computation. A newer extensively revised version of ODE is now available. This version is documented in complete detail in Reference 4.

Older versions of ODE were unable to successfully compute equilibrium compositions for aluminized propellants. This difficulty led directly to the development of certain of the sixteen chemical equilibrium codes previously mentioned. The more recent versions of the ODE program, however, are all capable of handling multiple solid phase products. For example, the SP273 version of ODE can successfully compute compositions with large amounts of solid phase carbon; a system with a history of difficulties.

The ODE program uses a free energy minimization technique, along with the following assumptions, to calculate the vacuum I_{sp} and related theoretical performance parameters.

- One dimensional flow.
- Chemical equilibrium between species and phases.
- Thermal and dynamic (velocity) equilibrium between condensed and gaseous phases.
- Adiabatic, isentropic flow.

The ODE program requires curve fit data for enthalpy vs. temperature. Seven coefficients ($a_1, a_2, a_3, a_4, a_5, a_6, a_7$) are required such that:

$$\frac{C_p^o}{R} = a_1 + a_2 T + a_3 T^2 + a_4 T^3 + a_5 T^4$$

$$\frac{H_T^o}{RT} = a_1 + a_2 T/2 + a_3 T^2/3 + a_4 T^3/4 + a_5 T^4/5 + a_6/T$$

$$\frac{S_T^o}{R} = a_1 \ln T + a_2 T + a_3 T^2/2 + a_4 T^3/3 + a_5 T^4/4 + a_7$$

Two sets of coefficients are required per species such that:

$$300^\circ\text{K} \leq T \leq 1000^\circ\text{K} \quad \text{for set 1}$$

$$1000^\circ\text{K} \leq T \leq 6000^\circ\text{K} \quad \text{for set 2}$$

The fits must be continuous across the juncture at 1000°K. NASA SP273 contains coefficients for 421 chemical species. A NASA/LRC program exists for the purpose of calculating thermodynamic data and outputting the above curve fit data. This program, called PAC, is described in Reference 23. A new all FORTRAN IV version of PAC is now available and has been found to be highly satisfactory.

The curve fit data is highly compact and computationally efficient but suffers from two major draw backs, which are:

- certain data cannot be accurately fit with only seven coefficients, especially over the range 300°K to 1000°K.
- curve fit data is awkward to produce since it requires use of the PAC program followed by careful comparison of the resulting fit to the original data.

NASA SP273 also contains elemental composition and enthalpy data (i.e., reactant cards) for 62 commonly used propellants.

Options available with the ODE program are:

Point Options:

- pressure and temperature
- enthalpy and pressure
- entropy and pressure
- density or volume and enthalpy

Problem Options:

- rocket option (i.e. chamber, throat, assigned area ratios, and/or pressures)

AFRPL Theoretical I_{sp} Program

This program also uses a free energy minimization technique to calculate theoretical performance, and employs the same assumptions listed for the ODE program. The AFRPL program contains several options not found in ODE, e.g. Air Augmented I_{sp}, Delta Velocity, Weight Optimization; however, these options are not of interest for the present purposes.

The AFRPL program requires curve fit data for specific heat vs. temperature. Ten coefficients ($z_1, z_2, z_3, z_4, z_5, z_6, z_7, z_8, z_9, z_{10}$) are required such that

$$C_p = z_1 + z_2 T^{-1} + z_3 T^{-2} + z_4 T^{-3} + z_5 T^{-4}$$

for $298^\circ\text{K} \leq T \leq 1200^\circ\text{K}$

and

$$C_p = z_6 + z_7 T + z_8 T^2 + z_9 T^3 + z_{10} T^4$$

for $1200^\circ\text{K} \leq T \leq 6000^\circ\text{K}$.

A curve fit program and an extensive library of fit thermodynamic data is maintained at AFRPL.

Either one of these two programs would be very satisfactory for the purpose of computing theoretical performance. Computer run times for both programs are short and are in no way a limiting factor. Computer core storage requirements are also modest (approximately 32K words) for both programs. Both programs feature excellent input methods. The ODE program was chosen for incorporation into the performance prediction methodology. The deciding factors were as follows:

1. The AFRPL program lacked the extensive documentation provided with the ODE program.
2. The ODE program has been adopted as a standard by JANNAF and is widely distributed.
3. The ODE program was already integrated into the One Dimensional Kinetics Program (ODK), which was adopted for the kinetics loss calculation. Replacing ODE with another program would have required a significant effort to link the new program to ODK.

3.2.2 Modifications To The ODE Program

For the present purposes the ODE program was modified to calculate the transport properties required by the Grain Design and Ballistics Module, 2-D, 2 Phase Module and Boundary Layer Module. In addition, the program has been modified to calculate the reference condition for the loss in performance due to finite rate chemical kinetics. This calculation is referred to as the "restricted equilibrium" solution and is discussed in more detail in section 3.4. ODE has also been modified to perform an equilibrium calculation at the exact area ratio corresponding to solidification. To reduce the length of the program the subroutines not required for the performance calculation were deleted. Thus, only the so-called rocket problem option of the ODE program can be exercised in the present context.

The transport properties calculated by the modified ODE program are the gas phase viscosity μ , thermal conductivity, ν , and Prandtl number, Pr. The viscosity and thermal conductivity of the individual gaseous species are calculated from formulas given in Reference 20:

$$\mu_i = \frac{4.15822 \times 10^{-8} \sqrt{M_{w_i} T}}{\sigma_i^2 \Omega_i} \quad (3-7)$$

$$\lambda_i = \frac{\mu_i R}{M_{w_i}} \left(1.45 + 1.32 \frac{C_{p_i}}{(e/M_{w_i})} \right) \quad (3-8)$$

The required Lennard Jones parameters, (σ_i, Ω_i) are internally stored in the computer program for 206 species. (See Subroutine MUK, Volume II, for a list of the species.) The viscosity of the mixture is calculated from Wilke's semi-empirical formula⁽²¹⁾

$$\mu = \sum_{i=1}^N \left[\mu_i \left(1 + \sum_{\substack{j=1 \\ j \neq i}}^N \epsilon_{ij} \frac{X_j}{X_i} \right)^{-1} \right] \quad (3-9)$$

where N is the number of species, X_i , the mole fraction of species i , and ϕ_{ij} is defined by:

$$\phi_{ij} = \frac{1}{2^{3/2}} \left[1 + \frac{M_i}{M_j} \right]^{-1/2} \left[1 + \left(\frac{\mu_i}{\mu_j} \right)^{1/2} \left(\frac{M_j}{M_i} \right)^{1/4} \right]^2 \quad (3-10)$$

The thermal conductivity, κ , is based on the equation given by Mason and Saxena (22), which is a slight modification of Eucken's relation,

$$\kappa = \sum_{i=1}^N x_i \left[1 + 1.065 \sum_{\substack{j=1 \\ j \neq i}}^N \phi_{ij} \frac{x_j}{x_i} \right]^{-1} \quad (3-11)$$

The Prandtl number is simply given by

$$Pr = \frac{\mu C_p}{\kappa} \quad (3-12)$$

A subroutine, ϕ MEGA, which performs a least squares fit for viscosity in the form $\mu = \mu^* (T/T^*)^\omega$ has also been added to ODE. This routine was necessary because the TD2P and TBL programs require viscosity to be in this form. The curve fits treat the chamber, throat and exit points; the throat values are treated exactly.

3.3 Grain Design and Ballistics Module

3.3.1 Grain Design Calculations

3.3.1.1 Approach

It was required that the SPP program be capable of calculating solid rocket motor delivered performance (i.e., pressure and thrust versus time as well as specific impulse and total impulse) for a wide range of motor designs and grain designs. At a minimum, end-burning, circular port, star port and spherical geometries, and at least two other geometries representative of modern production motors (e.g., slotted tube and finocyl), were to be considered.

The problem with constructing separate specialized subroutines for each geometry is that it is both cumbersome and limited. A multiplicity of individual geometry subroutines would add greatly to program length. The resultant program would also be limited, since the list of potential grain geometries is exhaustive. In addition, the geometry calculations do not stand alone; they have to be integrated with the ballistics calculations. Each separate, specialized geometry cal-

ulation would have to be individually integrated with the ballistics calculations. Clearly, a general method, that accomodates a wide range of geometries, is a more desirable means of fulfilling the objectives of this program.

Several grain geometry computer programs of more or less general capability are available. Some are limited to the geometry problem, some incorporate combustion and gasdynamics to provide an integrated interior ballistics capability. These candidate programs were reviewed in order to select the most appropriate. Selection criteria were principally geometric capability and adaptability to general interior ballistics analysis.

3.3.1.2 Review of Existing Computer Programs

3.3.1.2.1 Aerojet Basic Grain Design and Interior Ballistics (564)

This program solves the grain geometry and internal ballistics problems in a sequential manner. The geometric solution is two-dimensional, and the internal ballistics uses a simple burning rate law and one-dimensional gasdynamics.

Two-dimensional grain design can be very useful for symmetrical motors with sufficiently large length/diameter ratio that end effects become negligible. However, at lower length/diameter, or with end surfaces burning, or with partial burn surface restrictions, even a nominal two-dimensional geometry would require a three-dimensional treatment. Consequently, this program was not selected.

3.3.1.2.2 Lockheed General Grain Design Program (470)

This grain geometry program is basically two-dimensional, but can accommodate cylindrical grain designs in three dimensions. An important feature of this program is that it includes logic to account for nonuniform burning for ballistics adaptability. However, it was not selected because it is not fully capable of three-dimensional treatment.

3.3.1.2.3 Thiokol Generalized Grain Design Program (AGDA)

The AGDA program is a three-dimensional grain geometry program, but is not capable of handling internal ballistics. The program uses the Elkton-Moore method which is a vectorial approach to the geometric problem. It is capable of handling a broad range of grain designs, the complexity manifesting itself in the effort required for input.

This program was not selected because it does not incorporate combustion and gasdynamics analysis, and does not contain logic for coupling such analysis to the geometry calculations.

3.3.1.2.4 Boeing Internal Ballistics Computer Program (D2-125286)

The Boeing program is a three-dimensional grain design program incorporating one-dimensional gasdynamics and erosive burning. However, it was created for a special purpose and is therefore deficient in some respects and excessive in others. It is deficient in that it is restricted to certain types of grain geometries. It is excessive in the detail given to transients and high acceleration effects. Consequently, the program as presently constructed would not be best suited for the present purpose.

3.3.1.2.5 Hercules Grain Design and Internal Ballistics Evaluation Program (64101)

This program consists of two parts, the Basic Grain Design Program and the Internal Ballistics Evaluation Subprogram.

The Basic Grain Design Program examines a grain in three dimensions by analytical simulation of drafting techniques used in developing a grain design. It solves for geometric parameters used in internal ballistics calculations, and also for mass properties used in flight simulation calculations. It was developed in order to handle the most complex geometries used in modern production motors, and therefore has the desired general capability.

The Internal Ballistics Evaluation Subprogram uses simple one-dimensional gas-dynamics and erosive burning. It uses the geometry data computed for each burning station in the Grain Design Program, and feeds back the ballistics data at that location. It therefore accommodates nonuniform burning, and contains logic for coupling grain design with interior ballistics. Ignition and talloff transients are computed, but more for appearance than accuracy.

This program was selected because of its geometric generality and ballistics adaptability. Two correctible deficiencies were detected: the method of computing the radial slots in segmented grains, and the enormous size of the program (largely due to subroutines not required for the present purpose).

3.3.1.3 The Selected Program

The Hercules 64101 program is described in detail in Reference 8. With all of its options, it consists of six links and sixty subroutines. Only a fraction of these subroutines, fifteen in all, were found to be necessary for the requirements of the present program. Most of these are contained within LINK 2 of the original program, which deals with the geometry calculations. LINK 4 (a pseudo ballistics option) and LINK 5 (plotting routines) were eliminated since they could not be exercised when LINK 3 (the ballistic subroutines) is used. The mass properties subroutines within LINK 2 were also eliminated. LINK 3 was modified to incorporate the LPC ballistics analysis described in Section 3.3.2, and LINKS 0 and 1 (main driver and common regions between LINKS 2 and 3) were modified in accordance with the other insertions and deletions. These modifications resulted in an 80 percent reduction in the size of the program. Information regarding the operation of this modified program is presented in the Users' Manual portion of this report, Volume 3.

Basically, the geometry calculations compute volumes, and changes in volumes. Other geometric quantities are derivable from these volumes. Thus, for example, the burn area is equal to the rate of change of volume divided by the rate of change of web:

$$\dot{m} = \rho_p A_b r \quad (3-13)$$

$$\frac{dm}{dt} = \rho_p A_b \frac{dw}{dt} \quad (3-14)$$

$$A_b = \frac{dV/dt}{dw/dt} \sim \left. \frac{\Delta V/\Delta t}{\Delta w/\Delta t} \right|_{\text{mean value}} \quad (3-15)$$

- m = propellant mass
- \dot{m} = propellant mass flow rate
- ρ_p = propellant density
- A_b = propellant burn area
- r = propellant burn rate
- w = propellant web
- t = time
- V = propellant volume

The changes in web over a time increment are calculated from the ballistics subroutine, and the corresponding changes in volume are calculated from the geometry subroutines. The computations iterate on flow rate until a solution for pressure converges. Burn area is output as a matter of information, but is not used as such in the computations. Volumes form the basis of the computations in order to best satisfy the constraint that the weight expended must equal the weight loaded.

Inputs to the geometry calculations initially consist of the outer dimensions of the propellant grain, which is taken to be completely filled with propellant. Next, a series of inputs subtracts all initial void volumes representing the motor cavity. Such volumes may be represented by combinations of cylinders, cones, spheres, and prisms located by spatial coordinates; these volumes may intersect each other, but must not intrude into propellant. Supplementary parameters are available to define an inhibited surface, a corner round, a segmented grain slot face, and the symmetry of the grain. The grain is then divided into an X-Y computational mesh. Web fractions are also defined. When the web burns past a specified fraction, information may be output or internally transmitted between subroutines. The finer the mesh, the greater the accuracy, the smoother the output and the longer the computer time. The method by which the changing volumes are calculated for each mesh segment is presented in Ref. 8 and will not be repeated here.

3.3.1.4 Program Modifications

As far as the geometry calculations per se are concerned the only modification required was in the method of computing the volumes in the vicinity of opposed-face radial slots separating segmented grains. In the course of using the Lockheed 156-5 motor (a multiple segmented motor) as an early test case, there were pressure surges in the ballistics output. These were traced to excessive volumes being expended when the slots crossed the reference burn increments. In this type of situation, the calculations were expending triangular wedges of propellant (formed by the end face and the port to a certain length) rather than orthogonal webs. The error was magnified by the multiplicity of the segments. This deficiency was corrected by providing input logic to key the existence of a slot, and a single equation for the annular geometry of the slot to be used at that location.

A related problem was encountered with end-burning faces in general. Depending upon the selection of the mesh size and burn intervals, it is possible to have the same volume expended counted several times. This can be avoided by maintaining a certain relationship between these inputs, as discussed in the User's Manual. No program modification was required.

The aforementioned 80% size reduction from the original Hercules program was successfully accomplished. Care had to be exercised to assure that deletions would not destroy functionality. The retained subroutines are listed in the Program Description, Volume 2 of this report.

The revised ballistics analysis is discussed subsequently.

3.3.2 Ballistics Calculations

3.3.2.1 Approach

The interior ballistics analysis solves the conservation equations applied to the rocket motor cavity to predict pressure and mass flow as a function of time. In its most rigorous form, a ballistics calculation solves the time dependent equations governing conservation of mass, momentum and energy. The simplest type of ballistics calculations, widely used in rocket motor design, employ a steady-state mass balance. The sophistication required is determined by the purpose of the analysis and the accuracy required.

A comprehensive model of the energy exchange processes within a rocket motor was prepared by LPC for the prediction of duty cycles of controllable solid rocket motors⁽¹³⁾. The sophistication was warranted by the emphasis on transient phenomena: predictions of ignition delay times, ignition pressure spikes, extinguishment-reignition phenomena and transient performance integrals were required. The program would be recommended for such purposes. For present purposes however, which emphasize steady-state performance prediction, its size, complexity and run time would not be justified.

Computer programs such as Hercules 64101, Aerojet 564 and Lockheed 241 use a simplified one-dimensional treatment. Although the Hercules 64101 program was selected for its geometric capabilities, it would not be recommended for the computation of interior ballistics. It employs a three-stage

treatment with separate analyses for ignition, steady-state and talloff. The method of interfacing these stages is ill-defined. The transient stages do not employ an internal flow analysis, and the steady-state stage uses a simplified one-dimensional flow solution with time dependent terms omitted. A better approach, to avoid arbitrary division of the motor operation into stages, would be to employ one set of equations. The Boeing program takes this approach, but like Reference 13 was developed for a special purpose.

The most recent interior ballistics analysis, completed by Lockheed for the Air Force, resulted in the Lockheed 637 program⁽⁹⁾. This program couples a comprehensive ballistics analysis to a limited grain geometry capability. However, the methodology is compatible for use with the Hercules geometry analysis for more general capability. Therefore, this analysis was selected as best-suited to the requirements of the present program. The effort required was to reconstruct LINK 3 of the original Hercules program, using the ballistics analysis from Ref. 9 as the basis. The original designation for the ballistics subroutine in the Hercules program, MAIN3, was retained.

3.3.2.2 Flow Equations

The equations for one-dimensional flow used in the computer program are based on the following assumptions:

Particles occupy negligible volume compared to the gas.

Particle velocity and temperature are equal to the respective gas values.

The particle-gas mixture behaves as an "equivalent" perfect gas.

Mass is generated from the propellant without an axial component of velocity; although invalid for end-burners, the error will be negligible because of the large flow area downstream of the end face.

Transient effects are simply approximated.

With these assumptions, the conservation equations are:

$$P = cRT \quad (3-16)$$

$$\frac{\partial}{\partial t} (\rho A) + \frac{\partial}{\partial x} (\rho u A) = \dot{m}_e \quad (3-17)$$

$$\rho \frac{Au}{g} \frac{\partial u}{\partial x} + \dot{m}_e \frac{u}{g} + A \frac{\partial P}{\partial x} = 0 \quad (3-18)$$

$$C_p T + \frac{u^2}{2g} = C_p T_F \quad (3-19)$$

- P** = pressure, lb/ft²
ρ = gas density, lb/ft³
R = gas constant for the products, ft²/F
T = gas temperature, °F
t = time, sec
A = flow area, ft²
x = axial distance, ft
 \dot{m}_e = incremental mass flow rate, lb/ft-sec
u = gas velocity, ft/sec
g = gravitational constant, ft/sec²
C_p = gas heat capacity, ft²/R
T_F = flame temperature, °R

These equations are applied at each computational increment, as defined by the mesh for the grain geometry calculation.

The cross-sectional areas are supplied by the grain geometry calculations. The local mass flow increments, \dot{m}_e , are determined by the grain geometry and the local burning rate (see Section 5.1 for description of burning rate calculation).

At each time increment a solution is obtained in the following manner. The head-end pressure is estimated, and equations 3-16 to 3-19 are integrated down the port, step by step. When the end of the grain is reached the nozzle choking constraint is tested. The procedure is iterated, with successive head-end pressure estimates until the choking constraint is satisfied. The choking constraint is applied as follows. First, a throat stagnation pressure is defined as:

$$P_T = \frac{W(HN) C^*}{g AP(NN)} \quad (3-20)$$

- P_T** = throat stagnation pressure, lb/in²
W(HN) = mass flow through the throat, lb/sec
C* = flow characteristic velocity, ft/sec
AP(NN) = throat area, in²

Starting with P_T and a Mach number equal to one at the throat, the isentropic relations are used to calculate what the static pressure at the nozzle entrance must be if the throat is to be choked. This pressure, $P(NN)$, is compared to the static pressure resulting from the integration down the port, $P(N)$. Convergence (choking) is realized when these two pressures are within a specified tolerance. The C^* used in equation 3-20 is the theoretical C^* multiplied by an empirical C^* efficiency (Section 4.1) and an insulation dilution factor (Section 5.3).

The thermochemical properties required for the ballistics calculation are obtained from the Theoretical Performance Module. The nozzle erosion rate required to define the instantaneous throat area may be input as a table, or calculated internally based on the simple correlations presented in Section 5.2.

3.3.2.3 Other Mass Contributions

Mass may enter the rocket motor from a gas generator, an igniter, or insulation ablation. These are treated as lumped, rather than distributed, additions; hence, they influence the pressure magnitude but not the shape of the pressure distribution down the grain port. For lumped additions, it does not matter whether the mass enters at the head end or the aft end of the motor. In constructing the iterations, it was entered at the aft end (which best represents insulation in general). Therefore,

$$W(NN) = \int \dot{m}_e dx + WI + WIGN \quad (3-21)$$

or

$$W(NN) = W(N) + \rho_I A_I r_I + WIGN \quad (3-22)$$

- $W(N)$ = propellant flow rate
- ρ_I = insulation density
- A_I = insulation exposed area
- r_I = insulation ablation rate
- $WIGN$ = igniter or gas generator flow

These masses are input in tabular form. Igniter (or gas generator) flow is input as a function of time. Insulation density and burning rate are input constants, while exposed insulation area is input as a function of time. All of these masses are assumed to have the same thermochemical effects. All are optional and not required input. It should not be inferred from the inclusion of an igniter mass flow that the analysis can predict ignition delay; it does not do so. The analysis assumes that burning has started in a motor initially at ambient pressure, and will properly fill the chamber (also empty the chamber at burnout). Therefore, WIGN is an artifice and except where it is a significant contribution to the total impulse of the motor, can be included or excluded as desired. If the user is seriously interested in predicting the ignition transient, the method of Reference (13) should be employed.

3.3.2.4 Flow Across Radial Slots (Segmented Motor)

Pressure drop across a radial slot separating the segments of a segmented motor is treated for two cases: (1) where the gas velocity in the slot exceeds the gas velocity in the adjacent upstream port; (2) where it is less than that velocity. In either case, the state properties in the slot are assumed equal to the static values of the gas at the end of the upstream port; slot velocity is then determined from continuity in the slot:

$$u_s = \frac{W_{ADD}}{\rho A_s} \quad (3-23)$$

- u_s = slot gas velocity, in./sec
 W_{ADD} = flow rate of propellant from the slot faces, lb/sec
 A_s = slot width flow area, in²
 ρ = gas density, lb/in³

It is implied that pressure is constant in the slot. Further, it is asserted that burning rates are equal over the entire slot face and at the strand rate value. Propellant in the slot does not see radiating walls, and in practice the separation will be large enough to preclude erosive burning.

If the entering gas velocity from the slot exceeds the approaching gas velocity in the port, the slot pressure drop is calculated as one increment with the momentum equation. It is as though the slot were physically absent, being filled with propellant of high \dot{m}_0 . Thus the radial momentum is dissipated, and a

pressure drop equivalent to accelerating the added flow to port velocity is determined.

If the entering gas velocity from the slot is less than the approaching gas velocity in the port, an empirical relation is used to find the port area of the expanded stream tube over the slot:

$$A_{pi} = A_{pm} + (D_x^2/A_{pm}) (1 + \frac{u_s}{u}) \quad (3-24)$$

- A_{pi} = stream tube area
- A_{pm} = local port area
- D_x = slot separation distance

Knowing the area and static pressure in the streamtube, other parameters are determined by iteration. The pressure drop across this streamtube into the downstream port is determined with the assumption of an inlet efficiency:

$$P_{i+1} = P_i + \frac{1}{2} \frac{ETA_{IN}}{g} \left[(\rho u^2)_i - (\rho u^2)_{i+1} \right] \quad (3-25)$$

- P_{i+1} = downstream static pressure
- P_i = upstream static pressure
- ETA_{IN} = inlet recovery efficiency, typically 0.9 for sharp-edged entrance geometry

Optional capability is provided to refine the treatment to simulate a slot face which is not perpendicular to the motor axis. Causes of a non-normal face include variable ignition delays in the slot, grain slump, or tapered inhibitors. The corrections are used to locate the axial position of the outer slot diameter, knowing the position of the inner slot diameter at the grain port. Inputs relating to these effects are tables of the amount of burning slot diameter versus time, and lateral burn-back versus web.

The analysis of the slot ballistics is coupled to the analysis of the slot geometry, and overrides the normal grain geometry calculations. A card input keys the existence of a slot.

3.3.2.5 Delivered Performance

The various quantities which characterize delivered performance are also calculated with the Grain Design and Ballistics Module. The performance calculations within this module do not replace the ones previously described (Sections

2.3 and 3.1). They are supplementary; to be referred to only when the Grain Design and Ballistics Module is used in a stand-alone mode.

Delivered thrust (vacuum) is given by

$$F_D = W(N) \frac{V_e}{g} \eta_F + P_e A_e \quad (3-26)$$

$W(N)$ = propellant flow rate, lb/sec

V_e = exit velocity, ft/sec

η_F = input nozzle efficiency

P_e = exit static pressure, lb/in²

A_e = nozzle exit area, in²

Exit velocity and pressure are determined from the standard isentropic relations. The nozzle efficiency may be determined from the semi-empirical correlations, which are amenable to hand calculation. The exact calculations (TD2P, etc.) would not be available in the stand-alone mode. As used here, nozzle efficiency is an input value. Thrust delivered to the input, ambient pressure, P_a , is given by

$$F_{D_a} = F_D - P_a A_e \quad (3-27)$$

Ambient pressure may be a constant or a table to simulate a flight schedule.

Total impulse is calculated as the time integral of F_{D_a} . Specific impulse is calculated on an instantaneous basis by dividing F_{D_a} by $W(N)$, and on a total basis by dividing the integral of F_{D_a} by the integral of $W(N)$. Insulation weight is not included because of the convention to base performance on propellant weight only; however, both instantaneous and integrated insulation weight flow are output if such correction is desired.

3.4 Kinetics Module

3.4.1 Approach

The loss of performance in solid rocket motors due to finite rate chemical kinetics has been estimated to range between 0.2% for high pressure, low metal loading systems, to as high as 5%, or more, for low pressure, high metal loading systems. Hence, if the performance of solid propellant rocket motors is to be

accurately predicted over a wide range of configurations and operating conditions, the loss due to chemical kinetics must be accurately modeled.

The loss of performance which we attribute to finite rate chemical kinetics is usually associated with the difference between the maximum possible sensible heat release (chemical equilibrium) and the actual heat release due to chemical reactions which occur in the rocket nozzle. The loss is small if the reactions proceed at a rate comparable to a small fraction of the stay time in nozzle. However, if the recombination reaction rates are slow all of the heat released by combustion of the propellant cannot be converted into kinetic energy. As the ratio of nozzle stay time to a characteristic reaction time approaches zero, the so-called frozen performance limit is approached.

The selection of a method to compute the kinetics loss was not as straightforward as some of the other selection procedures. As pointed out in Reference 1, there are two basic techniques which have been used for calculating finite rate performance losses. The first method seeks numerical solutions to the exact one dimensional, two phase, reacting gas, equations of motion. The second technique is approximate, and is based upon application of a "sudden freeze" criteria.

Equilibrium flow is assumed up a given point in the nozzle, at which the flow is then frozen. The sudden freeze approximation is more applicable to liquid rockets than solid rocket motors. Such methods were not considered for the present program as their accuracy was not deemed to be high enough. The only existing program of the first type is that of Kliegel, et al⁽¹⁹⁾. As discussed below, this program was also considered inappropriate for the present purpose.

The one dimensional, two phase, reacting gas program of Reference 19 yields accurate one dimensional performance predictions, but does not directly yield an estimate for the kinetics loss alone. The two phase flow loss is presently calculated on a two dimensional basis using the TD2P program (Section 3.5). Thus, if the one dimensional, two phase, reacting gas program is to be used, the two phase and kinetics losses, which are coupled in this analysis, must be separated in order to avoid a redundancy.

An accurate method for separating the two losses could be developed by modifying the one dimensional equilibrium program (ODE) to handle finite particle

lags. Such an approach was discarded, however, due to the extent of the modifications required. Other, more approximate means of obtaining a kinetics loss could be developed, but not without compromising the resultant accuracy. The program described in Reference 19 is also complex, very large, long running, and not easy to use. For all of these reasons alternate means were considered.

Since the present effort was not to include any new computer program development, the JANNAF standard computer program for calculating one dimensional kinetics losses in liquid rockets, ODK, was considered. The ODK program is widely used and is computationally efficient. Complete documentation of the analysis and computer program are contained in Reference 5. In its existing form ODK was not applicable, however, since it contained no provision for solid or liquid phases.

The existence of a second phase in the flow can result in significant alteration of the axial distributions of the various flow quantities (T , ρ , u , etc.), and, hence, impacts the reaction rates and kinetic losses. The existence of finite lags between the particles and gas modifies the effect of two phase flow on the kinetics loss, but in a second order manner.

Various modifications could be made to the ODK program to include the effect of two phase flow on the kinetics loss. In its unmodified form the ODK program numerically integrates the exact one dimensional, finite rate kinetics, equations of motion for a gas only system. A modification of the program to allow it to treat the particles in an exact manner would have resulted in a program similar to that of Reference 19, and would have engendered the same problems. A modification based on the adoption of the constant fractional lag approximation was also considered. In this approximation the velocity and temperature lags of the particles are assumed to be finite, but constant. With this assumption the one dimensional, two phase, equations of motion can be reduced to those for an "equivalent" gas only system, thereby eliminating the need for solving a separate set of particle equations. The required modifications to the ODK program, and the ODE program (in order to generate a reference equilibrium solution), were determined to be substantially less than those required to implement a solution of the "exact" two phase flow equations. The effort required was, however, still greater than desired.

Another possible modification, actually a degenerate form of the previous one, was also evaluated. In the limit of vanishingly small lags, the constant fractional lag equations reduce to the so called equilibrium limit, i.e. particles and gas have the same velocity and temperature. The system of equations again reduces to that for an "equivalent" gas only flow, but the program modifications required to implement a no lag model were simpler and less extensive than those for the other alternatives examined. While this approach seemed attractive, a series of calculations was performed in order to estimate the effect of ignoring finite lags before it was adopted. As a result of these calculations it was determined that the zero lag assumption is quite adequate. It is estimated that the use of the zero lag approximation should impact the overall performance prediction by less than 0.1% (when the kinetics loss itself is but a fraction of a percent the impact should be closer to 0.01%).

In view of the previous discussion, the ODK program modified to treat particles on an equilibrium, no lag, basis, was adopted as the method to be used in computing the kinetics loss. A kinetic efficiency factor, η_{KIN} , is defined by taking the ratio of the I_{sp} (vacuum) calculated by ODK to an equilibrium I_{sp} obtained by exercising a special option which was incorporated in the ODE program. When approached in this manner the kinetics loss is obtained directly; without the need to separate out redundant two phase flow losses. The only requirement is that the particles be treated identically in ODK and ODE.

Both ODE and the modified ODK program assume the particles and gas are in thermal and dynamic equilibrium. The ODE program in its original form, allows for the gas phase to condense as it expands out the nozzle, i.e. the weight fraction of the condensed phase may increase. The modified ODK program, however, does not allow mass transfer between phases. Thus, to be consistent, and to preserve accuracy, a special option was added to the ODE program which allows it to "freeze" the concentration of the condensed phases at their chamber values. The same dictates of consistency and accuracy governed the treatment of particle solidification. The ODE program allows the liquid phase to solidify, and properly accounts for the resultant energy release. An analogous treatment of particle solidification was, therefore, incorporated into the ODK program.

The previously mentioned definition of the kinetic performance efficiency, as calculated, may be written in the following symbolic form,

$$\eta_{KIN} = \frac{I_{spODK}}{I_{spRE}} \quad (3-28)$$

wherein I_{spRE} denotes the specific impulse calculated using the so-called restricted equilibrium option to the ODE program. An additional advantage of using this reference method of calculating $\eta_{I_{sp}}$ is that only thermodynamically important species need be considered in the ODK and ODE-RE calculations. Thus, trace species, and reactions involving them, need not be included in the calculation.

The following is a brief summary of the ODK program (prior to modification). Further details regarding the details of the analysis and the program itself may be found in Volume II of this report and in Reference 2. The ODK program calculates the inviscid, one-dimensional, nonequilibrium, frozen, and equilibrium (the ODE program is incorporated into ODK), nozzle expansion of gaseous combustion products. The program can treat large, complex, chemical systems. A maximum of 150 distinct chemical reactions and 40 individual species can be included in a given calculation. Chemical reactions are input in standard reaction form and are translated by an input processor into a mathematical form suitable for computation. Chemical reactions can be added or deleted by adding (or deleting) a single input card per reaction. Up to 10 reactants and 10 products can be included in each reaction. There is also a convenient method for specifying third body efficiencies. The coupled set of nonlinear, ordinary differential equations, is integrated using a very efficient, stable, second order, implicit method. Under certain conditions, when efficient to do so, the program switches to an explicit integration method. The program is designed for engineering use, is well documented and user oriented.

The modifications to the ODK program accomplished during the present effort are described in the next section and in Volume II of this report. The reaction set and reaction rates, for aluminized propellants, that were employed in the calculations performed to date are described in Appendix A. The manner in which these reactions and rates were selected is also discussed therein.

3.4.2 Modifications To The ODK Program

Modifications to the ODK program were required in order to incorporate into it the ability to treat two phase expansions, with solidification. As discussed

in the previous section, particle-gas equilibrium (zero lag) was assumed. Thus, the gas and particle velocities and temperatures are taken to be equal. Other assumptions which were employed are:

- There is no phase change from the gaseous phase to either the liquid or solid state.
- The liquid particles of a given specie solidify at the melting point of the solid phase.
- The particles occupy zero volume and exert no pressure on the gas.

As would be expected for a program like ODK, a significant effort was required in order to identify, program and check out the requisite modifications. As mentioned previously, the zero lag assumption allows the two phase flow to be treated as an "equivalent" gas only flow. The existing equations employed in the ODK program can be made to correspond to the equations for an equilibrium (no lag) particle-gas mixture simply by treating the condensed phases as gas phase species with infinite molecular weights. Thus, the only the equation for the gas constant required special treatment. The gas constant is defined by

$$R = \sum c_i R_i \quad (3-29)$$

where

$$R_i = \frac{R}{M_{w_i}} \text{ for gas phase species}$$

$$R_i = \frac{R}{\infty} = 0 \text{ for condensed phase species}$$

A method for handling particle solidification also had to be incorporated into the program. Under the zero lag assumption, particle solidification must be handled in a special manner, since there is no explicit heat transfer term to govern the rate at which a particle solidifies. It is assumed that when the gas reaches the particle solidification temperature the gas temperature remains constant, i.e., $dT/dx = 0$, until the latent heat of solidification is given up by the liquid particles. This constraint yields an equation for the rate of change of the condensed phase mass fraction, as follows. By noting the constancy of the total enthalpy, and applying the restriction $dT/dx=0$, it is easily shown that the following equation must be satisfied:

$$-c_p \frac{dT}{dx} = 0 = u \frac{du}{dx} + \sum_{l=1}^{N_g} h_l \frac{dc_l}{dx} + h_l \frac{dc_l}{dx} + h_s \frac{dc_s}{dx} \quad (3-30)$$

where N_g is equal to the number of gas phase species. By using the following relations,

$$\frac{dc_g}{dx} = - \frac{dc_l}{dx} \quad (3-31)$$

$$h_l - h_s = \Delta H_m \text{ (heat of fusion)}, \quad (3-32)$$

equation (3-30) may be solved for the rate of change of the liquid phase mass fraction, yielding,

$$\frac{dc_l}{dx} = - \frac{1}{\Delta H_m} \left[u \frac{du}{dx} + \sum_{i=1}^{N_g} h_i \frac{dc_i}{dx} \right] \quad (3-33)$$

The ODK program integrates the quasi-one dimensional equations of motion either on a pressure defined, or area defined basis. Therefore, before equation (3-33) could be implemented the velocity derivative had to be replaced by either a pressure or area derivative. Using the equations of motion given in Reference 5, it can be shown that equation (3-33) can be written in the following alternate forms, for pressure, or area defined problems, respectively.

$$\frac{dc_l}{dx} = \frac{\gamma RT}{(\gamma-1)\Delta H_m} \left\{ \frac{\gamma-1}{\gamma} \frac{1}{P} \frac{dP}{dx} - B \right\} \quad \text{pressure defined} \quad (3-34)$$

$$\frac{dc_l}{dx} = \frac{\gamma RT}{(\gamma-1)\Delta H_m} \left\{ \frac{(\gamma-1)M^2}{1-M^2} \left(\frac{1}{a} \frac{da}{dx} - A \right) - B \right\} \quad \text{Area defined} \quad (3-35)$$

With dc_g/dx and dc_l/dx defined, the remaining equations can be integrated. This procedure is then applied at each succeeding integration step until the concentration of the liquid phase becomes equal to zero (i.e. all of the heat of fusion contained in the original mass fraction of liquid has been given up to the gas phase).

Since this part of the analysis is new, and cannot be found elsewhere, the partial derivatives of the rate of change of the liquid mass fraction, dc_l/dx (denoted $c_{l,x}$), with respect to all of the other dependent variables are given here, for completeness. These partial derivatives are required by the implicit integration scheme used in ODK.

Pressure Defined Equations

$$\frac{\partial c_{l,x}}{\partial V} = \frac{c_p}{\Delta H_m} \frac{\partial \bar{T}_x}{\partial V} \quad (3-36)$$

$$\frac{\partial c_{l,x}}{\partial \rho} = \frac{c_p}{\Delta H_m} \frac{\partial \bar{T}_x}{\partial \rho} \quad (3-37)$$

$$\frac{\partial c_{l,x}}{\partial \bar{T}} = \frac{1}{\Delta H_m} c_p \frac{\partial \bar{T}_x}{\partial \bar{T}} + \frac{d\bar{T}}{dx} \frac{\partial c_p}{\partial \bar{T}} - \frac{dc_l}{dx} \frac{(c_{p_l} - c_{p_s})}{\Delta H_m} \quad (3-38)$$

$$\frac{\partial c_{l,x}}{\partial c_i} = \frac{1}{\Delta H_m} c_p \frac{\partial \bar{T}_x}{\partial c_i} + \frac{d\bar{T}}{dx} c_{p_i} \quad (3-39)$$

Area Defined Equations

$$\frac{\partial c_{l,x}}{\partial V} = \frac{1-M^2}{1-\gamma M^2} \frac{c_p}{\Delta H_m} \frac{\partial \bar{T}_x}{\partial V} + \frac{dc_l}{dx} \frac{\gamma}{1-\gamma M^2} - \frac{\partial M^2}{\partial V} \quad (3-40)$$

$$\frac{\partial c_{l,x}}{\partial \rho} = \frac{1-M^2}{1-\gamma M^2} \frac{c_p}{\Delta H_m} \frac{\partial \bar{T}_x}{\partial \rho} \quad (3-41)$$

$$\begin{aligned} \frac{\partial c_{l,x}}{\partial \bar{T}} &= \frac{1-M^2}{1-\gamma M^2} \frac{c_p}{\Delta H_m} \frac{\partial \bar{T}_x}{\partial \bar{T}} + \frac{dc_l}{dx} \left(\frac{\gamma}{1-\gamma M^2} - \frac{1}{1-M^2} \right) \frac{\partial M^2}{\partial \bar{T}} \\ &\quad - \frac{dc_l}{dx} \frac{(c_{p_l} - c_{p_s})}{\Delta H_m} + \frac{dc_l}{dx} \frac{M^2}{1-\gamma M^2} \frac{\partial \gamma}{\partial \bar{T}} \\ &\quad + \frac{dc_l}{dx} \frac{1}{c_p} \frac{\partial c_p}{\partial \bar{T}} \end{aligned} \quad (3-42)$$

$$\begin{aligned} \frac{\partial c_{l,x}}{\partial c_i} &= \frac{1-M^2}{1-\gamma M^2} \frac{c_p}{\Delta H_m} \frac{\partial \bar{T}_x}{\partial c_i} + \frac{dc_l}{dx} \left(\frac{\gamma}{1-\gamma M^2} - \frac{1}{1-M^2} \right) \frac{\partial M^2}{\partial c_i} \\ &\quad + \frac{dc_l}{dx} \frac{M^2}{1-\gamma M^2} \frac{\partial \gamma}{\partial c_i} + \frac{dc_l}{dx} \frac{1}{c_p} c_{p_i} \end{aligned} \quad (3-43)$$

where $\bar{T}_x = d\bar{T}/dx =$ gas temperature derivative in the absence of solidification.

The QDK computer code has been dimensioned to handle up to 10 condensed phase species (or 5 doublets of solid and liquid phase) with 10 discrete melting points. This allotment should be adequate to handle any metalized propellant system of interest.

While strictly a modification to ODE, and not ODK, the manner in which ODE was modified to restrict the condensed phase mass fraction from changing is described here, as this "restricted equilibrium" modification serves only to provide a reference I_{sp} value for the kinetics loss computation.

For purposes of computing a reference (or base) I_{sp} for the kinetics loss calculation an option was incorporated into the ODE program which allows it to "freeze" the concentrations of the condensed phase species at their chamber values (except that corresponding liquid and solid phases are allowed to exchange, i.e., solidification is allowed).

In order to implement this option, the ODE program searches the list of species to see if aluminum (Al), beryllium (Be), boron (B), lithium (Li), magnesium (Mg), zinc (Zn), zirconium (Zr), or any compounds containing these elements, are present in either the liquid or solid phases. If any such species are found, the corresponding liquid and solid phases are renamed, but assigned their usual thermodynamic properties. This is done so that the program will not recognize them for what they are, thereby restricting these liquid-solid pairs from reacting with any species other than themselves. As far as the gaseous species are concerned, these condensed phases no longer exist, hence, additional amounts of condensed phase cannot be formed as the flow expands out the nozzle.

3.5 Two Dimensional Two Phase Module

3.5.1 Approach

Almost all rocket nozzles of practical interest have a loss in performance due to a nonaxial component of velocity at the nozzle exit plane. This loss is usually referred to as a divergence, or two dimensional flow, loss. If the propellant is metalized, there is an additional loss when the particles cannot maintain a state of dynamic and thermal equilibrium with the gas flow. This loss is referred to as the two phase flow loss.

The two dimensional and two phase flow effects are coupled. From the discussion in Section 2.4 it is clear that any analytical methodology for predicting two phase flow loss should be integrated with the calculation of divergence loss. This requires a two-dimensional flow field program with two phase capability. Both a survey conducted by JANNAF and the study reported in Reference 1 recom-

mended, as the best available computer program of this type, the Two Dimensional Two Phase Flow computer program developed by Kliegel and Nickerson⁽⁶⁾. This program was, therefore, adopted for use in the present performance prediction methodology. The basic assumptions employed in the TD2P program are:

- The flow is at the choked steady state condition for an axially symmetric converging - diverging nozzle.
- The gas and particle phases each have constant thermodynamic properties.
- There are no mass or energy losses from the system.
- The gas is inviscid except for its interactions with the condensed particles.
- The volume occupied by the condensed particles is negligible.
- The thermal (Brownian) motion of the condensed particles is negligible.
- The condensed particles do not interact.
- The condensed particle size distribution may be approximated by groups of different size spheres.
- The internal temperature of the condensed particles is uniform.
- Energy exchange between the gas and the condensed particles occurs only by convection.
- The only forces on the condensed particles are viscous drag forces.
- There is no mass transfer from the gas to the condensed phase during the nozzle expansion.

The overall method of solution consists of essentially two distinct parts: a transonic solution; and a supersonic solution. The transonic solution is required in order to provide an initial line for the supersonic solution.

The transonic solution is obtained by an approximate technique. The nozzle geometry is assumed to consist of a conical inlet section joined smoothly to a constant radius of curvature throat. The flow in the conical inlet portion of the nozzle is assumed to be a one-dimensional sink flow. The flow in this region is coupled to a two dimensional, Sauer type, expansion solution in the throat region. The output from this analysis is a set of flow properties along a supersonic start line. The flow field from this initial line out to the nozzle exit is obtained numerically using the method of characteristics to solve the exact two phase flow equations of motion.

This overall procedure works quite well in most cases, however, the nature of the transonic solution introduces certain restrictions on the problems which can be solved. As previously mentioned the transonic analysis requires that the

convergent portion of the nozzle be conical and that the throat be circular, with a single radius of curvature. Nozzles not of this shape must be "fitted" to conform to this geometry in order to obtain a solution. While this can often be accomplished without introducing significant error, the "fitting" procedure is subjective, which is undesirable, and the size of the error introduced is not known a priori. The transonic method of solution will also fail when the nondimensional throat radius of curvature (radius of curvature divided by throat radius) is less than about 1.5, and when the conical inlet angle exceeds approximately 45°. This fact results in two additional restrictions on the nozzle geometries which may be considered.

It is clear from this discussion that a more exact, less restrictive, method for solving the two-dimensional, two-phase flow equations would be desirable. With presently available numerical techniques such a method of solution could, and should, be developed.

There is one additional limitation of the TD2P program that has yet to be mentioned. If the exhaust nozzle is contoured in such a manner that the particles impinge upon it before reaching the exit plane, the supersonic solution will fail (terminate) at the first point of impingement. It is a relatively simple matter to modify the program to continue the calculation in an artificial manner after impingement occurs. It is not quite so simple, but not too difficult, to incorporate a simple, but reasonable, physical model of impingement into the program.

In order to use the TD2P program it is necessary to determine appropriate average values for the perfect gas and particle phase properties. A method for obtaining such properties was developed by Kliegel and Nickerson and was formalized in the Average Gas Properties (AGP) computer program⁽²³⁾. This program uses the one-dimensional equilibrium (zero lag) approximation to find a set of "equivalent" perfect gas properties such that the solidification area ratio is identical to the value computed by the ODE program. There are other details involved in this computation which will not be discussed at this point. An updated, modified, version of the AGP program has been incorporated in the TD2P program, and is fully described in Volume II of this report (see subroutine AGP).

Because the two-phase flow loss is an important source of performance loss and is a function of particle size, the ability to predict particle size will have an important impact upon the success of the computer program over a broad range of conditions. The present method for predicting particle size is described

in detail in Section 5.4. The correlation described therein yields the mean particle size. The distribution function employed, and the method for selecting the diameter of each of the particle groups is described in the subroutine DIST write up in Volume II.

3.5.2 Modifications to the TD2P Program

Numerous modifications and additions to the TD2P program were accomplished during the present effort: The more significant of these changes are discussed below.

The TD2P program was originally written in FORTRAN II, and the common linkages were completely unsatisfactory for use as a module element. The program had only blank common with multiply defined entries. These were eliminated and data storage replaced by multiple labeled common statements. These modifications were necessary to reduce program size to the 55K requirement for the combined program. The TD2P overlay structure was revised accordingly.

The number of options for describing the nozzle wall contour was increased. In particular, the ability to use a cubic spline fit contour, rather than a point by point specification, was added. A cone, defined by the nozzle end point only, option was also incorporated into the program. The maximum number of wall points allowed was also increased from 60 to 150 to allow better definition of the contour.

The TD2F input was revised to be more convenient for the user. Certain input items were built into the program, while others were modified or eliminated.

The particle size correlation presented in Section 5.4 was incorporated into the program, as was a subroutine (DIST) to provide a log-normal distribution into the specified number of particle groups.

The AGP program⁽²³⁾ was modified and then incorporated into the TD2P program. The AGP program provides a rational means for selecting perfect gas properties to use in the TD2P calculation. Previously, this program had to be executed separately and the requisite parameters input to the TD2P program. The AGP program was modified to calculate I_{sp} on a one-dimensional, zero lag, basis, to serve as a reference value for the two-dimensional, two-phase loss calculation. The manner in which the AGP program calculates specific heats, and the way it treats solidification, was also modified.

The TD2P program was also modified to provide certain quantities to the Boundary Layer Loss Module. These quantities are the internally tabulated wall geometry, the Mach number distribution along the wall streamline, the two-dimensional, two-phase, mass flow rate, and the total pressure and total temperature at the wall initial line point. The latter two quantities are provided to allow the TEL calculated wall pressure and velocity distributions to closely approximate the corresponding TD2P values.

The object of the TD2P Module is, of course, to calculate a performance loss efficiency. The manner in which the program was modified to do this is described in the next sub-section.

3.5.3 Performance Loss Calculation

The TD2P Module provides three types of quantities to the Master Control Module for use in the overall delivered performance calculation. These quantities are the nozzle discharge coefficient, C_D ; and two-dimensional, two-phase, specific impulse, I_{spTD2P} , and specific impulse efficiency, η_{TD2P}^i , as functions of area ratio.

The discharge coefficient, C_D , is obtained as a direct result of the TD2P transonic solution. It is used in obtaining the combustion efficiency from the c^* efficiency - equation (3-4), and in computing the ambient pressure correction to delivered I_{sp} - equation (2-4).

The specific impulse calculated by the TD2P program I_{spTD2P} , is used in the performance calculation, but never on an absolute basis. At every wall point in the TD2P characteristics solution a two-dimensional, two-phase flow, I_{sp} efficiency, $\eta_{TD2P}^i(\epsilon)$ is calculated by ratioing the TD2P I_{sp} to a one-dimensional, zero lag, I_{sp} computed at the same area ratio. This one-dimensional, reference I_{sp} , is obtained from the subroutine used by the modified AGP program (AGP was incorporated into the TD2P program) using the same ideal gas properties as employed in the TD2P program. By using a ratio calculated in this manner, instead of using the absolute I_{sp} number from TD2P, the effect of neglecting real gas effects is minimized. Also, extra care was taken to accurately calculate the reference I_{sp} during solidification so as to avoid the use of different assumptions in the two calculations. The equations used in calculating the one dimensional reference I_{sp} are given below.

The following equations were iterated using the method of secants to calculate the one dimensional reference I_{sp} for a given expansion ratio, ϵ . The three sets of equations reflect the regions of interest. These are before solidification of the condensed phase begins, during solidification, and after solidification ends. In the first and last regions, temperature was used as the independent variable, while during solidification, the ratio of the amount of solidified condensed phase to total condensed phase was used.

Before solidification begins: $\epsilon < \epsilon_m$

$$u_g = \left[\frac{2C_p}{B} (T_f - T_g) \right]^{1/2}$$

where,

$$B = \frac{1 + \dot{\omega}_p / \dot{\omega}_g}{1 + \frac{\dot{\omega}_p}{\dot{\omega}_g} \frac{C_{p,s}}{C_{p,g}}}$$

$$\epsilon = \left[\frac{\bar{\gamma} - 1}{2} \frac{T_g}{T_f - T_g} \right]^{1/2} \left[\frac{2}{\bar{\gamma} + 1} \frac{T_f}{T_g} \right]^{1/2} \frac{\bar{\gamma} + 1}{2(\bar{\gamma} - 1)}$$

During solidification: $\epsilon_m < \epsilon < \epsilon_{\text{end of solidification}}$

$$u_g = \left[u_{g_m}^2 + 2\Delta H_m \left(\frac{\dot{\omega}_p / \dot{\omega}_g}{1 + \dot{\omega}_p / \dot{\omega}_g} \right) \left(\frac{\dot{\omega}_s}{\dot{\omega}_p} \right) \right]^{1/2}$$

$$\epsilon = \epsilon_m \frac{u_{g_m}}{u_g} \exp \left(\frac{\dot{\omega}_s}{\dot{\omega}_p} \frac{\dot{\omega}_p}{\dot{\omega}_g} \frac{\Delta H_m}{R T_m} \right)$$

where,

u_{g_m} = gas velocity at beginning of solidification

ϵ_m = expansion ratio at beginning of solidification

$\dot{\omega}_s$ = weight flow of solid condensed phase

$\dot{\omega}_g$ = weight flow of the gas

$\dot{\omega}_p$ = weight flow of the total condensed phase (liquid plus solid)

T_m = melt temperature of the solid phase

After solidification: $\epsilon > \epsilon_{\text{end of solidification}}$

$$u_g = \left[u_{ges}^2 + \frac{2 C_{p,g}}{B_s} (T_m - T_g) \right]^{1/2}$$

where,

u_{ges} = gas velocity at the end of solidification

$$B_s = (1 + \dot{\omega}_p / \dot{\omega}_g) / \left(1 + \frac{\dot{\omega}_p}{\dot{\omega}_g} \frac{C_{p,s}}{C_{p,g}} \right)$$

In all regions the one-dimensional zero lag vacuum I_{sp} , I_{spIDOL} , is calculated as follows:

$$I_{spIDOL} = \frac{u_g}{32.174} \left[1 + \frac{T_g}{u_g^2} \frac{\bar{R}}{\left(1 + \frac{\dot{\omega}_p}{\dot{\omega}_g} \right)} \right]$$

The efficiency, η_{TD2P}^i , embodies only the combined two-dimensional two-phase flow effect on performance, as the TD2P and reference I_{sp} calculations are identical in all other respects. When the nozzle throat erodes, nozzle exit area ratio, and, hence, η_{TD2P}^i is time dependent. The program calculates a time averaged 2-D, 2 phase, efficiency in the manner shown in equation (3-3).

The specific impulse calculated by the TD2P program (as a function of area ratio) is also used to compute the erosion loss. While this loss could have been estimated based on one-dimensional results (using the ODE program), it was felt that a two-dimensional calculation would be superior. As defined herein, the erosion loss is equal to the ratio of the 2-D, 2-phase I_{sp} at the time averaged expansion ratio, to the specific impulse calculated at the initial expansion ratio, i.e.,

$$\eta_{erosion} = \frac{I_{spTD2P}(\bar{\epsilon})}{I_{spTD2P}(\epsilon_1)} \quad (3-44)$$

It should be noted that, here again, I_{spTD2P} values are used on a relative, rather than an absolute, basis. This efficiency is not reported separately, but is combined with the time averaged two-dimensional two phase efficiency, $\bar{\eta}_{TD2P}^i$, to yield a single value, η_{TD2P} - see equation (3-2).

In the present analysis, the fact that the two phase flow loss tends to decrease with increased throat diameter (erosion) was intentionally ignored, since it was felt that the added loss due to throat roughness would compensate for this effect.

3.6 Boundary Layer Loss Module

3.6.1 Approach

Two dimensional two phase flow solutions indicate that the bulk of the particulate matter gets channeled towards the centerline of the motor due to initial effects in the throat region of the nozzle. As a result of this phenomena gas phase only boundary layer calculations can usually be made without fear of introducing significant error due to the neglect of the particulate matter.

The usual boundary layer loss mechanisms which must be accounted for in

rocket engine performance predictions are the energy loss through the walls due to heat transfer, and the momentum loss due to shear stress at the wall. As discussed in Reference 24, these losses can either be found by properly integrating the stress tensor along the wall (pressure plus skin friction) or by calculating the momentum deficit in the boundary layer at the nozzle exit plane. The latter method is the simplest and easiest to use, and is the recommended JANNAF procedure⁽²⁵⁾. Following this procedure the boundary layer loss may be calculated as

$$\Delta F_{BL} = (2\pi r_e U_e^3 \theta \cos \alpha) \left[1 - \frac{\delta^*}{\theta} \frac{P}{\rho U_e^2} \right] \quad (3-45)$$

where r_e , ρ , U and P are the nozzle radius, density, velocity and pressure at the wall exit station, respectively, δ^* and θ are the boundary layer displacement and momentum thicknesses, and α is the angle between the slope of the nozzle contour and the centerline.

It should be pointed out that this equation gives the complete boundary layer loss. The reduction in fluid momentum due to both shear and heat transfer losses to the wall is properly accounted for.

The boundary layer edge conditions that are required in this formula are supplied by the TD2P Program. This allows the effect of two dimensional flow in the nozzle to be incorporated into the boundary layer solution. This is the same procedure as adopted by JANNAF in the liquid propellant performance methodology (i.e. the TDK - TBL interface).

The boundary layer thicknesses δ^* and θ may be calculated in several ways, categorized below in order of increasing accuracy:

- Simple correlational techniques
- Integral methods
- Finite difference and related numerical methods

The correlational techniques are normally based on semi-empirical correlations of experimental data for flat plate-zero pressure gradient-flows. In many cases the relations are based on incompressible results and are applied to compressible, variable property flows, through the use of compressibility transformations and reference temperatures (enthalpies). Normally, one of several forms of Reynolds analogy is applied to relate skin friction to heat transfer. As

a result of their simplicity, these methods have proven to be of great utility in preliminary design calculations; however, final engine design calculations are normally based on more accurate techniques.

The majority of rocket engine heat transfer and boundary layer loss calculations are currently carried out using integral methods such as the TBL program described in Reference 7. The integral methods are based upon solutions of various integral forms of the differential equations of motion. These methods give two ordinary differential equations for the momentum thickness, θ , and energy thickness, δ_T^* , (one equation for θ only, when the energy equation is replaced by the Crocco relation relating the temperature profiles to velocity, as is the case in TBL). These equations cannot be solved without additional assumptions for the form or shape factor, h^*/θ , the surface shear stress, τ_w , and heat transfer, q_w , and the boundary conditions such as wall temperature and pressure gradients.

The accuracy of integral methods is limited by the types of relations which are adopted for computing τ_w , q_w , etc. The majority of the integral methods that have been applied to rocket nozzle flows proceed on the basis of all or most of the following assumptions:

τ_w can be calculated from correlations based on zero pressure gradient flows.

q_w can be calculated using Reynolds analogy.

The shape factor, $H=h^*/\theta$, can be determined using power law velocity profiles (usually a 1/7th power is taken).

The Crocco relation can be used to calculate the temperature profiles.

Reference temperature or enthalpy methods such as Eckert's can be used to account for variable properties in the boundary layer.

All of these assumptions are violated to various degrees in variable property flows in cool wall rocket motors; however, integral methods of the above type, including TBL, give results which in many cases compare fairly well with experimental data. In the supersonic portion of the nozzle, TBL heat transfer predictions are generally within 20% of the measured values, while in the general region of the throat, discrepancies of 50% or more have been noticed⁽²⁶⁾. The large discrepancies between the integral theories of TBL type and the convergent section-throat data can be attributed to the presence of large pressure gradients in the throat region which seriously violate some of the assumptions upon which

the analysis is based, the occurrence of "laminarization" of the boundary layer due to the pressure gradients, and the sensitivity of the calculations to assumptions made about the boundary layer flow in the chamber.

While of major importance to local heat transfer calculations these discrepancies in the throat region are not serious from the standpoint of performance calculations. For most rocket motors TEL, or related integral methods, should be able to calculate boundary layer losses within about 20%. Considering that boundary layer losses are usually about 1%, and rarely exceed 2% (small motors, of short firing duration being one of the exceptions), the total impact of such a 20% error on overall performance loss should be restricted to several tenths of a percent; an amount that should prove tolerable in most cases.

There are more accurate methods available for calculating boundary layer performance loss, such as the Mass Addition Boundary Layer Program⁽²⁷⁾ and the BLIMP Program⁽²⁸⁾. These methods, are based on finite difference or other numerical solutions of the turbulent boundary layer partial differential equations. While the advances achieved in recent years allow such solutions to be achieved in reasonable amounts of computer time, the trade-off between increased accuracy and increased operational complexity (as well as run time) did not appear to favor the use of a finite difference type approach in the SPP Program. This conclusion follows from the usually restricted size of the boundary layer loss, which logically precludes a major effort to calculate it.

The previous discussion outlines why it is felt that integral methods, and TEL in particular, are adequate for the task at hand. More accurate methods such as MAEL and BLIMP are not warranted for general solid rocket motor performance prediction. However, in certain cases the increased generality of programs like these may be the only way to obtain an adequate prediction for boundary layer performance loss. If such cases can be identified, a program like MAEL can serve, not as an integral part of the performance prediction methodology, but as an addendum to it; to be used as required. On the other hand, there will be classes of motors for which data and/or correlations exist which will adequately be able to characterize the boundary layer loss. This will be especially true for the class of motors for which boundary layer losses are small. In such cases the use of any analytical boundary layer solution may be obviated.

The SPP Program has been structured to account for all of these possibilities. The TEL program was selected as the standard method for computing the boundary layer loss, and was incorporated into the program as a module. Two other methods for determining the boundary layer loss have been explicitly provided for. A simplified semi-empirical boundary layer loss correlation can, on option, be utilized in lieu of the TEL program. This correlation is described in Section 4.2.4. The boundary layer loss can also be directly input to the SPP Program. In such a case, the input value of the loss is used in deference to all others. In this manner, should the circumstances warrant it, a more exact boundary layer method may be utilized to calculate the boundary loss in an external, uncoupled, fashion. The computed value may then be input to the SPP program.

The TEL program does not allow for a direct assessment of the time dependent nature of the boundary layer loss. For motors of all but very short firing duration, this is of little consequence to the accuracy of the overall performance prediction. Since wall temperature is an input to the TEL program, the variation of the boundary layer loss with wall temperature (and therefore with time) may be evaluated by performing a series of boundary layer solutions wherein the nozzle wall temperature distribution is varied. To perform this calculation in a rational manner a thermal analyzer type, transient, heat conduction code should be externally coupled to the boundary layer solutions to provide the required wall temperature distributions.

3.6.2 Modifications to the TEL Program

Very little modification was required to implement the TEL program as a module in the SPP program. Most of the modifications were related to the incorporation of additional labeled commons to allow TEL to communicate with other modules, as appropriate. Many of the items that must normally be input to TEL are instead obtained through this linkage. For most problems, the need to specify the bulk of the remaining input items was obviated by presetting them in program data statements. Thus, very little user specified input is normally required to execute TEL as an element of the SPP performance prediction methodology.

The only other modification of substance to TEL was the incorporation of a calculation of the boundary layer induced performance loss decrement, $\Delta I_{SP_{TEL}}$.

This quantity was calculated as follows:

$$\Delta I_{SP\text{TBL}} = \frac{\Delta F_{\text{BL}}}{\dot{m}_{\text{TD2P}}} \quad (3-46)$$

where ΔF_{BL} is given by equation (3-45), and \dot{m}_{TD2P} is the nozzle mass flow rate calculated in the TD2P module.

The TBL calculation is carried out at the average chamber pressure, and the initial expansion ratio. The boundary layer loss is assumed to be independent of erosion induced effects for the present purposes.

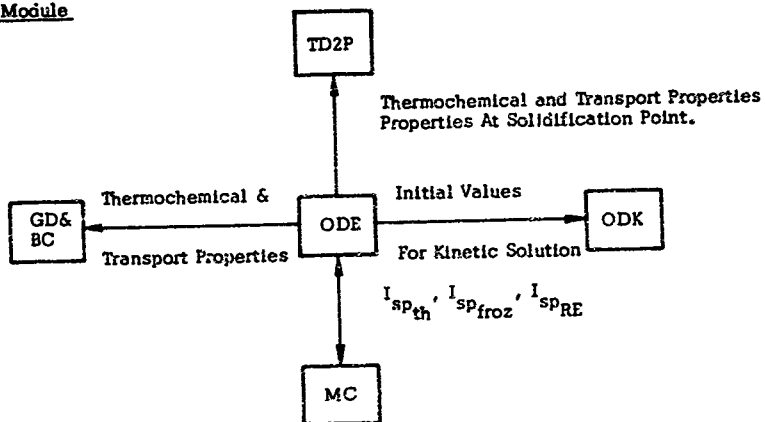
3.7 Inter-Module Interfaces

In order for the various programs contained within the SPP program to function together, automatically, the program modules must be able to communicate with each other, as required. A perfunctory description of the inter-module interfaces is given here to provide the reader with an overall idea of how the elements of the SPP program are linked together. More detailed descriptions of the program linkage structure may be found in Volumes II and III of this report.

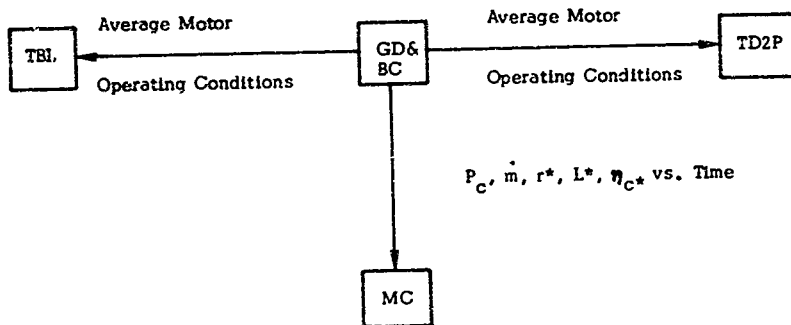
The following five simplified diagrams are designed to indicate only the nature of the information which flows out of the five basic computational modules, and its ultimate destination. In actuality, all of the inter-module communications are processed through the Master Control Module. Each block in these diagrams represents a module. The following abbreviations are used for convenience:

Master Control Module: MC
Theoretical Performance Module: ODE
Grain Design and Ballistics Module: GD&BC
Kinetics Module: ODK
Two-Dimensional Two-Phase Module: TD2P
Boundary Layer Module: TBL

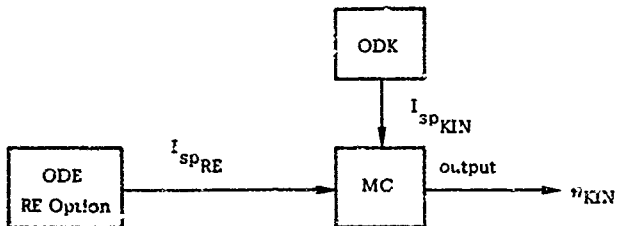
ODE Module



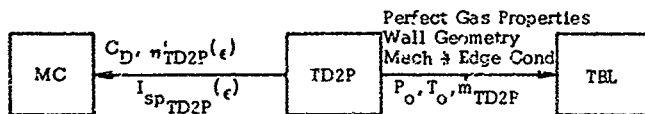
GD&BC Module



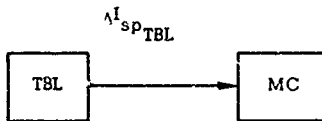
CDK Module



TD2P Module



TBL Module



4. PERFORMANCE LOSS CORRELATIONS

4.1 Combustion Efficiency

4.1-1 Approach

The combustion efficiency of aluminized solid propellants is ordinarily close to 100 percent. Departures from ideal characteristic velocity generally result from wall losses (as can exist with an exposed steel chamber in subscale test hardware), from particle lags in the throat region, and from dilution by ablatives (generally corrected out in data reduction). These three effects will be further commented upon subsequently. Exceptions to the efficient combustion of aluminum are found with low burning rate propellants, operation at low chamber pressure, and tests in combustors of exceptionally low L^* . Interest in spacecraft motors, upper-stage motors and sustainer operation has provided substantial data showing the loss of combustion efficiency at low chamber pressures and burning rates⁽¹⁴⁾.

Therefore, the correlation approach began with a theory that aluminum combustion efficiency is a function of propellant burning rate. Burning rate bears directly on those processes which influence the competition between extensive metal agglomeration and rapid metal ignition at the propellant burning surface⁽¹⁴⁾. Burning rate directly influences the combustion zone temperature gradient, the particle heating rate, and the gas velocity normal to the propellant surface. Reported effects of propellant formulation are relatable to changes in burning rate^(14, 15) as long as the oxidizer and binder provide enough energy for metal ignition (always true in aluminized propellants of practical interest, not always true for other metals). Likewise, reported effects of pressure are relatable to burning rate. The motor L^* does not appear to be important so long as it is greater than approximately 50 in., according to experiments measuring complete combustion directly⁽¹⁶⁾, the implication is that complete combustion is largely determined by what happens at or near the propellant surface. Motor C^* efficiency data were accumulated in several groups for the purpose of constructing, verifying and refining the correlation with burning rate, and finally to demonstrate the completed correlation on an a priori basis.

Statistical analysis is a useful diagnostic tool to provide insight into the nature of poorly-understood phenomena, but has proven misleading when used to generate correlations for refined predictions. The present computer program devel-

opment was predicated upon the premise that factors affecting the specific impulse efficiency of aluminized propellants are not poorly understood, and that existing theories and models can be evaluated and combined to achieve the desired accuracy. Further, statistical analysis is not warranted when the data base is insufficient compared to the potential scope of application. While the amount of BATES motor data is considerable, the fact that it is a standard motor becomes restrictive; potential governing parameters will vary together in a corresponding manner and so cannot be meaningfully separated. It is also true that the great majority of the BATES data are at a standard test condition, and cover a fairly narrow range of burning rates and aluminum concentrations. Therefore, the use of statistical analysis was limited to a supplementary role.

Data groups that were studied are listed in Table 1.

4.1.2 The Basic Correlation with Burning Rate

The basic correlation of C^* efficiency with burning rate is shown in Figure 4-1. These data consist of Groups I and II, excluding data for propellants having aluminum concentrations below 10 percent or greater than 24 percent. Each point represents an average for a series of firings of a given propellant, in a given motor, at a particular test condition. Where BATES data for a given propellant existed in groups, each group was averaged separately. It is observed that the bulk of the data exist between burning rates of 0.3-0.6 in./sec. and, within that range, the correlation is not meaningful at first glance. It is only when a broad range of burning rates are examined that the correlation appears significant.

It is observed that C^* efficiency falls rapidly below burning rates of 0.25 in./sec. This effect persists in the full-scale motors which are included in that range. Therefore, C^* efficiency is not expected to depend upon scale. The problem with the steep behavior at low burning rate is that the uncertainty in predictability becomes large in that regime. At high burning rate, the efficiency appears to approach 100 percent.

4.1.3 BATES Motor Reproducibility

The basic correlation with burning rate was examined in the light of the reproducibility of the BATES motor C^* efficiency data, particularly in view of the above-mentioned confinement of most of the data.

Table 4-1

DATA USED TO DEVELOP, REFINE AND VERIFY
 C* EFFICIENCY CORRELATION

GROUP I DATA - CONSTRUCTION OF CORRELATION

a) Propellants in 5 x 11.4 Rohm & Haas Motors

LPC-343-1401		Ref (17)
LPC-343-1402		Ref (17)
LPC-343-1403		Ref (17)
LPC-580A		Company Records
LPC-582A		
LPC-586A		
LPC-625C		
NOTS X-32		
RHP-112		
TPH-1011		
LPC-365-19AL (NAS 1-9182)		Ref (14)
NASA/Langley (NAS1-10956)		Ref (18)

b) Full-Scale Motors

ASTROBEE-F (Sustainer)	Aerojet	
AVANTI	Lockheed	Company records
ATS (End-Burner)	NASA/JPL	Ref (29)
ATS (Internal-Burner)	NASA/JPL	Ref (29)
HARPOON (Lockheed Testweight)	Lockheed	Company records
156-6	Lockheed	Ref (30)

GROUP II DATA - BATES MOTORS, VERIFICATION AND REFINEMENT¹

a) Conventional Propellants

RHP-112	LPC-543A
RHP-113	LPC-543D
RHP-161	LPC-580A
RHP-162	RDS-501
RHP-163	RDS-507
TFG-3016D	RDS-510
TPH-1085	UTP-11475
TPH-1011	C55A
TPH-1066	VBB
TPH-8163	SPIS-31
ANP-2969	SPIS-32
ANB-3066	
ANB-3105	
AAB-3318	

¹All data furnished as reduced computer output by C. Beckman, AFRL.

Table 4-1 (Continued)

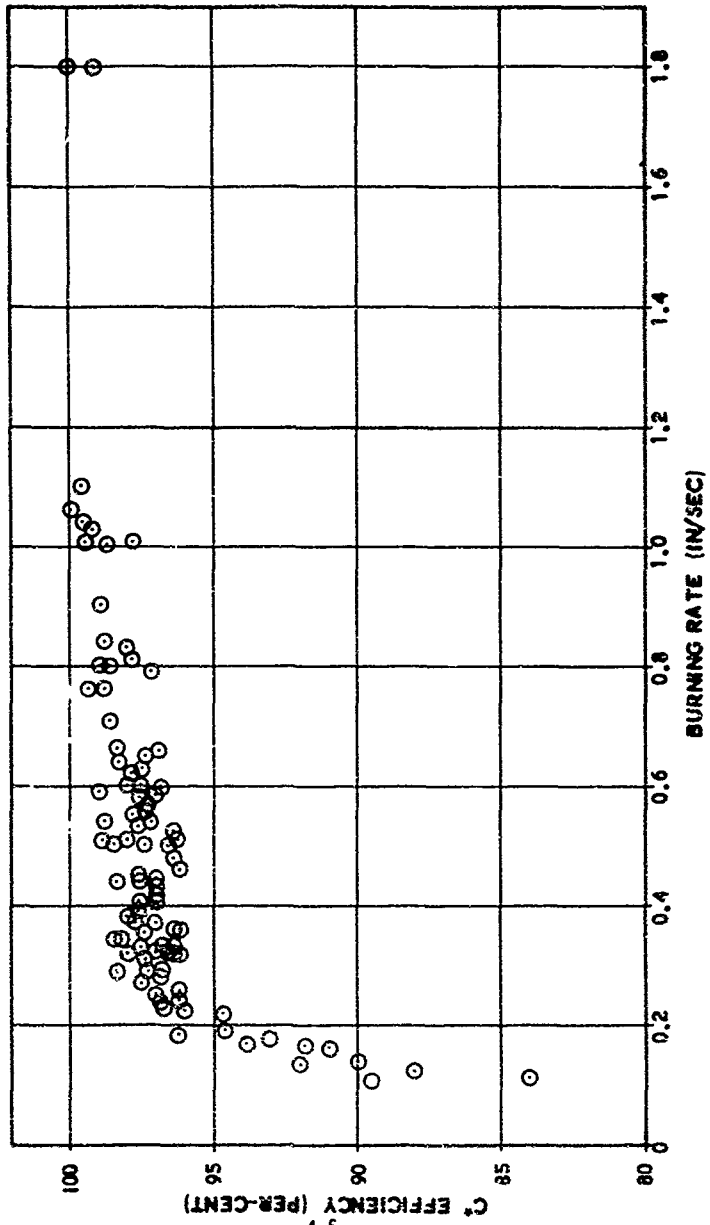
b) Advanced or Experimental Propellants

ARCHT-9015	RHU-105
ARCHT-9018	DLH-258
ARCHT-9021	ANB-3406
ARCHT-9024	ANP-3413
ARCHT-9027	ARCEF-147
ARCHT-9030	LXA-100
UTP-15908	SPIS-26
UTX-14617	SPIS-27
UTX-14682	
UTX-14631	
UTP-15151	
VLU	
VLZ-II	
VMO	

GROUP III DATA - DEMONSTRATION OF CORRELATION

2.75 FFAR	Aerojet	Ref (31)
2.75 FFAR	Hercules	Ref (32)
SRAM	Lockheed	Ref (33)
HYDAC	Lockheed	Ref (34)
HI-EX (Experimental)	Lockheed	Ref (35)
MINUTEMAN III 3rd	Aerojet	Ref (36)
FW-4S	UTC	Ref (37)
SURVEYOR RETRO	Thiokol	Ref (38)
ANTARES I	Hercules	Ref (39)
ANTARES II	Hercules	Ref (40)
SPARROW	Rocketdyne	Ref (41)
SAM-D	Thiokol	Ref (42)
SPARTAN-2nd	Thiokol	Ref (43)
156-5	Lockheed	Ref (30)

FIGURE 4-1 BASIC CORRELATION OF C EFFICIENCY WITH BURNING RATE



Within the range of burning rates 0.3-0.6 in/sec, the correlation exhibits a maximum deviation of 1.2 percent and an average deviation of 0.5 percent. All groups of BATES data were examined for reproducibility. The maximum deviation within a group was found to be as high as 2.0 percent, and the average deviation within a group was found to be as high as 1.4 percent. These results were not flash-in-the-pan. One group consisting of eight nominally identical firings exhibited an average deviation of 1.2 percent, and average deviations covering all groups were typically greater than 0.5 percent. The accumulated average deviation was 0.8 percent. Thus, the accuracy of the correlation could be said to be comparable to the reproducibility of the data. This was not particularly satisfying because unsound correlations might turn out just as good within this range of burning rates, forcing reliance on the data outside of this range to support the proposed correlation.

Some attention was devoted to the reason for the data scatter in the BATES motors. The principal uncertainty in the C^* measurement is caused by nozzle erosion; C^* requires relating the measured pressure integral with an average throat area, a factor not present in the specific impulse measurement. All other factors, including instrumentation and propellant weight, are also present in the specific impulse measurement. Average deviations in specific impulse efficiency ranged from 0.1-0.3 percent, clearly and significantly superior to the C^* error. Reported nozzle erosion rates, and throat averaging, are based upon pre-fire and post-fire measurements. They do not reveal the nature of the throat behavior in the course of the firing. A cause of variability in throat erosion behavior is the repetitive use of the same nozzle insert for economy. It was confirmed by AFRPL that this was the general practice and, within a given group of data, one can observe this taking place from the initial throat sizes. The effect is aggravated in high erosion situations. Therefore, unless this data scatter in C^* is acceptable, it would be recommended that fresh or noneroding nozzles be used on each test for improved accuracy.

The improved accuracy of the specific impulse measurement afforded an alternative opportunity to look for burning rate effects through specific impulse.

4.1.4 Effect of Burning Rate on Specific Impulse Efficiency

Additional confirmation of the effect of burning rate on performance appears in the specific impulse efficiency data, which are more accurate than the C^* efficiency

data, and, therefore, lend more credence to the effect. This is shown for Group IIA propellants in Figure 4-2. Specific impulse efficiency is plotted versus aluminum concentration, as is often done. Each datum point here is an average of an over all series of tests for each propellant. The number placed next to the datum point is the average burning rate. Note that, at each aluminum concentration, increasing burning rate increases specific impulse efficiency. This is believed to reflect C^* efficiency changes. Therefore, wide variations in burning rate can explain why specific impulse efficiency cannot cleanly be plotted versus aluminum concentration.

The darkened points in Figure 4-2 denote one type of propellant in which aluminum concentration was systematically changed, with burning rate approximately constant. All of the other ingredients are the same. Thus, the darkened points would basically reflect the expected change in nozzle efficiency with increasing aluminum concentration.

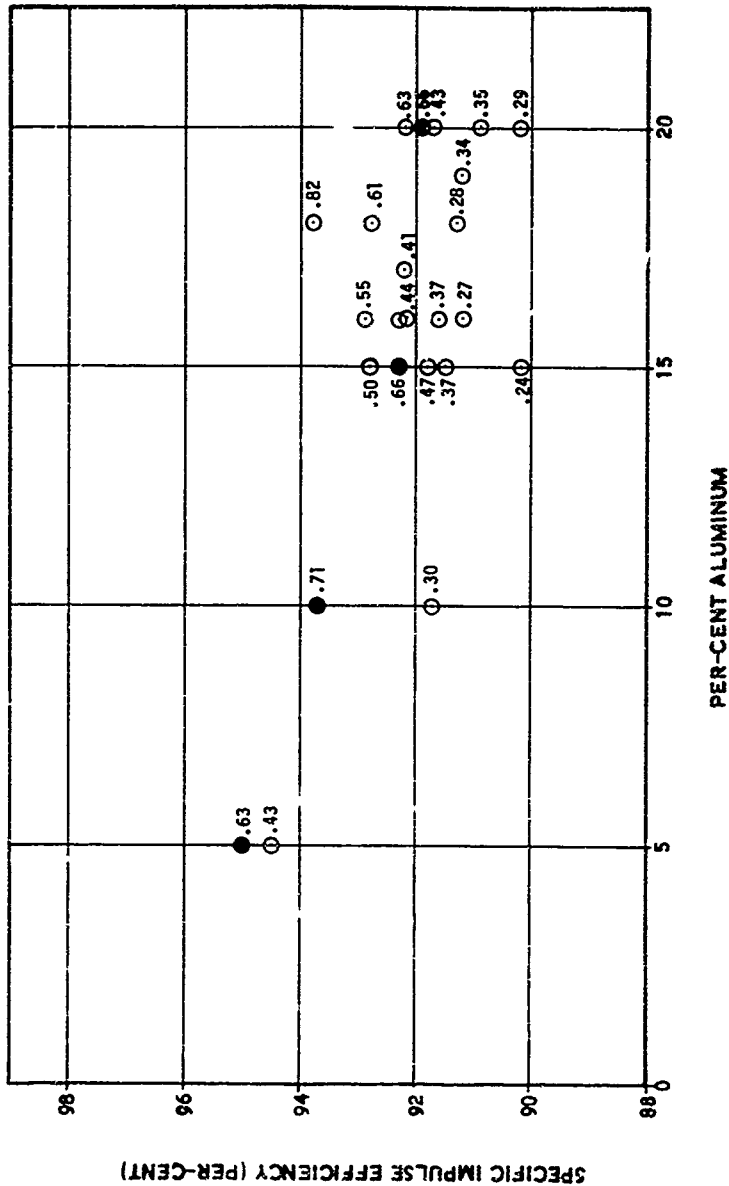
Assuming the burning rate correlation to be valid guide to C^* efficiency, the nozzle efficiency was then computed from this correlation and the specific impulse efficiency data. Results are plotted versus aluminum concentration in Figure 4-3. Note that the spread of data points is considerably less in Figure 4-3 than in Figure 4-2. This reflects normalization of the influence of burning rate.

4.1.5 Effect of Binder on Specific Impulse Efficiency

A curious oddity appears in Figure 4-3. Except for the propellant in which aluminum concentration was systematically varied, it cannot be concluded that efficiency decreases from 15 percent aluminum to 19 percent aluminum. Rather, the data indicate that efficiency is higher at 16-18 percent aluminum than at 15 percent. Upon closer examination of these conditions, it was found that the anomaly could be explained by a binder effect. Data from 15 percent to 19 percent aluminum could be systematically organized by binder, and the more efficient binders were coincidentally at the higher aluminum concentrations. Within the Group IIA propellants, the order in the direction of increasing efficiency was polyurethane, NC/NG, CTPB and HTPB, PBAA and PBAN.

This binder effect was incorporated as a correction on the correlation of C^* efficiency with burning rate. By correcting C^* efficiency for binder, the Figure

FIGURE 4-2 CORRELATION OF SPECIFIC IMPULSE EFFICIENCY WITH ALUMINUM CONCENTRATION SHOWING BURNING RATE EFFECTS



SPECIFIC IMPULSE EFFICIENCY (PER-CENT)

4-3 data should collapse into place and clearly show the expected dependence of specific impulse or nozzle efficiency on aluminum content. This is shown in Figure 4-4, which incorporates all Group II data and similar corrections for Group IIB binders.

The value of the C^* correlation in specific impulse efficiency correlation is summarized as follows:

- a) If specific impulse efficiency in BATES motors is correlated only with respect to aluminum concentration, the standard deviation is 0.8 percent and the probability of accuracy within 2 percent is 94 percent.
- b) If the burning rate correlation is taken into account, the standard deviation is 0.4 percent and the probability of accuracy within 2 percent is better than 99 percent.
- c) If both binder and burning rate effects are taken into account, the standard deviation is 0.2 percent, and the probability of accuracy within 2 percent is better than 99 percent; this is comparable to the reproducibility of the specific impulse data.

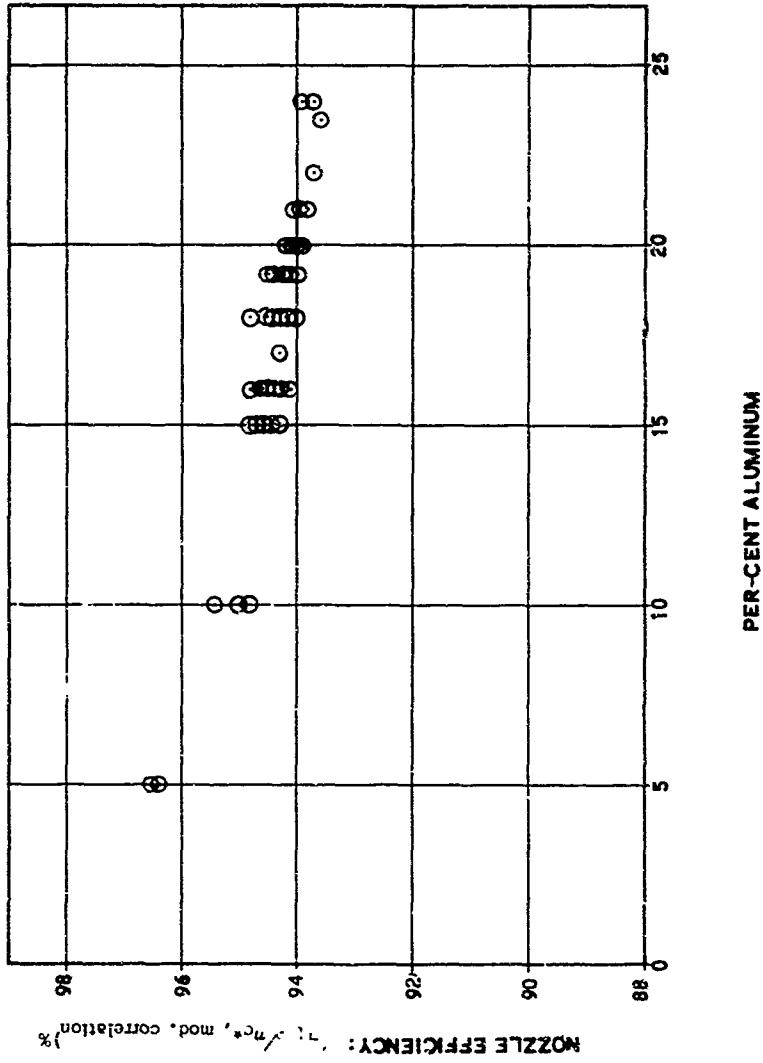
Thus, the BATES motors were successfully correlated within the limits of the data received.

4.1.6 Effects of Extremes of Aluminum Content on C^* Efficiency

The data correlations do not include propellants having aluminum concentrations in excess of 24 percent. Such propellants were tested in BATES motors as a matter of academic interest, but are too fuel-rich to be of practical interest. As might be expected, values of C^* efficiency fell below the Figure 4-1 correlation, metal agglomeration was undoubtedly extensive. On the other hand, values of nozzle efficiency increased. The increase in nozzle efficiency could be explained by a reduced total particle concentration resulting from the fuel-richness. In any event, it was concluded that should propellants, of practical interest, having high aluminum concentration ever be developed, they would probably obey the correlation. Therefore, the correlation is not modified for high aluminum content.

C^* efficiency data for low burning rate propellants having aluminum concentrations below 10 percent fell above the Figure 4-1 correlation. Aside from this fact, a correction would be warranted by the premise that combustion inefficiency

FIGURE 4-4 CORRELATION OF SPECIFIC IMPULSE EFFICIENCY WITH ALUMINUM CONCENTRATION, NORMALIZED FOR BURNING RATE AND BINDER



stems from the aluminum; therefore, some means should be afforded to approach the unmetallized propellant condition. A correction factor in the form of an equation was added to accomplish this.

4.1.7 Effect of Scale on C^* Efficiency

The C^* correlation should be unaffected by scale inasmuch as Group I data include large motors. However, there is one factor related to scale which does need to be addressed. A large motor is likely to be fully insulated, whereas a subscale test motor (including BATES motors) is likely to have exposed walls. Measurement of heat loss in BATES motors⁽⁴⁴⁾ indicates that a 1 percent loss may be assigned to the chamber. A fully insulated motor would have negligible heat loss because the thermal energy in the insulation is recovered by ablation until the last instant of the firing. Therefore, in constructing the final correlation, all subscale data were shifted upward by one percent, and a one percent loss factor was included in the correlation for an uninsulated motor.

4.1.8 Treatment of Discharge Coefficient Effect

In addition to combustion and heat losses, C^* efficiency also embodies a two phase two dimensional discharge coefficient effect. The effect of C_D on performance is calculated within the TD2P module, so the danger that a performance loss would be counted twice in the specific impulse calculation was presented. To assure that this would not happen, the following approach was taken.

The value of C^* efficiency determined from the correlation was accepted as valid, being based upon motor data. In the overall performance calculation the C_D related portion of the C^* efficiency is isolated, and removed. The remainder is a combustion efficiency factor (and heat loss). This procedure is detailed in Section 3.1. In the Grain Design and Ballistics Module the C^* efficiency is used directly in the calculation of chamber pressure.

4.1.9 Verification of Correlation

The final C^* efficiency correlation consists of a table look-up, with correction factors in equation form, and is presented in Table 4-2. A comparison with motor C^* efficiency data from Group III is presented in Table 4-3.

Table 4-2

C* EFFICIENCY FUNCTION

$$\eta_{C^*} = \left[K + \frac{10-a}{10} (100 - K) \right] \times b \times c$$

a = percent aluminum; a = a for a ≤ 10, a = 10 for a > 10

b = 1.00 for fully insulated motor, 0.990 for uninsulated motor

c = binder constant

NF, C = 1.008

PGA/NC, C = 1.008

PBAA, C = 1.006

PBAN, C = 1.006

HTPB, C = 1.003

CTPB, C = 1.000

NC, C = 0.998

PU, C = 0.992

K = burning rate constant

<u>r</u>	<u>k</u>	<u>r</u>	<u>k</u>
0.11	91.4	0.50	98.6
0.12	93.1	0.60	98.9
0.13	94.0	0.70	99.1
0.14	94.6	0.80	99.2
0.15	95.1	0.90	99.3
0.16	95.6	1.00	99.4
0.17	96.0	1.20	99.6
0.18	96.4	1.40	99.7
0.19	96.7	1.60	99.8
0.20	97.0	1.80	99.9
0.30	97.7	≥ 2.00	100.0
0.40	98.2		

If $\eta_{C^*} > 100.0$, $\eta_{C^*} = 100.0$

Table 4-3

PREDICTABILITY OF PRODUCTION MOTOR C* EFFICIENCY FOR MOTORS NCT
USED IN DEVELOPING THE METHOD

	<u>MOTOR C* EFFICIENCY</u>	<u>PREDICTED C* EFFICIENCY</u>	<u>DEVIATION</u>
2.75 FPAR (HFC)	100	99.8	-0.2
2.75 FPAR (AGC)	98.9	98.8	-0.1
SRAM	99.4	100.0	+0.6
HYDAC	98.9	98.4	-0.5
III-LX	98.0	97.8	-0.2
MINUTEMAN III-3	98.2	97.9	-0.3
FW-4S	96.7	97.0	+0.3
SURVEYOR RETRO	97.1	97.5	+0.4
ANTARES I	99.1	99.0	-0.1
ANTARES II	97.2	97.5	+0.3
SPARROW	98.2	99.1	+0.9
SAM-D	97.6	97.5	-0.1
SPARTAN-2	99.0	99.2	+0.2
156-5	99.0	99.6	+0.6

RANGE OF VARIABILITY = 3.3

AVERAGE DEVIATION = 0.4

Group III motors were selected because of certain features bearing upon specific impulse predictability. In the C* context, they also afford a wide range of burning rates, aluminum concentrations and binder types. The range of variability of 3.3 percent in C* efficiency provides a reasonable basis for testing the method; clearly, the test has little meaning if the range is comparable to the accuracy.

It is observed that the average deviation of the predictions is 0.4 percent. Although the predictions are uniformly distributed between high and low values, the overpredictions tend to be larger in magnitude. This would be consistent with the uncertainty of accounting for insulation dilution in the actual data. Insulation dilution was not considered in these predictions (this effect is discussed in Section 5.3). Because these motors were not used in developing the correlation, and the accuracy is a small fraction of the range of variability, it is concluded that the Table 4-2 correlation is satisfactory.

4.2 Specific Impulse Efficiency

4.2.1 Approach

The development of simple expressions for each source of specific impulse loss affords a means for the rapid and convenient assessment of motor delivered performance. Such expressions therefore provide an important and useful supplement to the analytical computer program subroutines which deal with these losses in a more exact and detailed manner.

In order to enhance the scope of applicability of the simplified method, a semi-analytical rather than statistical correlative approach was adopted. The disadvantages of the statistical approach were discussed in the context of combustion efficiency correlations. In correlating specific impulse efficiency, there is the added consideration that it is a function of numerous, interrelated processes. Depending upon the propellant and the motor design, different physical mechanisms may dominate the loss. Therefore, correlations of delivered specific impulse or total nozzle efficiency in terms of aluminum concentration and scale parameters will be deficient to the extent that the individual loss components do not vary systematically with these variables. An approach that addresses the individual loss components is preferred, and a semi-analytical approach is better able to do so.

The resulting expressions were derived from analytical or semi-empirical expressions appearing in the literature, or by fitting the results of the analytical computer programs used in the SPP program. A group of motors was selected that would serve to highlight various loss components, and furnish a basis for their verification. The final expressions were compared to the measured total loss for all of these motors.

The motors selected for this exercise, and the reasons for their selection, are listed in Table 4-4. These motors represent extremes of the motor design variables that influence delivered performance. The nozzle efficiencies of the production motors are plotted versus aluminum concentration in Figure 4-5, and are compared to the Figure 4-4 BATES correlation. It is observed that there is no correlation with aluminum content. It is also interesting to note that most of the production motors deliver lower performance than the BATES motor even though most are larger. Therefore, factors other than aluminum content, or size per se, must be important. These factors do not vary appreciably in BATES motors used as a standard propellant reference, but must be considered in predicting motor performance in general. The factors which distinguish production motors are contained within the expressions for the loss components.

The semi-empirical efficiencies described in Sections 4.2.2 through 4.2.7 are in terms of per cent nozzle thrust coefficient, C_p , losses instead of fractional I_{sp} efficiencies.

4.2.2 Divergence Loss

The simple half-angle correction, modified for contoured nozzles⁽¹⁾, is employed. Thus, the details of the source flow from the throat region, and the coupling of the two-dimensional particle lags, are not taken into account here. This is a potential source of error in the simplified analysis. There is insufficient information to isolate these coupled effects, either experimentally, or from parametric TD2P solutions, to create a justifiable simplified expression. One difficulty in performing a parametric analysis is that the full shape of the nozzle has an important influence on the coupling of the two-dimensional and two-phase flow effects.

The expression used for divergence loss is as follows:

$$\eta_{DIV} = 50 \left[1 - \cos \left(\frac{\alpha + \theta_{EX}}{2} \right) \right] \quad (4-1)$$

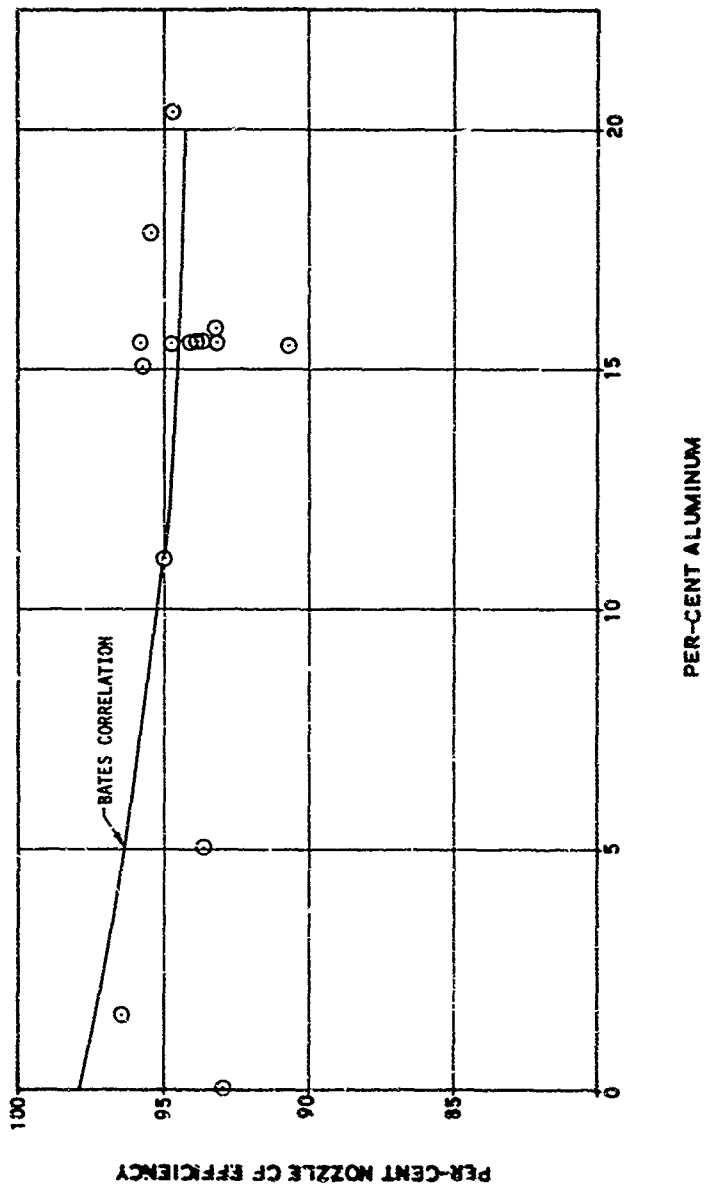
α = half angle of conical nozzle, included angle of contoured nozzle
 θ_{EX} = exit angle of conical nozzle

Table 4-4

SELECTED MOTOR FOR VERIFICATION OF SIMPLIFIED LOSS EXPRESSIONS

STAR (Aeroflot)	Smallest motor with aluminumized propellant; multiple nozzles with narrow divergence and smallest throats; high chamber pressure, highest nozzle erosion rate; short burn time; low L^* .
STAR (Hercules)	Smallest motor with unmetallized propellant; multiple steel nozzles with narrowest divergence and lowest expansion ratio; shortest burn time.
RAM	End-burner with large L^* and small physical nozzle; highest chamber pressure and burning rate; contoured nozzle with narrow divergence.
RAM	Small L^* for a motor of its physical size.
HI EX	Systematic variation of expansion ratio to highest values; low chamber pressure and burning rate; lowest nozzle erosion rate; long burn time.
MIN. THERMAL EFFICIENCY	Contoured nozzle with wide divergence and deep submergence to high expansion ratio; noneroding throat; long burn time; large L^* .
MIN. WEIGHT	Conical nozzle with highest divergence to high expansion ratio; low burning rate.
MIN. SIZE	Spherical motor; conical nozzle with deepest submergence to high expansion ratio.
MIN. WEIGHT AND SIZE	Largest motor with low aluminum propellant; lowest chamber pressure and burning rate for low aluminum propellant; highest expansion ratio for low aluminum propellant.
MIN. WEIGHT AND SIZE	Highest aluminum content propellant.
MIN. WEIGHT AND SIZE	Low aluminum content propellant; conical nozzle with wide divergence and low expansion ratio.
MIN. WEIGHT AND SIZE	Intermediate aluminum content propellant; conical nozzle with narrow divergence; high chamber pressure.
MIN. WEIGHT AND SIZE	Largest motor at high chamber pressure; contoured nozzle with widest divergence.
MIN. WEIGHT AND SIZE	Largest motor, L^* and throat size; long duration; high aluminum content propellant; low expansion ratio.
MIN. WEIGHT AND SIZE	Selected data showing effects of aluminum content.
MIN. WEIGHT AND SIZE	Selected data showing effects of aluminum content and advanced binders.

FIGURE 4-5 ABSENCE OF PRODUCTION MOTOR PERFORMANCE CORRELATION
WITH ALUMINUM CONTENT OR SCALE



4.2.3 Kinetics Loss

The kinetics loss expression originally proposed simply stated that this loss is 1/3 of the difference between theoretical shifting and theoretical frozen performance at the particular expansion ratio. It came from a study of various propulsion systems, including liquid engines and fluorinated propellants under conditions that would emphasize this loss⁽⁴⁵⁾. However, subsequent comparison with results of the kinetics calculations from the ODK program indicated that a pressure correction should be provided to reduce the predicted loss at higher pressures. The final form of the kinetics loss expression is therefore:

$$\eta_{KIN} = 33.3 \left[1 - \frac{\text{theoretical frozen Isp}}{\text{theoretical shifting Isp}} \right] \cdot \left(\frac{200}{P} \right)_{P > 200 \text{psi}} \quad (4-2)$$

A thermochemical calculation is necessary to exercise this expression, and care should be taken that the frozen result is for the same expansion ratio as the shifting result (some computer programs furnish optimum results at different expansion ratios). The difference between shifting and frozen performance will vary with propellant chemistry, pressure and expansion ratio.

4.2.4 Boundary Layer Loss

Boundary layer loss is expressed in the form of a time-dependent heat transfer expression, with a correction term for nozzle expansion ratio:

$$\eta_{BI} = C_1 \frac{P^{0.8}}{D_t^{0.2}} \left[1 + 2 \exp(-C_2 P^{0.8} t / D_t^{0.2}) \right] \left[1 + 0.016 (\epsilon - 9) \right] \quad (4-3)$$

P = pressure, psi

D_t = throat diameter, in

t = time, sec

ε = expansion ratio

Ordinary Nozzle : C₁ = 0.00365
 C₂ = 0.000937

Steel Nozzle: C₁ = 0.00506
 C₂ = 0

The time-dependence is in exponential form to represent transient heat-up. Wall heating with time is an important factor to consider in motors of short burn time (e.g., less than 4 seconds). The heat transfer variables are combined in the well-known form for pipe flow. The dependence on expansion ratio represents the effect of increased nozzle surface area.

The bracket term containing the time-dependence states that the heat transfer with a cold nozzle ($t=0$) will be a factor of 3 greater than with a fully heated nozzle ($t \rightarrow \infty$). This factor comes from comparing a typical equilibrium wall temperature-gas temperature difference with the difference between ambient temperature and the gas temperature. It is consistent with the differences between hot wall and cold wall heat losses derived from computer calculations, and plotted in Ref. 1. The time constant (C_2) comes from an analysis of the transient heating of a standard BATES motor. The coefficient (C_1) was judiciously selected based upon a study of the following: a direct measurement of heat loss in a BATES motor (Ref. 44); computer calculations of boundary layer loss (Ref. 1); measurement and analysis of nozzle heat transfer coefficients (Refs. 46, 47); deductions of the boundary layer losses in standard 3KS and 16KS motors by knowing the total measured loss with unmetallized propellant (Ref. 48, 49) and assuming that divergence loss and kinetics loss are correctly described by the equations above.

The constant preceding the expansion ratio term was deduced from the HI-EX motors as follows. The motor data revealed a decrease in nozzle efficiency with increased expansion ratio. A series of TD2P calculations provided results showing an increase in nozzle efficiency (decrease in 2-D lag losses) at high and increasing expansion ratios*. Assuming the expression for kinetics loss to be correct, the remainder was assigned to differences in boundary layer loss with expansion ratio.

A second set of constants is provided for a "steel nozzle," which is primarily addressed to the Hercules 2.75 motor. These constants assume a constant cold wall ($C_2=0$), and a higher temperature potential (higher C_1). They should be limited to a motor employing a solid steel nozzle of relatively thick walls.

*An important practical application of this result is that propellants of higher metal content and total solids may be considered for high expansion ratio than the optimum at low or standard expansion ratios.

4.2.5 Two-Phase Flow Loss

The expression for two-phase flow loss is more complicated, attempting to take into account different regimes of concentration effects and interdependencies of particle size and throat size effects. The form of the expression and the values of the various constants were obtained by fitting detailed solutions appearing in References 1, 50-52, and from parametric TD2P solutions obtained during the present effort.

The two-phase flow loss is given by:

$$n_{TP} = C_3 \frac{\xi C_4 D_P^{C_5}}{P^{0.15} \epsilon^{0.08} D_t C_6} \quad (4-4)$$

ξ = mole fraction of condensed phase, moles/100 gm

D_P = particle size, μ

P = pressure, psi

ϵ = expansion ratio

D_t = throat diameter, in.

If $\xi \geq 0.09$, $C_4 = 0.5$

$D_t < 1$: $C_3 = 9.0$, $C_5 = 1.0$, $C_6 = 1.0$

$1 < D_t < 2$: $C_3 = 9.0$, $C_5 = 1.0$, $C_6 = 0.8$

$D_t > 2$ and $D_P < 4$: $C_3 = 13.4$, $C_5 = 0.8$, $C_6 = 0.8$

$4 \leq D_P \leq 8$: $C_3 = 10.2$, $C_5 = 0.8$, $C_6 = 0.4$

$D_P > 8$: $C_3 = 7.58$, $C_5 = 0.8$, $C_6 = 0.33$

If $\xi < 0.09$, $C_4 = 1.0$

$D_t < 1$: $C_3 = 30.0$, $C_5 = 1.0$, $C_6 = 1.0$

$1 \leq D_t \leq 2$: $C_3 = 30.0$, $C_5 = 1.0$, $C_6 = 0.8$

$D_t > 2$ and $D_P < 4$: $C_3 = 44.5$, $C_5 = 0.8$, $C_6 = 0.8$

$4 \leq D_P \leq 8$: $C_3 = 34.0$, $C_5 = 0.8$, $C_6 = 0.4$

$D_P > 8$: $C_3 = 25.2$, $C_5 = 0.8$, $C_6 = 0.33$

$$D_P = 0.454 P^{1/3} \xi^{1/3} \left[1 - \exp(-0.004L^*) \right] \left[1 + 0.045L_t \right] \quad (4-5)$$

L^* = motor characteristic length, in.

The expression branches first as a function of exhaust condensibles. It then branches as a function of throat diameter, and then with particle diameter, for large throat diameters. In general, the dependencies upon particle size and throat size increase as these quantities get smaller. There is a slight dependence upon expansion ratio. Effects of pressure, exhaust condensibles, throat size and particle size are coupled, in that particle size is a function of the other three; the result is that the loss will increase slightly with pressure, strongly with exhaust condensibles, and go through some optimum respecting throat size.

The expression for particle size combines theories of particle growth by condensation in the chamber and collisions in the nozzle, as discussed in Sec. 5.4.

4.2.6 Submergence Loss

The expression for submergence loss is in the form suggested by Kordig and Fuller (53), with constants modified based upon the data appearing in Ref. (1).

$$\eta_{SUB} = 0.0584 \left(\frac{P\xi}{A^*} \right)^{0.8} \frac{S^{0.4}}{D_t^{0.2}} \quad (4-6)$$

P = pressure, psi

ξ = mole fraction of condensed phase, moles/100 gm

A* = nozzle entrance area/nozzle throat area

S = length of submergence/length of internal motor

D_t = throat diameter, in.

4.2.7 Losses Not Considered

Expressions were not included for the following: flow separation in highly over-expanded nozzles; shock losses stemming from rough nozzle surfaces caused by nonuniform erosion or spalling, expansion ratio losses stemming from erosion or nonoptimum expansion by design. The last item is not really a loss, and may be accommodated by comparing predicted and measured performance at the actual average expansion ratio. It has significance in a priori prediction where the actual throat erosion is not known. Analyses of shock losses and nonuniform erosion are not yet well-developed for a priori prediction. Separation requires considerable over-expansion, not likely except during portions of ignition and tail-off which are generally inconsequential among the total impulse.

4.2.8 Verification of Simplified Loss Predictions

Results of applying the simplified methodology to the selected group of motors are listed in Table 4-5. The simplified performance predictions were obtained in the following manner. The individual nozzle loss per cent efficiencies given by equations (4-1) to (4-4), and (4-5) were combined to yield an overall nozzle C_F efficiency,

$$\eta_{CF} = 100 - (\eta_{BL} + \eta_{DIV} + \eta_{KIN} + \eta_{SUB} + \eta_{TP}) \quad (4-7)$$

In performing this calculation average values for pressure, expansion ratio and L^* had to be estimated. Particle size was obtained from equation (4-5). A C^* efficiency was obtained from Table 4-2, and combined with the C_F efficiency to yield an overall delivered i_{sp} efficiency,

$$\eta_{i_{sp}} = \eta_{C^*} \eta_{CF} \quad (4-8)$$

The measured values of i_{sp} efficiency were obtained by dividing the measured delivered specific impulse (delivered to ambient pressure) by the theoretical specific impulse (at ambient back pressure) calculated at the estimated average expansion ratio.

It is observed that all predictions are within 1.5 percent of data, and that the average deviation is 0.5 percent over a range of variability of 5.9 percent. The overpredictions and underpredictions of efficiency appear to be equally distributed in number, but the overpredictions tend to be greater in magnitude.

The BATES motor results are added to the production motor results in order to comment upon the performance of NF propellants relative to standard propellants. These results indicate that the superior performance of the NF propellants in BATES motors was an artifact of the particular propellants and the BATES motor. The NF propellants were of substantially higher burning rate, improving C^* efficiency in addition to the inherent improvement from the binder itself. The higher burning rate necessitated a larger throat size, which in itself improved the nozzle efficiency 1 percent due to lower two-phase flow losses. Thus, the indicated 2 percent improvement would not be predicted to be maintained in a full-scale motor where burn rate and throat size would be fixed by design. The inherent improvement in combustion efficiency could also be compromised by an increased kinetics loss with fluorine at high expansion ratios.

Table 4-5
SUMMARY OF SIMPLIFIED LOSS PREDICTIONS

	<u>"HL</u>	<u>"DIV</u>	<u>"KAN</u>	<u>"SUB</u>	<u>"TIP</u>	<u>"QF</u>	<u>"C*</u>	<u>"ISP</u>	<u>Measured</u>	<u>Error</u>
A Bates	1.5	1.7	0.2	0	2.1	94.5	98.1	92.7	92.7	0
B Bates	2.0	1.7	0.2	0	2.0	94.1	98.1	92.3	92.3	0
A Bates (NF)	1.7	1.7	0.2	0	1.2	95.0	99.5	94.8	94.9	-0.1
B Bates (NF)	2.0	1.7	0.2	0	1.0	95.0	99.5	94.5	94.2	+0.3
SRHM	1.3	0.3	0.1	0	3.3	95.0	100.0	95.0	94.0	+1.0
156-5	0.3	2.3	0.2	0.4	2.4	94.4	99.6	94.0	94.4	-0.4
H ¹	1.1	2.1	0.2	0	2.2	94.2	98.4	92.7	92.8	-0.1
H ²	0.6	1.7	0.0	0	2.6	94.4	97.8	92.3	93.0	-0.7
(r=150)	1.3	1.7	0.9	0	2.3	93.8	97.8	91.7	92.1	-0.4
(r=300)	1.9	1.7	1.1	0	2.2	93.1	97.8	91.1	91.5	-0.4
2.75 (ASPC)	3.6	1.0	0.1	0	4.8	90.5	98.8	89.4	89.6	-0.2
2.75 (HI)	4.9	0.8	0.2	0	0	94.2	99.0	94.0	93.0	+1.0
MM III, 3	0.5	2.2	0.5	0.8	1.1	95.0	97.9	93.0	94.0	-1.0
FW-48	0.9	3.0	0.6	0.5	2.4	92.6	97.0	89.8	90.0	-0.2
Surveyor	0.8	1.7	0.8	0.8	1.8	94.1	97.5	91.8	91.2	+0.6
Antares I	0.4	1.7	0.3	0	0.3	97.3	99.0	96.3	95.5	+0.8
Antares II	0.4	1.7	0.5	0	1.4	95.9	97.5	93.5	92.0	+1.5
Sparrow	2.3	2.6	0.4	0	0.9	94.0	99.1	93.1	91.9	+1.2
SAM P	1.1	0.9	0.2	0	1.7	96.1	97.5	93.7	92.7	+1.0
Spartan, 2	0.9	3.0	0.3	0	2.1	93.7	99.2	93.0	92.9	+0.1

Range of variability = 5.9%
Average deviation = 0.5%

5. OTHER CONSIDERATIONS

5.1 Burning Rate

5.1.1 Approach

Motor burning rates cannot, as yet, be predicted on a strictly a priori basis. Therefore, burning rate predictions must be based on experimentally measured strand burning rates for the propellant of interest. The problem of calculating motor burning rate then reduces to accounting for the factors which cause it to differ from the strand burning rate.

At a given set of conditions (i.e. pressure, temperature) strand burning rate is a constant. Motor burning rates are design dependent, however, being a function of the local convective and radiative heating at the burning surface^(13,16). The differences between motor burning rates and strand burning rates are often large enough to impact pressure and thrust to a greater extent than the desired tolerance level of five percent; hence, these differences must be accounted for. The sophistication of the analysis used to convert strand data to motor burn rate is dictated by a compromise between accuracy and the information readily available for an a priori calculation.

One of the more comprehensive coupled analyses of motor burning rate appears in Reference 13. That analysis was constructed for the special purposes of predicting ignition delay, ignition spikes, the success or failure of command termination, and delivered impulse during transient start-up and shut-down in multiple stop-restart operation. For those purposes, a comprehensive combustion and energy exchange analysis was required, including an in depth heat transfer solution for the solid phase. The accurate prediction of steady-state ballistics followed as a by-product of the accurate prediction of transient ballistics. The disadvantages of this analysis are its complexity, size and run time. The run time and size, with a limited number of axial increments, are comparable to goals established for the entire Grain Design and Ballistics Module; coupling it to the much finer grid required by the grain design solution was considered impractical for a priori predictions. Therefore, the use of this analysis should be limited to the detailed study of transient ballistics for which it was created. The present program is chiefly concerned with steady or quasi-steady ballistics.

The approach that was taken was to construct a closed-form expression consisting of an erosive term, a radiation term, and a transient term:

$$r = r_0 (1 + \Delta r) (1 + r') \quad (5-1)$$

r_0 = strand rate, in./sec.

Δr = steady-state corrections

r' = transient correction

5.1.2 Erosive Burning

An extensive review of erosive burning was performed by LPC in association with the development of a computer program to predict the ballistics of nozzleless rocket motors^(9,54). All of the erosive burning laws were found to be deficient in some respect, but the best and most comprehensive equation appears to be that of Lenoir and Robillard:

$$\Delta r = \frac{c_1 G^{0.8}}{x^{0.2}} \exp\left(-\frac{c_2 \rho_s r}{G}\right) \quad (5-2)$$

c_1, c_2 = constants

G = local port mass flux, lb/in²-sec.

x = local axial position, in.

ρ_s = propellant density, lb/in³.

In this work, the r appearing in the exponential was changed to r_0 to remove the iterative step; it is a minor correction, within the uncertainty in the values of c_1 and c_2 . The dimensionless c_2 was left at 53 per Lenoir-Robillard. The constant c_1 may be expressed in analytical form, but then includes other constants of more or less uncertainty. The value of this constant was therefore established from selected motor data wherein erosive burning would be expected to be significant: 0.0068 in in⁻⁶-pound⁻⁸-second⁻⁸ units.

5.1.3 Radiation Contributions

Radiation can be a significant source of combustion augmentation in large motors⁽¹³⁾. In the case of unmetallized propellant, radiation will be imparted by hot nozzle and insulation surfaces as well as by the hot gases flowing inside the motor. In the case of metallized propellant, the particle-gas cloud shields the propellant from the hot nozzle and insulation surfaces but is itself a source of significant radiation heating.

Radiation contributions to motor burning rate have been studied using the sophisticated transient analysis computer programs of reference (13) which dealt with motors containing unaluminized propellant and Reference (55) dealt with motors containing aluminized propellant. Closed form expressions are constructed as ratios of radiation flux to combustion flux: a) in the case of unaluminized propellant,

$$\Delta r = \frac{\sigma}{1.8 \rho_s C_{sO} r_o T_F} \left\{ 0.1 \left[(0.125 T_F^4 - T_S^4) (A_I/A_B) + (0.410 T_F^4 - T_S^4) (A_N/A_B) \right] + \left[1 - \exp(-\lambda P) \right] (T_F^4 - T_S^4) \right\} \quad (5-3)$$

b) in the case of aluminized propellant

$$\Delta r = \sigma \frac{[1 - \exp(-\lambda P)] (T_F^4 - T_S^4)}{1.8 \rho_s C_{sO} r_o T_F} \quad (5-4)$$

where:

- σ = Stefan-Boltzmann constant, $3.52 \times 10^{-14} \frac{\text{BTU}}{\text{in.}^2 \text{-sec.}^{\circ} \text{K}^4}$
- 0.1 = average view factor from walls, based on Ref. (13) computations
- T_F = thermochemical flame temperature, $^{\circ}\text{K}$
- T_S = propellant surface temperature, $^{\circ}\text{K}$ =850 for AP composite propellants, 523 for double-base propellants
- 0.125 = fourth power of ratio of insulation wall temperature to propellant flame temperature, taken from typical Ref (13) output
- A_I = exposed insulation area, in.^2
- A_B = propellant burn surface area, in.^2
- A_N = projected annular nozzle area, radiating surface, in.^2
- 0.410 = nozzle analogy to 0.125 above
- λ = emissivity, $(\text{lb./in.}^2)^{-1}$
- P = pressure, lb/in.^2
- C_s = propellant heat capacity, $\frac{\text{BTU}}{\text{lb}^{\circ}\text{R}}$
- 1.8 = conversion factor

and

$$\lambda = \left[0.001 + 0.04 (\text{Percent Aluminum})/100 \right] / 14.69 \quad (5-5)$$

from Reference (55).

Results obtained for motors wherein the radiation contribution was significant indicates that equations (5-3) and (5-4) yield good results, without having to apply any additional "correction factors".

5.1.4 Transient Term

Effects of \dot{P} on instantaneous burning rate were approximated using the expression derived by Paul and Von Elbe:

$$r' = \frac{n\alpha\dot{P}}{2r_o^2 P} \quad (5-6)$$

n = pressure

α = thermal diffusivity, in²/sec

P = rate of change of pressure

5.1.5 Other Effects

Effects of acceleration on burning rate, brought about by spin-stabilization of motors, were not included in the program. If desired, such effects can be incorporated at a later date.

Burning rate augmentation along bondlines has been encountered in certain motors. The phenomenon has been attributed to propellant nonuniformity. No attempt was made to account for it because it is to be avoided in the future.

Recent analyses have begun to address two-dimensional erosive burning. In these analyses burn rate differences between the tips and valleys of stars and keyhole slots are accounted for in addition to longitudinal differences. Although progress along these lines is encouraging, the incorporation of two-dimensional erosive burning into the program would have required further new developments, and, therefore, was beyond the scope of the present effort.

Conditioning temperature is accounted for through program input, i.e., the input strand burning rates should correspond to the conditioning temperature of interest.

5.1.6 Strand Data as Input

In recognition of the fact that the burning rate pressure exponent, n , is not a constant, and that conditioning temperature effects vary with pressure and temperature, it was decided to input strand burning rate data in tabular form. Logarithmic interpolation is used within this table.

5.2 Nozzle Throat Erosion

5.2.1 Approach

Changes in nozzle throat area with time mainly impact the chamber pressure. Thrust and specific impulse will be affected to a lesser extent, but the effect can become significant if the throat area changes appreciably.

Because nozzle erosion is a time-dependent athermochemical effect, it is not sufficient to correlate erosion by steady-state heat transfer, parameters which would include pressure, throat size and temperature. The time-dependence of nozzle heating rates must be accounted for, particularly for short burn time. A parameter related to the oxidation potential of the combustion products is also required. Combustion of contemporary propellant formulations produces exhaust gases which contain several chemical species that are reactive with the free carbon contained in throat materials. It follows that these additional considerations will vary with the formulation of the propellant and the type of throat material.

The prediction of erosion rates in carbonaceous and graphitic throat materials has been the subject of several computer program developments combining chemical kinetic theory and heat transfer. These efforts are very sophisticated and include experimental work as well as theoretical analysis. However, when applied to motor firings, accuracies could not confidently be expected to be better than 30 percent without a posteriori adjustment of constants.

According to the original program plan the nozzle erosion rate was to be specified by means of a user determined input table. During the development of the computer program it was agreed that provision for some means of calculating the erosion rate would be desirable, since not all potential users could be expected to have the capability to independently determine it. Rather than burden the SPP program with additional complexity, it was decided to incorporate an erosion rate capability on a semi-empirical basis. Towards this end, the CMA⁽⁵⁶⁾ and ASTHMA⁽⁵⁷⁾ computer programs were run for a matrix of conditions consisting of two propellants (zero aluminum and 16 percent aluminum), three pressures (500 psi, 1000 psi, 2000 psi), and three materials (carbon phenolic, ATJ graphite and pyrolytic graphite). For each material the calculated erosion rates were fit as a tabulated function of temperature and parameters characterizing heat transfer and combustion products. Temperature, in turn, is derived from the propellant flame temperature and a time-

dependent heat transfer expression. Final adjustment of constants followed application to motors representing each material. The exact nature of the erosion rate as a function of time has been retained. Thus, when warranted, the present correlations may be overridden by data, or the results of another analysis, deemed more appropriate for the problem at hand.

5.2.2 Form of the Nozzle Erosion Correlation

Nozzle erosion rate was correlated in the following form:

$$\dot{r}_t = \frac{12}{\rho_m} \beta'_c C_H \quad (5-7)$$

where C_H is a time dependent film coefficient having the form,

$$C_H = \frac{c_3/c_p}{D_t^{0.2}} \left(\frac{\dot{m}}{A_t} \right)^{0.8} \frac{\kappa}{\mu} \quad (5-8)$$

- c_3 = a constant, including conversion factors
- D_t = throat diameter, in.
- \dot{m} = propellant weight flow rate, lb/sec
- A_t = throat area in²
- κ = gas thermal conductivity, BTU/in.-sec.-°R
- μ = gas viscosity, lb/in.-sec
- c_p = gas heat capacity, ft²/R
- \dot{r}_t = erosion rate, in./sec
- ρ_m = material density, lb/ft³
- β'_c = dimensionless erosion rate parameter
- C_H = heat transfer parameter, lb/ft²-sec
- 12 = conversion factor

For each of the three materials considered, equation (5-7) yields the relation,

$$\dot{r}_t = 0.173 \beta'_c C_H \quad \text{Carbon Phenolic} \quad (5-9)$$

$$\dot{r}_t = 0.109 \beta'_c C_H \quad \text{A7 Graphite} \quad (5-10)$$

$$\dot{r}_t = 0.086 \beta'_c C_H \quad \text{Pyrolytic Graphite} \quad (5-11)$$

The Aerotherm computer programs (56,57) calculate β'_C as a function of wall temperature, for a given propellant and material. The results were found to be dependent on temperature and the corrosivity of the propellant combustion products, but were essentially independent of pressure. Thus, the erosion parameter β'_C , was correlated in the following form,

$$\beta'_C = c_4(T) f(\beta) \quad (5-12)$$

where $c_4(T)$ is a tabular function of temperature, and $f(\beta)$ is a function of the propellant products corrosivity parameter, β . The temperature in equation (5-12) should be wall temperature, however, wall temperature was converted to flame temperature by assuming the equilibrium wall temperature to be 70 percent of the flame temperature. The flame temperature is obtained from a thermochemical equilibrium solution (ODE program). The time dependence of the wall temperature, expressed as a flame temperature, is obtained from a standard form of transient heat flux expression:

$$T_g = T_o + (T_F - T_o) \left\{ 1 - \exp \left[-c_5 \left(\frac{\dot{m}}{A_t} \right)^{0.8} t \right] \right\} \quad (5-13)$$

At time equal to zero the temperature is equal to the initial temperature, T_o (°K), while at longer times, the temperature approaches the propellant flame temperature, T_F (°K). The constant c_4 is found by linearly interpolating in a stored table, with T_g as the argument. There is a separate table for each of the three materials considered.

The corrosivity of the combustion products is characterized by the parameter β :

$$\beta = \frac{M_g}{M_g(1-\xi) - \xi M_o} \sum_{i=1}^5 X_i \quad (5-14)$$

M_g = molecular weight of gaseous combustion products

M_o = molecular weight of metal oxide

ξ = concentration of metal oxide, moles/100 gm

X_i = mole fraction concentration of the i^{th} oxidizing species.
There are 5 oxidizing species considered, H_2O , CO_2 , $1/2 O_2$, C , OH

The parameter β is computed by the ODE program and transmitted to the Grain Design and Ballistics Module, where it is used. Based on the matrix of calculations that were carried out, the following relations were obtained for $f(\beta)$ (see eq. 5-12):

$$f(\beta) = 1 \quad \text{Carbon Phenolic (no dependence on } \beta) \quad (5-15)$$

$$f(\beta) = \left(\frac{\beta}{0.24}\right)^{1.2} \quad \text{ATJ Graphite} \quad (5-16)$$

$$f(\beta) = \frac{\beta}{0.24} \quad \text{Pyrolytic Graphite} \quad (5-17)$$

Thus, to summarize, for each material the erosion rate, \dot{r}_t , is found from the one of the equations (5-9) - (5-11). C_H is given by equation (5-8) and β_C by equation (5-12) (with the subsidiary relations (5-13) - (5-17)). The constants c_3/c_p , in equation (5-8), and c_5 in equation (5-13) were adjusted based on comparisons with a limited amount of erosion data for each of the three materials. The final values selected for these constants are:

$$\begin{aligned} c_3/c_p &= 1.682 \\ c_5 &= 3.368 \end{aligned} \quad (5-18)$$

Other nozzle materials can be added to the computer program by repeating the previously described procedure for the materials of interest.

For operating pressures below 300 psi, the phenomenon of nozzle deposition rather than erosion is likely to be encountered in aluminized propellants. Deposition has not been studied to the degree of erosion. Limited data suggest a rate of -0.001 in./sec. for every 50 psi below 300 psi. This is offered as a guide in constructing an input table for use with low-pressure motors.

5.3 Insulation Degradation

5.3.1 Approach

Insulation has a minor effect on the interior ballistics of motors. However, it is enough to warrant accounting for this effect, but not enough to conduct detailed analyses. Therefore, a simple methodology was adopted.

5.3.2 Performance Degradation

From the standpoint of program accuracy and efficiency multiple thermochemical calculations, as the insulation becomes an increasing fraction of the total mass flow, would not be justified. Instead, one matrix of thermochemical calculations was performed varying aluminum content from 0 to 25% and insulation/propellant ratio from 0 to 0.1. The following expressions were fit to the results:

$$\frac{C^*}{C^*_0} = \begin{cases} 1 - [0.5 - 0.025 (\%Al)] R \\ 1 \text{ for } \%Al > 20 \end{cases} \quad (5-19)$$

$$\frac{I_{SP}}{I_{SP_0}} = \begin{cases} 1 - [0.7 - 0.035(\%Al)] R \\ 1 \text{ for } \%Al > 20 \end{cases} \quad (5-20)$$

$$\frac{T_F}{T_{F_0}} = \begin{cases} 1 - 1.9 R \\ 0.81 \text{ for } R \geq 0.1 \end{cases} \quad (5-21)$$

where R denotes the insulation/propellant weight flow ratio, and the subscript o refers to values with no insulation. The performance degradation due to insulation is considered only in the Grain Design and Ballistics Module and is not transmitted to the Master Control Module.

5.3.3 Determination of the Insulation Weight Flow Ratio

Coupling the insulation exposure to the grain regression pattern would not be justified by the magnitude of the insulation effect. Rather, a table is provided for a priori input of exposed area versus time. Ablation rate and insulation density are single inputs. Therefore, at any time, the flow rate of insulation is determined and, by comparison with the propellant flow rate, the value of the ratio is established. The thermochemical parameters used in the ballistics analysis are then degraded accordingly.

5.4 Aluminum Oxide Particle Size

5.4.1 Approach

The two-phase flow loss is an important source of performance loss and is a strong function of particle size, therefore, the ability to predict particle size will have an important impact upon the success of the computer program over a broad range of conditions.

Considerable particle size data have been reported in the literature. Although the collection methods and the relevance of the results have been open to question (58), the existing data must be accepted in lieu of anything better. A number of mathematical models of oxide particle formation and growth have also been published in the literature.

The approach that was taken was to construct a semi-empirical expression for the mean particle size. The form of the expression is analytical in origin, and the constants result from a fit of data covering a wide range of conditions. A log-normal distribution is constructed about the mean, and selected sizes representing distribution intervals are used in the TD2P module.

5.4.2 Experimental Data and Pure Empiricism

Aluminum oxide particles were first collected and measured by Brown⁽⁵⁹⁾ and Sehgal⁽⁶⁰⁾. Brown's work provided the first indication of their rough-order-of-magnitude size, and Sehgal showed the size to be a function of pressure. Cheung and Cohen⁽⁶¹⁾ extended Sehgal's work to show dependences not only upon pressure but also upon residence time and aluminum concentration; no effect of propellant aluminum particle size was detected. Since that time, the Air Force has investigated particle size in a variety of motors⁽⁶²⁾ which has formed a basis for Air Force performance investigations⁽⁴⁴⁾. Having acquired data over a wide range of motor sizes, the Air Force chose a simple correlation based on nozzle throat diameter.

The problem with a correlation based on throat diameter is that it does not address the controlling physical phenomena. This is a drawback of empirical performance correlations based on size parameters, in general. The reason that such correlations work in an approximate sense is that many of the parameters tend to vary together (e.g., throat size, motor L^* , propellant weight or weight flow, burn time, all tend to increase in larger motors). However, when improved accuracy is desired, it is necessary to accommodate variables outside of the correlation range including combinations of these variables which are exceptions to general trends (e.g., a decrease in L^* with increasing motor size) and therefore sources of inconsistency or error. Because the scope of computer program application may encompass a wide range of variables, singularly and in combination, the throat size correlation would not be expected to produce the desired accuracy.

The throat diameter correlation was constructed from data over a relatively narrow range of pressure and aluminum content, but over a wide range of sizes, wherein L^* and throat diameter tended to vary together. Effects of pressure and particle concentration, as well as L^* , must be included if the scope of propellants and operating conditions is to be adequately covered. Cheung and Cohen actually found a decrease in particle size with increasing throat diameter in their data because they increased throat diameter in order to reduce pressure (and average L^*) in fixed hardware. Similarly, nozzle efficiencies reported from BATES motor data^(44,63,64), again in a fixed size, tend to infer a smaller particle size with decreasing pressure (increased throat size and smaller mean L^*). The BATES data also indicate a smaller particle size with decreasing aluminum content, and with changes in binder type that would result in decreasing Al_2O_3 concentration. The phenomena of oxide particle formation and growth must be addressed in some manner in order to account for these detailed effects.

5.4.3 Models and Semi Empiricism

Mathematical models of oxide particle growth have been reviewed by Brown⁽⁶⁵⁾. The Cheung and Cohen paper included a model describing particle growth by condensation and agglomeration, assuming that all particle growth takes place within the motor cavity. They used this model to correlate their data and explain the trends observed. They then extrapolated to large boosters and predicted the sizes actually measured from these motors two years later. The principal effect was residence time, relatable to the motor L^* . The model also predicts particle size to be dependent upon pressure to the one-third power and Al_2O_3 concentration to the one-third power. The residence time dependence is more complicated because condensation and agglomeration have different functional time-dependencies. Assuming that these time dependencies can be combined in a single term represented by L^* to a power, there results the following semi-empirical expression:

$$D_p \sim P^{1/3} \xi^{1/3} L^{*m} \quad (5-22)$$

This expression was fit to the Air Force data, and resulted in a very good correlation as shown in Figure 5-1 ($m=0.8$). The correlation was superior to one simply based upon throat diameter. However, when other data were considered, including lag loss implications in large motors having small nozzles, the L^* dependence was concluded to be too . . .

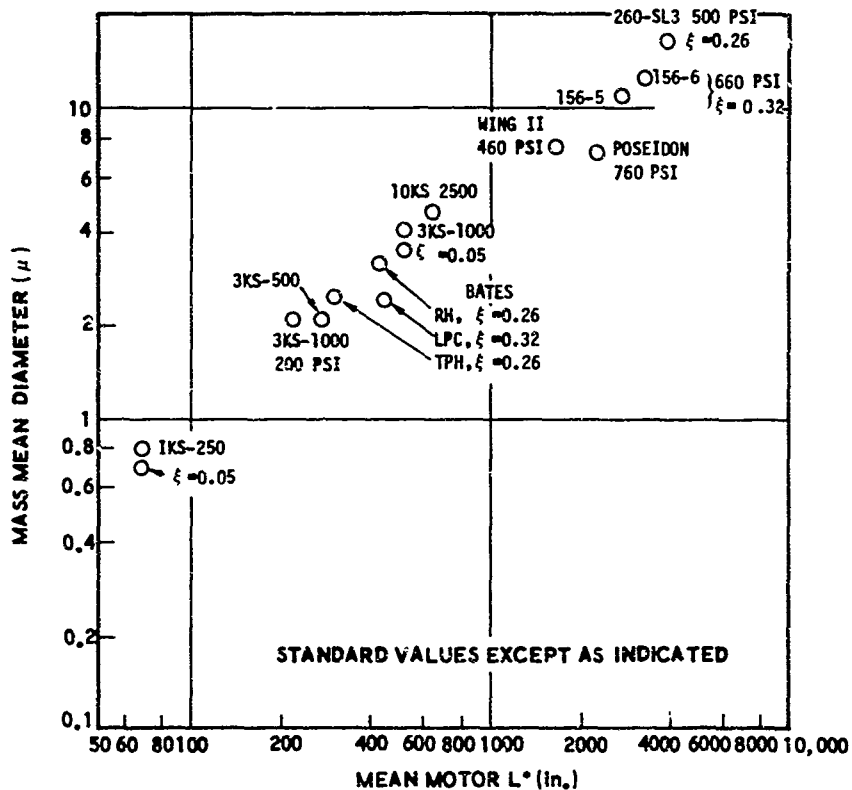


FIGURE 5-1 PARTICLE SIZE CORRELATION WITH MOTOR L*, CORRECTED FOR VARIATIONS IN PRESSURE AND ALUMINUM CONTENT

Another class of models assumes that particle growth occurs chiefly in the nozzle by collisions resulting from velocity gradients. Such a model would not have an L^* -dependence, nor does it address pressure and concentration effects from the standpoint of physical chemistry. The model of Crowe and Willoughby⁽⁶⁶⁾ is representative of this class. A semi-empirical correlation of the data was constructed based on this model, and was found to be poor. Therefore, it was concluded that a model of particle growth should not emphasize growth in the nozzle. This is fortunate from the standpoint of the complexity of the lag loss analysis.

Finally, a correlative expression was constructed combining the elements of the Cheung-Cohen and Crowe-Willoughby analyses. This assumes that particle growth occurs in both the chamber and the nozzle, but each to a lesser extent than predicted by either theory alone. It also serves the purpose of reducing the L^* -dependence of growth in the chamber under the circumstances where it was found to be excessive. The expression fit to the data is as follows:

$$D_p = 0.454 P^{1/3} \xi^{1/3} [1 - \exp(-0.004L^*)] (1 + 0.045 D_t) \quad (5-23)$$

D_p in microns

P in lb/in²

ξ in moies/100 gm

L^* in inches

D_t = throat diameter, in inches

Thus, a limiting diameter is reached in the chamber at large L^* , depending upon pressure and concentration, and additional growth occurs in the nozzle depending upon throat size. A comparison with the data is shown tabulated in Table 5-1. The average deviation is 18 percent, which represents a variance in specific impulse efficiency of less than 0.5 percent.

Additional studies of particle formation and growth are in progress in the context of particle damping of combustion instability. Observed trends support the theory that substantial growth must occur in the motor cavity. Results of these studies may be useful in future modification of the above correlation.

Table 5-1

COMPARISON OF PREDICTED AND MEASURED PARTICLE SIZES

Motor	Predicted (μ)	Measured (μ)
IKS-250 (low Ai)	0.4	0.4
IKS-250 (standard)	0.7	0.8
15 BATES	1.6	2.2
3 KS-500	2.1	2.1
3 KS-1000 (low P, L*)	1.1	1.2
3 KS-1000 (low Al)	1.6	2.0
3 KS-1000 (standard)	3.1	4.1
70 BATES (Thiokol)	2.3	2.1
70 BATES (Lockheed)	2.9	2.5
70 BATES (Rohm & Haas)	2.8	3.2
10 KS-2500	3.3	4.7
Wing II Minuteman	4.2	5.8
Poseldon	4.8	6.2
120-Inch	6.4	8.6
156-5	10.2	10.1
260-SL3	11.5	13.2

Range of variability = 12.8 μ
 Average deviation = 17.7%

6. COMPARISONS WITH MOTOR FIRING DATA

While the SPP program was, by design, based almost entirely on pre-existing, proven, analytical and semi-empirical techniques, there was no guarantee that the integration of all of these methods was properly implemented. Nor could it be known, ahead of time, if the combined techniques would be capable of meeting the accuracy goals which had been set (i.e., delivered Isp to $\pm 2\%$, delivered thrust and total impulse to $\pm 5\%$); for a wide range of motors, propellants and operating conditions.

In order to validate the present computer program, a series of comparisons with full scale motor firing data was carried out. To date, four program-data comparisons have been completed. The first three comparisons were basically used as vehicles to check out the operation of the computer program. The three check out cases were selected to provide a reasonable range of motor sizes, propellants and operating conditions. The motors considered are listed below, together with some of the characteristics that led to their selection.

Thiokol Extended Delta: complicated three dimensional grain, relatively large size, high expansion ratio.

Aerojet 2.75: small, short burn time, multiple nozzles, high throat erosion.

Lockheed SRAM: end burner, unusual nozzle shape, high pressure, low expansion ratio.

As a result of their diversity, these motors provided a reasonable thorough basis for evaluating the performance of the program. The fourth comparison with motor data was carried out after the previously mentioned comparisons were completed. This was a so-called sealed envelope comparison. The Air Force selected the motor to be considered and transmitted to us only the information required to execute the program. The motor chosen for this comparison was the C-4 Third Stage. It represents a motor of much current interest, having a high energy propellant, complex grain geometry and reasonably high expansion ratio. The completely a priori performance predictions for this motor were then delivered to AFRL and evaluated.

The results of each of these four comparisons are individually discussed below. The results for all of these cases are then summarized in Section 6.5.

6.1 Extended Delta Motor (67)

The present results for the Extended Delta motor were obtained by executing the complete performance prediction methodology on a completely coupled basis. For reasons discussed subsequently, this was the only one of the first three check-out cases for which this was done.

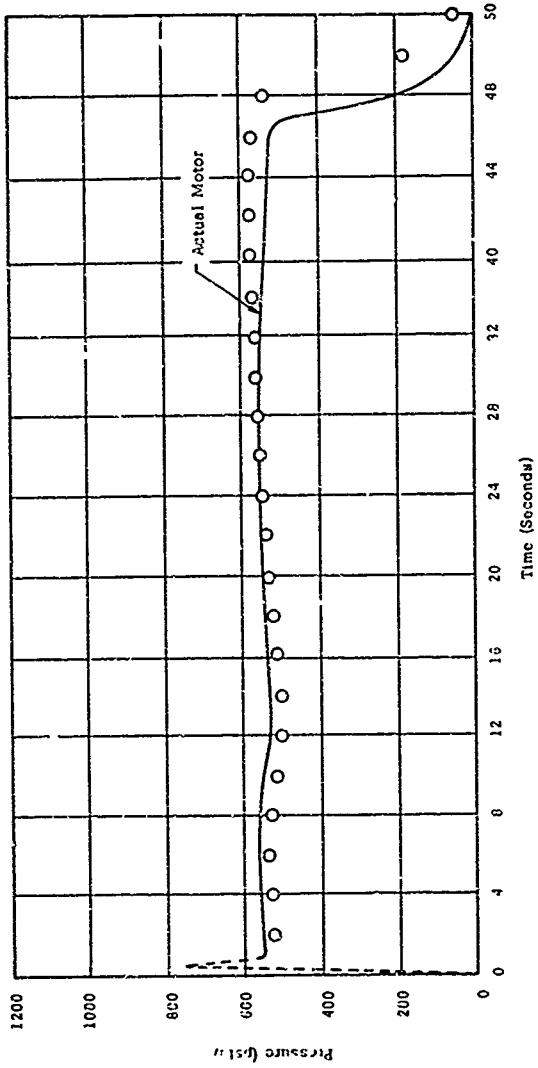
The theoretically calculated delivered specific impulse for this motor was found to be 0.45% less than the measured value. The simplified semi-empirical performance prediction correlations under predicted the measured value by 0.79%. The results of the ballistics calculations are discussed below.

The predicted pressure-time curve for the Extended Delta motor is compared to the actual pressure trace in Figure 6-1. It is observed that the qualitative and quantitative features of the data are well-predicted. Pressure is slightly underpredicted for the initial portion, and slightly overpredicted for the latter portion. The action time is somewhat overpredicted.

The predicted action time average pressure was 534 psia, compared to the actual result of 545 psia, for an error of 2.0%. Average thrust was underpredicted by 3.1%. The action time was overpredicted by 4.3%, in part because of a propellant weight error attributed to the fact that the web dimensions had to be measured from a motor drawing. Correcting for the pressure and assigned web errors, burning rate was underpredicted by 2.4%. This burning rate error in part explains the low initial pressure and longer action time. The pressure becomes high near the end of the burn in part because the throat erosion was underpredicted by 18.7% and in part because of the increased input web. As a result of compensating effects (i.e., thrust underprediction, weight flow overprediction) the predicted total impulse was only 0.5% above the measured value.

A burning rate error of 2.4%, if uncompensated by errors in the other parameters governing motor pressure, would produce a 3.4% pressure error for a 0.3 exponent and a 6.1% pressure error for a 0.6 exponent. Therefore, an error even in the course of strand burning rate measurement could make it difficult to predict pressure to within 5%. Sources of compensating (or aggravating) error would be in the grain geometry, nozzle erosion and C^* efficiency

Figure 6-1 Predicted and Actual Pressure Traces For Extended Delta Vector



computations. That there is a grain geometry error is evident in Figure 6-1 in that the predicted pressure dip precedes the actual pressure dip even though the predicted burning rate was low. It follows that the predicted pressure dip should have occurred later than actual. However, the prediction of the basic character of the pressure curve shows that the grain design program is properly computing the geometry in general. In this case, the error in the throat erosion partially compensated for the error in the burning rate.

6.2 SRAM First Pulse (33)

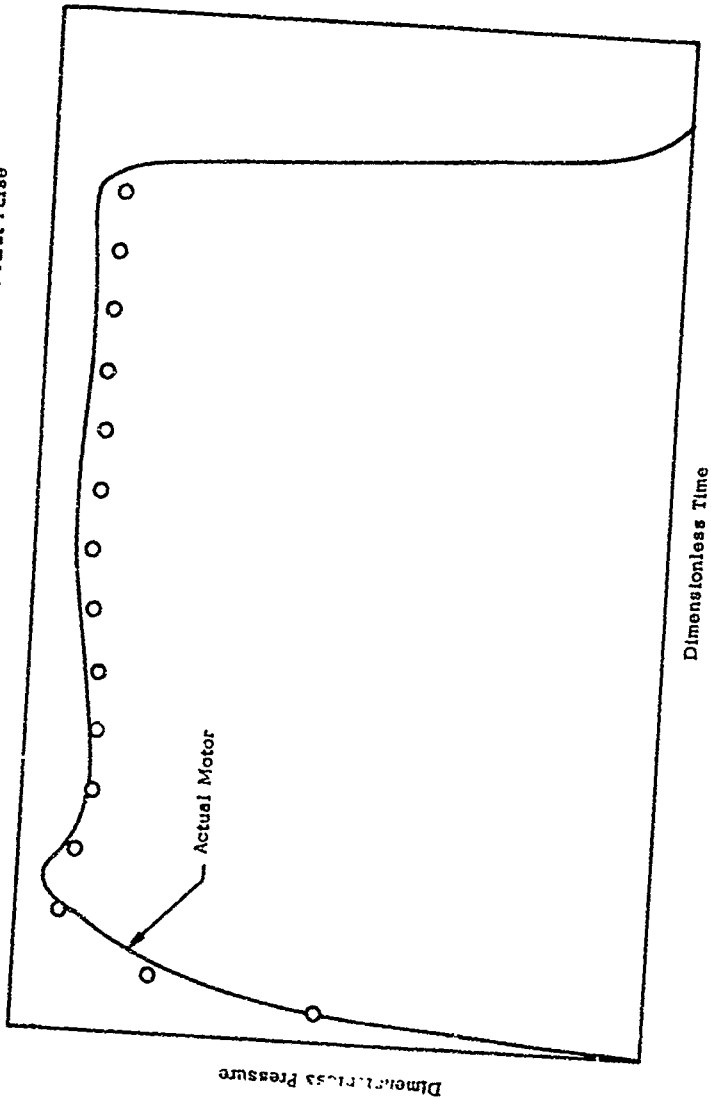
The primary reason for selecting SRAM as a validation case was to provide a means to check out the grain geometry and ballistics computations for an end-burner. The motor also has a unique nozzle geometry and high operating pressure. A full SRAM firing consists of two pulses. Calculations were carried out only for the first pulse.

The current grain design analysis does not contain a model for the meniscus burning phenomenon encountered in the SRAM motor. Thus, the ballistics predictions for the SRAM motor had to be corrected for the effect of meniscus burning. Neglecting meniscus burning, the computed pressure and thrust levels were expected to be, and were, low. The computer output was corrected for meniscus burning by raising the pressure at each instant of time and by reducing the value of each time in accord with the increase in effective burning rate. Thus, the fact that a given K_N is encountered sooner, was accounted for. The basis for the pressure correction at each instant was the previously known effect of the phenomenon on the grain regression. Although the important result was the successful operation of the computer program for an end-burner, the corrected pressure-time trace is shown compared with data in Figure 6-2.

The shape of the pressure trace is well-predicted. The predicted action time average pressure was low by 1.5%. The predicted motor burning rate as corrected was low by 1.3%, and was compensated by an underprediction of throat erosion of 2.5%. Action time average thrust was underpredicted by 0.8%. The underprediction of pressure was compensated by a 0.9% overprediction of delivered specific impulse, which is well-within the program goal.

The specific impulse prediction for this case was not based on the motor operating conditions output by the Grain Design and Ballistics Module, due to the

Figure 6-2 Predicted And Actual Pressure Traces For SRAM First Pulse



neglect of the previously mentioned motor burning phenomenon. Average motor pressure and erosion rate, based on the data were input to the program, together with an average motor L^* , and the ODE, TD2P and TBL Modules were executed. The Kinetics Module was not utilized since the loss is insignificant at the SRAM operating pressure (the simplified kinetics loss correlation predicts a 0.1% kinetics loss for this case).

6.3 Aerojet 2.75 FFAR(31)

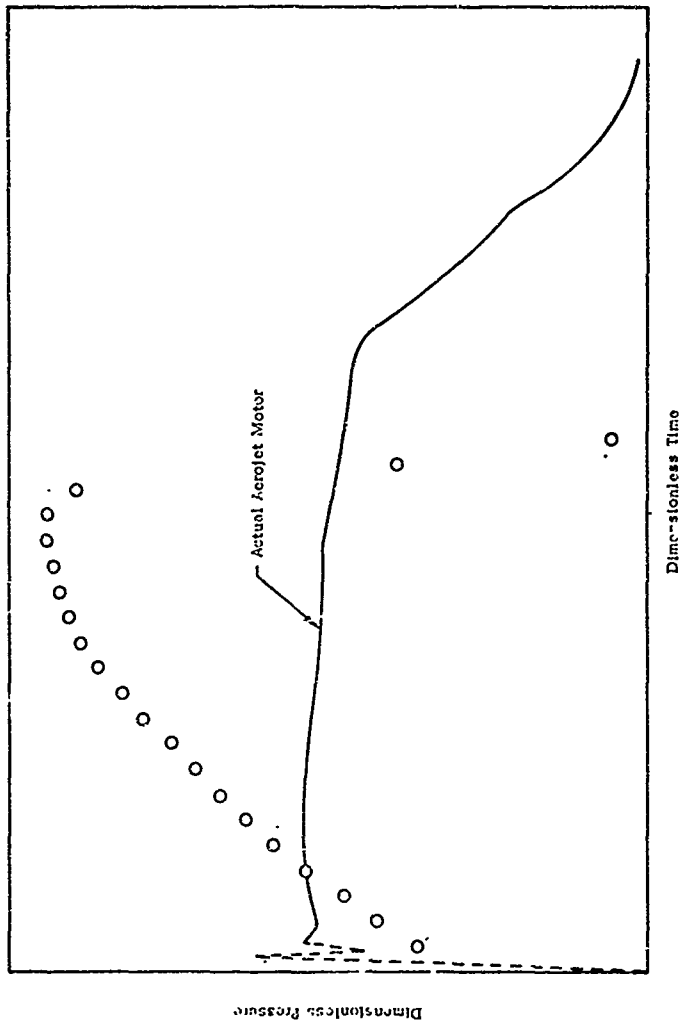
The ballistics prediction for the Aerojet 2.75 inch motor (Ref 31) encountered an anomaly. As shown in Figure 6-3, there is no resemblance between the predicted and actual pressure-time trace. A disturbing circumstance was an oscillograph trace for a "2.75 inch motor" which had been previously furnished to Ultrasonics by AFRPL, and which showed progressive burning. This piece of data will be discussed further subsequently. In view of this startling result, an investigation was conducted as to the nature of the problem.

After checking the inputs to the computer program, a discussion was held with members of the LPC Engineering Department who had 2.75 inch motor experience. It was reported that there is no reasonable way in which a circular-port grain could show a neutral pressure trace, and that inhibiting the aft portions would have little effect on the progressivity.

Nevertheless, Ref (31) was checked against the engineering drawing of the grain and there appeared a basis for suggesting a modification to the input description of the inhibited surfaces. A test case was run with this modified input, but showed little change in the progressivity. However, because a different answer did result, it was possible to conclude that the grain geometry subroutine was at least recognizing inhibited surfaces and probably correctly accounting for them.

The next step was a conversation with Aerojet. It was established that the neutral character of the pressure trace was reproducible over an extensive test history. The explanation offered was a combination of super erosive burning and considerable nozzle throat erosion. However, this explanation proved unsatisfactory for the following reasons:

Figure 6-3 Predicted and Actual Pressure Traces For Aerojet 2.75-inch Motor



- a) The computer program adequately predicted the reported measured throat erosion (11.3% error). It was verified that a single nozzle had not mistakenly been utilized in the calculation (the motor has four nozzles).
- b) An approximate calculation established that the rate of throat erosion would have to be increased by a factor of 2 in order to produce a neutral pressure trace. Discussion with LPC engineers indicated that a different throat material, such as an asbestos-based material, would be required to produce such a rate.
- c) The computer program closely predicted the reported measured motor burning rate, when corrected for the difference between predicted and measured average pressure (1.4% error). Therefore, the factor increase between motor and strand rates was satisfactorily predicted.
- d) The initial port-to-throat diameter ratio of the motor is 2, which is too high a value for exceptional erosive burning. Moreover, the aft end port, which would be expected to exhibit the highest erosivity, was inhibited.
- e) An approximate calculation established that, to produce the measured average burning rate and a neutral pressure trace with the measured throat erosion, the initial erosive burning would have to exceed that produced in nozzleless rocket motors and the burning rate G-dependence would have to be equal to the pressure-dependence (like a hybrid rocket fuel containing some AP). Both of these requirements are unrealistic.
- f) The long tail-off exhibited by the motor is indicative of some anomaly. In seeking to explain the anomaly, discussions were held with LPC engineers regarding the possibility of unbonds, inhibitor failure or cracks. An unbond was considered unlikely in view of the encapsulation of the propellant in this particular design. Inhibitor failure would not significantly alter the progressivity, as mentioned earlier. The possibility of a reproducible cracking of the grain was then assessed.

An LPC stress analyst was aware of a reproducible crack occurring at the interface between an inhibited surface and an uninhibited surface. This occurred in an Aerojet Minuteman motor. The motor had been stress-analyzed in its initial configuration, but not when a fillet was formed from burning at the interface:



The problem manifested itself as a motor failure some time into the burn, and therefore, warranted detailed study. (Such is not the case with the 2.75 inch motor in question, which to all intents and purposes, performs as required.) Under separate contract, UTC performed a stress analysis of the Minuteman Motor taking the fillet into account and the problem was subsequently identified and resolved.

A series of K_N^* curves was then constructed for an idealized cylindrical 2.75 inch motor and are shown in Figure 6-4. The first curve shown is for the absence of port inhibition, or complete inhibitor failure on the port. The second is for a partial inhibition, or a part failure. The third is for port inhibition per the Aerojet design without failure. The fourth curve takes the Aerojet design without inhibitor failure, and adds a diagonally circumferential crack beginning at the fillet and prepropagating at a 45° angle to the wall. In each case, the K_N is adjusted for the measured throat erosion by assuming a constant rate with web burned.

Each K_N curve is normalized to the initial K_N of the Aerojet design without a crack or inhibitor failure. It is verified that the port inhibition does not significantly alter the progressivity: the design inhibition is about 10% more progressive than no port inhibition. However, the assumed ideal crack does produce a near-neutrality. Moreover, the initial K_N was determined to be consistent with the initial pressure of the motor assuming the predicted erosive burning to be valid and not a super erosive burning.

The ballistics prediction for the Aerojet motor is qualitatively compared to the pressure trace furnished by AFRPL in Figure 6-5. The AFRPL motor has the same grain design as the Aerojet motor, but differs from the Aerojet motor as to propellant, nozzle configuration, and complete lack of grain inhibition. The following significant aspects may be noted: The AFRPL motor shows progressivity; it

*Ratio of propellant burn area to nozzle throat area.

Figure 6-4 Diagnostic K_N Curves For 2.75 Motor,
Including Measured Throat Erosion

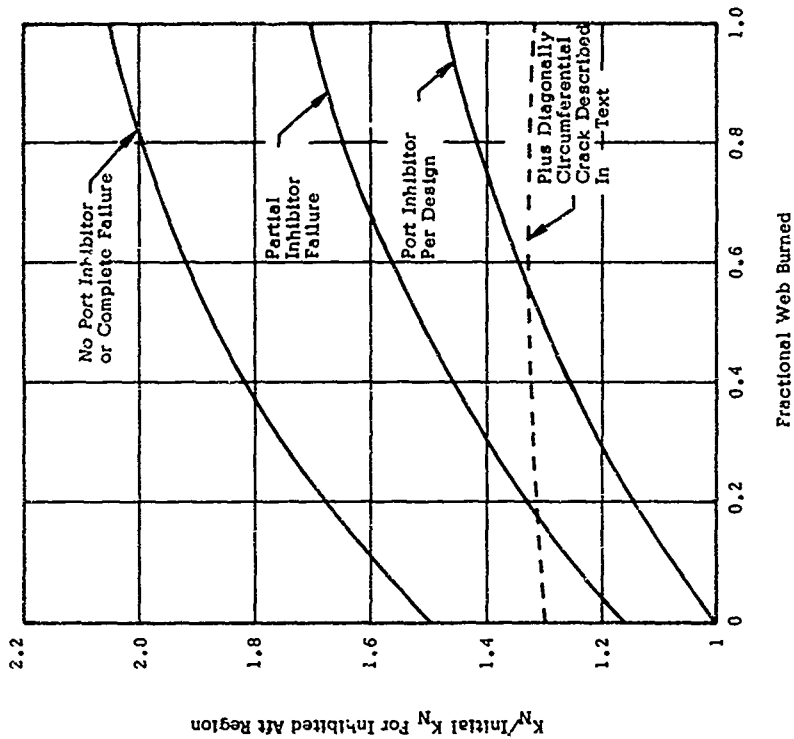
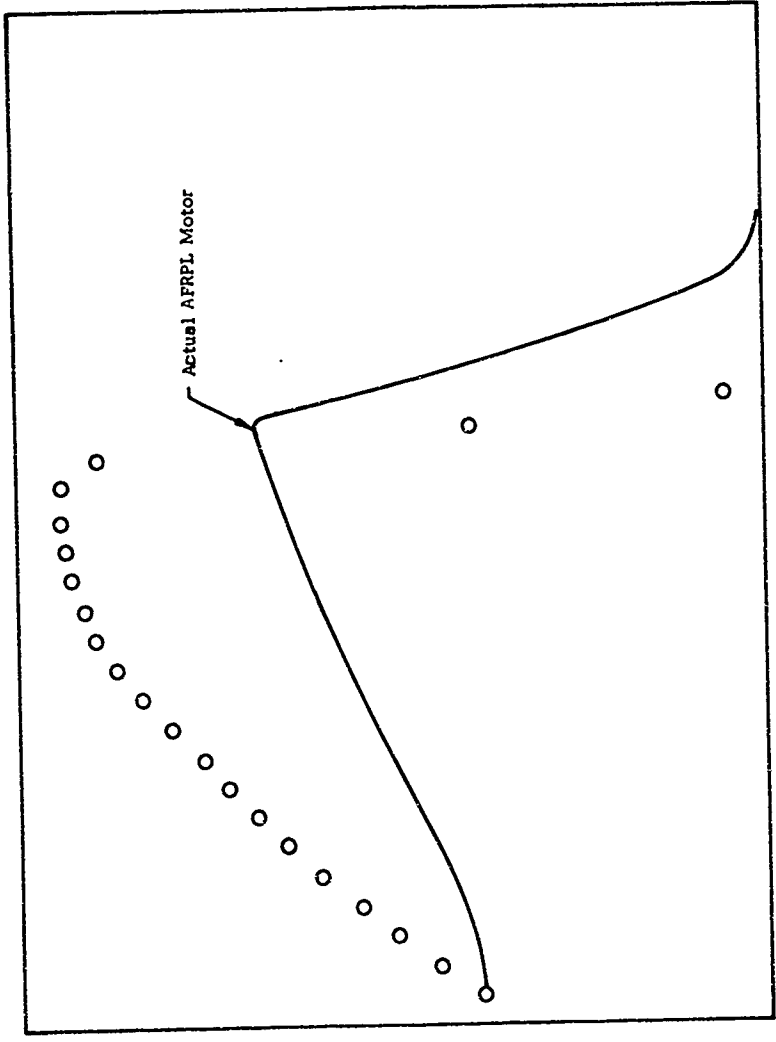


Figure 6-5 Comparison Of Predicted Pressure Trace For Aerojet 2.75 Motor With Actual Trace For AFRPL 2.75 Motor



was verified that its progressivity is consistent with its change in K_N ; the sharpness of its tail-off is closer to the predicted Aerojet motor than the actual Aerojet motor. The AFRPL motor shows less progressivity than the predicted Aerojet motor because of its complete lack of grain inhibition. It is apparent that the AFRPL motor does not exhibit any super erosive burning with high G-dependence, and does not exhibit any anomaly.

For all of the foregoing reasons, it is concluded that the Aerojet 2.75 inch motor exhibits some reproducible anomaly, that this anomaly is probably a crack emanating from the inhibitor interface, and therefore, it is impossible to predict the observed ballistics. On the other hand, the ballistics of the AFRPL 2.75 inch motor would probably have been successfully predicted were that the test case.

Since a satisfactory ballistics solution for the 2.75" motor could not be obtained, quantitative comparisons with the measured pressure and thrust versus time, and total impulse, are not indicative of the accuracy of the program, and are not given. A valid comparison with the delivered specific impulse was obtained, but in a somewhat non-apriori manner. Using one of the many operational modes of the SPP program, the measured average chamber pressure and erosion rates were input, together with an estimate for the average motor L^* . The Theoretical Performance (ODE), Two-Dimensional Two-Phase (TD2P), and Boundary Layer (TEL), Modules were then executed. At the high pressure for this motor the execution of the Kinetics Module (ODK) is not warranted as the loss is quite small, but the amount of computer time that would be required is relatively large. The simplified kinetics loss correlation should be adequate at pressures of 1000 psi, or more for conventional aluminized propellants.

Proceeding in the aforementioned fashion, the predicted delivered I_{sp} was found to be just 0.3% above the measured value for this motor. The simplified performance prediction correlations yielded a value 0.93% less than the measured value for this case. Both of these results are quite satisfactory.

6.4 Sealed Envelope Predictor: C-4 Third Stage

This prediction was a special challenge because it was a blind prediction of a motor containing a complex grain geometry and a high-exponent propellant. As would be expected for such a case, the complete capability of the program was utilized in the calculation. The specific impulse prediction for this case was also

excellent. The theoretically determined delivered specific impulse was only 0.4% higher than the reported motor firing value, while the simplified performance prediction correlations yielded a value of 0.6% on the low side.

The predicted pressure trace is compared to the actual motor data in Figure 6-6. The result is similar to the Extended Delta result in that pressure is underpredicted during the initial portion of the firing, and overpredicted at later times. Because the pressure exponent is high, the extent of the pressure departures is greater than in the Delta. The grain geometry calculations appear to be better here in that the pressure peak and dip are predicted to occur at a later time, which is consistent with the predicted slower initial burning. The compensating errors produce a near-correct prediction of action time, and the tail-off is well-predicted.

Action time average pressure was underpredicted by 0.7%, the best result of all test cases. Burning rate was underpredicted by 1.3%. The throat erosion was underpredicted by 41% of the average throat erosion; fortunately, the magnitude of the throat erosion was small and hence, was negligible in performance prediction. It is thought that this error in erosion rate stems from extrapolation of the semi-empirical throat erosion constants to a new high temperature regime, and should be subject to adjustment in future work. Action time average thrust was underpredicted by 1.3%. Total impulse was underpredicted by 2.1%; this resulted from an error in computed propellant weight, on the low side. The inputs for the grain geometry had to be prepared from a small, relatively crude grain drawing, and strand burning rate was provided to us at only one condition. In view of this, the accuracy of these ballistics predictions is quite good.

A summary of the results for this case may be found in Table 6-1. A breakdown of the individual losses, and a comparison between the theoretical and simplified predictions is presented in Table 6-2.

6.5 Summary of Results

The results of the four previously described comparisons with motor firing data are summarized in Table 6-1. Except for the anomalous pressure behavior

TABLE 6-1 SUMMARY OF RESULTS

Quantity	Percent Deviation From Motor Firing Data		
	Extended Delta	SRAM	2.7s (Aerojet) ²
Average Burn Rate ¹	- 2.4%	-1.3%	1.4%
Average Throat Erosion Rate	-18.7%	-2.5%	-11.3%
Action Time Pressure	- 2.0%	-1.5% ³	-
Action Time Thrust	- 3.1%	-0.84% ³	-
Thrust Impulse	0.46%	1.3%	-
Specific Impulse (Exact)	- .45%	0.95%	0.33%
Specific Impulse (Simple)	- .79%	X 1.0%	X - .93%
			C-4 Third Stage ¹
			- 1.3%
			-41.2%
			- 0.72%
			- 1.3%
			- 2.1%
			0.4%
			- 0.6%

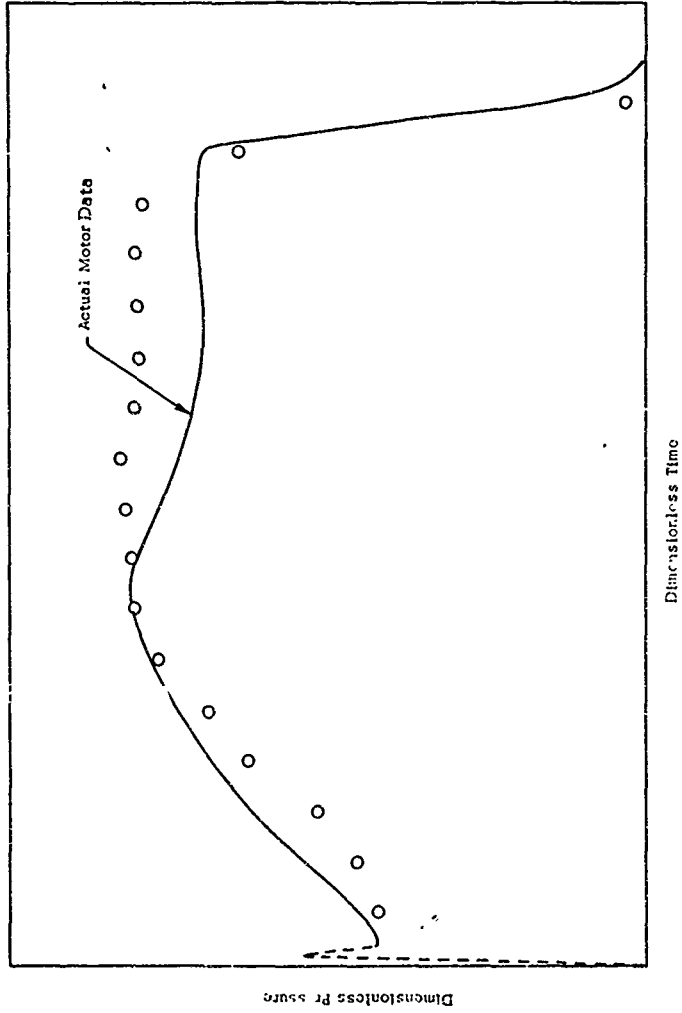
¹ Sealed envelope predictions

² Corrected for pressure error-effect

³ Corrected for meniscus burning effect

X Motor used in developing or evaluating the correlation

Figure 6-6 Predicted And Actual Pressure Traces For Blind Prediction Test Case



observed in the 2.75" motor (discussed in Section 6.3) all of the predicted results were well within the accuracy goals for the program.

A breakdown of the individual losses for the two cases in which the complete methodology was executed (Extended Delta and C-4 Third Stage) is presented in Table 6-2. The results of both the theoretical and simplified methods are indicated. In this way the relative magnitudes of the different losses can be assessed. The erosion loss, normally included in η_{TD2P} (see equation 3-2) has been listed separately for the same reason. In order to facilitate comparison between the theoretical and simplified 2D-2phase losses, the simplified 2D and 2 phase losses have been combined (the theoretical loss cannot be separated into its components).

As a result of the nozzle throat geometry restrictions of the TD2P module, the actual nozzle geometry could not be analyzed for the three high performance motors: Extended Delta, SRAM, and C4 Third Stage. The transonic flow solution for the TD2P module is limited to a simple circular arc throat geometry and the ratio of the throat radius of curvature to the throat radius must be greater than 1.5. The two-phase flow loss is usually the largest single loss for highly aluminumized propellants, and the magnitude of this loss is sensitive to the throat geometry. Therefore, the inability of the TD2P module to treat the actual nozzle geometry is cause for some concern. An effort to remove this limitation would be warranted. In the mean time, the magnitude of the error resulting from the use of a rationally selected approximate nozzle geometry should be ascertained.

Table 6-2 Breakdown Of Individual Losses

MOTOR	METHOD	η_{KIN}	η_{TD2P}	$\eta_{erosion}$	η_{SUP}	η_{CE}	ΔI_{SPRL}
EXTENDED DELTA	calculated	.9959	.9514	.9962	X	.9843	1.68
	correlation	.9939	.9597	X	.9921	.9735	1.74
C4 THIRD STAGE	calculated	.9969	.9488	.9979	X	1.00	1.62
	correlation	.9964	.9522	X	.9929	.9883	2.92

X: Not calculated by present methodology

7. CONCLUSIONS AND RECOMMENDATIONS

7.1 Conclusions

The goal of this effort was to develop a computerized performance prediction methodology that was capable of predicting delivered specific impulse to $\pm 2\%$, and delivered thrust and total impulse to $\pm 5\%$, for a wide range of solid rocket motor geometries, propellant, and operating conditions.

The Solid Rocket Performance Program (SPP) described herein, and in the other two volumes of this report, was designed to achieve the goal. Six existing computer programs were integrated with a central logic to form a strong analytical foundation for the program. To supplement the theory, where necessary, and to increase the flexibility of the program, a number of existing and newly developed semi-empirical correlations were incorporated into the program.

The program is modular in structure, and allows the user to exercise the various modules individually, all together, or in any predetermined combination, as required. For those cases where speed and simplicity are paramount (e.g. large parametric studies) the analytical portions of the program may be bypassed completely in favor of the performance loss correlations which have been incorporated into the program. Alternatively, one, or more of these correlations may be employed in lieu of the corresponding analytical calculation when the particular performance loss is either known to be small, or adequately characterized by the correlation.

Ballistics and performance predictions, obtained with the SPP Program, were compared with firing data for four widely varying full scale motors. Except for the anomalous pressure-time behavior of one of the motors (an explanation for which is proffered), all of the predicted results were within the accuracy goals originally set for the program. In each case the difference between the predicted and measured delivered specific impulse was less than one percent. This included one case which was predicted to within 0.4% on a sealed envelope basis. The simplified performance loss correlations also gave good results for each case. Conclusive statements regarding the accuracy and range of validity of the SPP program cannot be made until additional verification efforts are conducted. The following tentative conclusions have been drawn:

- The accuracy of burning rate prediction is comparable to, and will be limited by, the error in measuring strand burning rates.
- Action time average thrust and pressure appear to be predictable to within 5%; compensating errors in the various parameters entering into the computations of pressure and thrust being helpful in this regard.
- Delivered specific impulse appears to be predictable to within 2%, and probably to within 1% in most cases which do not involve unusual circumstances.
- The simplified method of computing specific impulse efficiency is adequate for its intended purpose.

As a result of the limitations of the present analysis (see Section 7.2) the accuracy of the calculated results may be influenced by compensating errors. For instance, the geometric limitation of the TD2P analysis that requires the actual nozzle shape to be approximated in many cases (including 3 of the present cases), the possible errors in particle size distribution, the neglect of throat roughness, etc., all impact the calculated two-phase flow loss. No attempt to quantify the magnitude of the possible errors resulting from these and other assumptions was made during the course of this investigation. Further verification efforts, parametric studies and future experimental and analytical investigations will undoubtedly be illuminating in regards to the adequacy of the individual assumptions and the program as a whole.

The SPP program treats the complete solid rocket motor performance problem, i.e., grain geometry, ballistics and efficiency, within the context of a single, automated, entity. As a result, accurate analytical predictions of solid rocket motor performance can be obtained in a single computer run. It is hoped that the convenience of the present approach will help stimulate more widespread application of theoretical techniques in solid rocket motor development programs.

7.2 Recommendations

The SPP program has many virtues; it also has its limitations. Recognition of these limitations serves a dual purpose: first, to allow the program, as it exists, to be more fruitfully employed; secondly, to yield a better perspective on the nature of the improvements and/or extensions of the program that should be considered. The following is a list of the more significant limitations of the SPP program.

1. The TD2P currently terminates if particle impingement occurs in the nozzle.
2. The two-dimensional two-phase transonic analysis is inadequate in a number of respects: the analysis will fail for normalized radii of curvature < 1.5 and for inlet angles $> 45^\circ$; the wall geometry is limited to a conical inlet and single radius of curvature throat.
3. The TD2P program also: neglects real gas effects; cannot handle shock waves; does not explicitly allow no particle cases to be computed (the program can be "fooled" into doing so), prohibits gas phase condensation and particle growth in the nozzle.
4. The present boundary layer analysis (TBL) is not deemed to be accurate enough when boundary layer losses are relatively large.
5. A method for determining nozzle wall temperature has not been integrated into the methodology.
6. The nozzle erosion correlations in the program are limited, and not as accurate as would be desired.
7. Throat roughness, and erosion induced discontinuities are not addressed.
8. The analysis is inadequate in transient dominated cases.
9. The grain design analysis is inefficient for "simpler" grain geometries.
10. The effects of acceleration on burn rate, and nozzle flow separation have not been considered.
11. Three dimensional flow effects have not been considered.

The state-of-the-art in solid rocket performance prediction was recently reviewed at the last JANNAF Performance Standardization Working Group meeting⁽³⁾. As a result of this meeting seven deficiency areas were identified. These areas included some, or all, of the items listed under numbers 2, 3, 7 and 11, above. In addition, they included more adequate particle size determination, and better burn rate modeling. So-called "deficiency statements" were recently prepared by several of the committee members, in which the nature of these limitations, and methods for alleviating them are explored in detail. Based on these statements, and our own predilections, it is recommended that any future efforts to modify the SPP program should begin with items 1, 2 and 7, as listed previously. Item 1 is a relatively simple matter to take care of, items 2 and 7 would require significant effort, but are entirely possible to overcome with currently available numerical techniques.

Most of the other items in this list represent limitations which are encountered less frequently (e.g., large boundary layer losses, nozzle separation, transient dominated motors, etc.), or ones which would require inordinate effort to overcome (e.g., 3-D effects). Some of these limitations can currently be overcome through the use of existing analyses on an uncoupled (to SPP) basis, (e.g., boundary layer and throat erosion). Which of these remaining limitations will be addressed will most likely be a function of the predilections of future users, and the requirements of future motors.

In passing, one other recommendation should be made. The existing knowledge regarding the kinetics of typical metalized solid propellant exhaust species is, as pointed out in Appendix A, meager, at best. In most cases this is of little consequence in conventional aluminized propellants, as the kinetics loss tends to be small. At low pressure, however, the kinetics loss can be significant, and unless additional work towards identifying the controlling reactions, and their rates, is forthcoming, substantial predictive errors can be expected in such cases.

8. REFERENCES

1. NASA SP 8039, "Solid Rocket Motor Performance Analysis and Prediction," May 1971.
2. Cohen, N. S., et al, "Solid Rocket Performance Prediction Techniques", AIAA/SAE 10th Propulsion Conference, AIAA Paper No. 74-1200, Oct. 1974.
3. JANNAF Performance Standardization Working Group, Solid Performance Subcommittee, Minutes of July 30-31, 1974 meeting at NASA Johnson Space Center, distributed by CPIA.
4. Gordon, S., and McBride, B. J., "Computer Program for Calculation of Complex Chemical Equilibrium Compositions, Rocket Performance, Incident and Reflected Shocks, and Chapman-Jouguet Detonations," NASA SP 273 (1971).
5. Nickerson, G. R., Coats, D. E., and Bartz, J. L., "The Two-Dimensional Kinetic (TDK) Reference Computer Program," Engineering and Programming Manual, Ultrasystems, Inc., Dec. 1973, prepared for Contract No. NAS9-12652, NASA JSC.
6. Nickerson, G. R., and Klegel, J. F., "Axisymmetric Two-Phase Perfect Gas Performance Programs, Volume 1 Engineering and Programming Description" prepared for NASA MSC under Contract NAS9-4358, April 1967.
7. Weingold, H. D., "The ICRPG Turbulent Boundary Layer (TBL) Reference Program," prepared for ICRPG perf. Std. Working Group, July 1968.
8. Barron, J. G., Jr., Cook, K. S., and Johnson, W. C., "Grain Design and Internal Ballistics Evaluation Program, Program No. 64101," Hercules Powder Co., Bachus Works, July 1967, AD 818321.
9. Harry, D. P., Price, C. F., Small, K. R., and Taylor, D. E., "User's Manual for Nozzleless Rocket Motor Internal Ballistics Computer Program," AFRL TR-73-20, March 1973.
10. Air Force Rocket Propulsion Laboratory. Theoretical I_{sp} Program, User's Manual.
11. Air Force Rocket Propulsion Laboratory, Theoretical I_{sp} Program, Listing and Sample Cases.
12. McBride, B. J., and Gordon, S., "Fortran IV Program for Calculation of Thermodynamic Data," NASA TND 4097, August 1967.
13. "Ballistic Predictions for Mass-Augmented Solid Rocket Motors", AFRL-TR-71-133, Lockheed Propulsion Company, Redlands, CA., (Dec 1971).
14. Cohen, N. S., and Derr, R. L., "Metal Combustion Efficiency Improvement," 7th JANNAF Combustion Meeting (CPIA Publication 204, Vol II, pp. 1-12, Feb. 1971).

15. "Combustion Instability of Aluminized Propellants," NWC-TP-5060, U.S. Naval Weapons Center, China Lake, CA. (April 1971).
16. "Combustion Tailoring Criteria for Solid Propellants," AFRPL-TR-69-190, Lockheed Propulsion Company, Redlands, CA. (May 1969).
17. "Propellant Tailoring Techniques for Controllable Rocket Motors," AFRPL-TR-71-25, Vol II, Lockheed Propulsion Company, Redlands, CA. (Mar. 1971).
18. Northam, G. J., and Sullivan, E. M., "Evaluation of Mg-Al Eutectic to Improve Combustion Efficiency in Low Burning Rate Propellants," 9th JANNAF Combustion Meeting (CPIA Publication 231, Vol I, pp 1-10, Dec. 1972).
19. Kliegel, J. R., et al., "One-Dimensional Two-Phase Reacting Gas Non-equilibrium Performance Program," Vol. 1 Engineering Analysis, Report MSC-11780, TRW Systems (Aug. 1967).
20. Svehla, R. A., "Estimated Viscosities and Thermal Conductivities of Gases at High Temperatures," NASA TR-132, 1962.
21. Bird, R. B., Stewart, U. E., and Lightfoot, E. N., Transport Phenomena, John Wiley & Sons, 1960.
22. Mason, E. A., and Saxena, S. C., Physics of Fluids, Vol. 1, no. 5, pp. 361-369, 1958.
23. Nickerson, G. R., et al, "Average Gas Properties Computer Program," Dynamic Science Report No. TR-024, Dec. 1969.
24. Alber, I. E., "Comparison and Prediction of Computer Program Results for Rocket Engine Performance Prediction, Chapter V, Boundary Layer Friction and Heat Transfer," Dynamic Science Report No. SN-82, prepared for ICRPG, April 1968.
25. Pieper, J. L., "ICRPG Liquid Propellant Thrust Chamber Performance Evaluation Manual," CPIA 178, Sept. 1968.
26. Back, L. H., Cuffel, R. F., and Mossier, P. F., "Laminarization of a Turbulent Boundary Layer in Nozzle Flow-Boundary Layer and Heat Transfer Measurements with Wall Cooling," ASME Journal of Heat Transfer, Aug. 1970, (to be published).
27. Levine, J. N., "Transpiration and Film Cooling Boundary Layer Computer Program, Vol. 1. Numerical Solution of the Turbulent Boundary Layer Equations with Equilibrium Chemistry," Final Report, Contract NAS7-791, NASA JPL, June 1971.
28. Evans, R. M., and Morse, H. L., "Interim User's Manual for Boundary Layer Integral Matrix Procedure," Version J, Aerontherm Report UM-74-41, prepared for NASA MSC, Contract No. NAS8-29667.

29. Static Test Report, ATS-EBM-1, Jet Propulsion Laboratory, Pasadena, CA (May 1969).
30. "156-Inch Diameter Motor Liquid Injection TVC Program," AFRPL-TR-66-109, Lockheed Propulsion Company, Redlands, CA. (1966); "Rocket Motor Manual" (CPIA Publication M-1, Unit 464).
31. Aerojet 2.75 Final Report, AFRPL-TR-69-90, (C).
32. Bullard, D., and Holden, J., "Design and Development of 2.75-Inch Mark 4 Mod 8 Rocket Motor," Report NAVWEPS 8647, NOTS-TP-3688, U.S. Weapons Center, China Lake, CA. (April 1965); "Rocket Motor Manual" (CPIA Publication M-1, Unit 505).
33. Broksbank, R. M., "Performance of Two Lockheed AGM-69A Solid Propellant Rocket Motors for the Short Range Attack Missile (SRAM)..." Report AEDC-TR-70-259, Arnold Air Force Station, TN (Dec. 1970).
34. "Report on Static Test of Hydac Motor," Motor H22-3 (July 1964), Motor H25-8 (Oct. 1964), Motor H25-9 (Dec. 1964), Lockheed Propulsion Company, Redlands, CA.; "Rocket Motor Manual" (CPIA Publication M-1, Unit 451).
35. "Design and Development of the High Expansion Ratio Rocket Motor," AFRPL-TDR-64-31, Lockheed Propulsion Company, Redlands, CA. (Oct. 1964); "Rocket Motor Manual" (CPIA Publication M-1, Unit 400).
36. Domal, A. F., et al; "Research and Development Testing of the Minuteman III Stage III Solid Propellant Rocket Motor ..." Report AEDC-TR-68-195, Arnold Air Force Station, TN (Oct. 1968); "Preliminary Flight Rating Test of the Minuteman III Stage III Solid Propellant Rocket Motor ..." Report AEDC-TR-68-249, Arnold Air Force Station, TN (Jan. 1969); "Qualification Testing of the Aerojet Minuteman III (LGM-30G) Stage III Solid Propellant Rocket Motor ..." Report AEDC-TR-70-89, Arnold Air Force Station, TN (July 1970); "Rocket Motor Manual" (CPIA Publication M-1, Unit 457).
37. Merryman, H. L., "Performance of a UTC FW-4S Solid Propellant Rocket Motor ..." Report AEDC-TR-68-253, Arnold Air Force Station, TN (Nov. 1968); "Rocket Motor Manual" (CPIA Publication M-1, Unit 522).
38. Domal, A. F., et al., "Simulated High Altitude Testing of a Flightweight TE-364-1 Solid Propellant Retrograde Rocket Motor for the Surveyor ..." Reports AEDC-TR-64-260, 65-21, 65-41 and 65-50, Arnold Air Force Station, TN (Jan-Apr 1965); "Rocket Motor Manual" (CPIA Publication M-1, Unit 361).
39. Morash, R. T., "Final Report on Rocket Motor ... Antares I," Report ABL/R-53, Allegheny Ballistics Laboratory, Hercules, Inc., Cumberland, MD. (Nov. 1963).
40. "Rocket Motor Manual" (CPIA Publication M-1, Unit 421).

41. "Sparrow III Alt 7F Pre-Flight Rating Test Report," Raytheon Co., Bedford, MA. (April 1968); AD 514 402L; "Rocket Motor Manual" (CPIA Publication M-1, Unit 476, 477).
42. "Rocket Motor Manual" (CPIA Publication M-1, Unit 510).
43. "Rocket Motor Manual" (CPIA Publication M-1, Unit 467).
44. Beckman, C. W., "Solid Propellant Impulse Scaling Prediction Techniques," AFRPL-TR-71-7, Air Force Rocket Propulsion Laboratory, Edwards, CA. (Feb. 1971).
45. "Study of a Fluid-Controlled Solid Rocket Motor for a Mars Orbiter," Report LPC-929F on Contract NAS7-701, Vol. II, Lockheed Propulsion Company, Redlands, CA. (Feb. 1969); also cf. "Fluorine-Hydrogen Performance Evaluation," Report NASA CR-72038, Rocketdyne Division of Rockwell International Corp., Canoga Park, CA. (April 1967).
46. Colucci, S. E., "Experimental Determination of Nozzle Heat Transfer Coefficient," TP106SRP, Aerojet Solid Propulsion Company, Sacramento, CA. (May 1960).
47. Grover, S. S., "Analysis of Nozzle Heat Transfer Coefficient," TM 113 SRP, Aerojet Solid Propulsion Company, Sacramento, CA. (April 1960).
48. Collection of internal memoranda from L. J. Gordon, J. P. Goughlin and R. M. Smith, Aerojet Solid Propulsion Company, Sacramento, CA. (1960-1964).
49. "Development of a Specific Impulse Scaling Technique for Smokeless Propellants," Technical Report S-286, Rohm & Haas Co., Huntsville, AL. (Nov. 1970).
50. Smith, P. W. and Stetz, G. A., "Impulse Scaling Prediction," AFRPL-TR-66-297, Air Force Rocket Propulsion Laboratory, Edwards, CA. (Nov. 1966); also, cf. Ref (3).
51. Kliegel, J. R., "Gas Particle Nozzle Flows," 9th International Combustion Symposium (Academic Press, New York, 1963) 811-826.
52. Kliegel, J. R. and Nickerson, G. R., "Flow of Gas-Particle Mixtures in Axially Symmetric Nozzles," ARS Progress in Astronautics and Rocketry, Vol. 6: Detonation and Two-Phase Flow (Academic Press, New York, 1962) 173-194.
53. Kordig, J. W. and Fuller, G. H., "Correlation of Nozzle Submergence Losses in Solid Rocket Motors," J. AIAA 5, 175-177 (Jan. 1967).
54. "Nozzleless Rocket Motor Internal Ballistics Computer Program," AFRPL-TR-73-19, Lockheed Propulsion Company, Redlands, CA. (Mar. 1973).

55. "Hydroquench Thrust Termination Analysis," AFRPL-TR-73-62, Lockheed Propulsion Company, Redlands, CA. (Aug. 1973).
56. "User's Manual - Aerotherm Charring Material Thermal Response and Ablation Program, Version 3," AFRPL-TR-70-92, Aerotherm Corp., Mt. View, CA. (April 1970).
57. "User's Manual - Aerotherm Ax1-Symmetric Transient Heating and Material Ablation Computer Program (ASTHMA 3)," AFRPL-TR-72-24, Aerotherm Corp. Mt. View, CA. (Jan. 1972).
58. Courtney, W. G., "Review of Particle Size Determination Techniques," AFRPL Two-Phase Flow Conference, AFRPL-TR-67-223, Vol. I, Air Force Rocket Propulsion Laboratory, Edwards, CA. (Mar. 1967).
59. Brown, B. and McCarty, K. P., "Particle Size of Condensed Oxide from Combustion of Metallized Solid Propellant," 8th International Combustion Symposium (Williams and Wilkins, Baltimore, MD. 1962), 814-823.
60. Sehgal, R., "An Experimental Investigation of a Gas-Particle System," TR-32-238, Jet Propulsion Laboratories, Pasadena, CA. (Mar. 1962).
61. Cheung, H. and Cohen, N. S., "Performance of Solid Propellants Containing Metal Additives," J. AIAA 3, 250-257 (Feb. 1965).
62. Smith, P., et al., "Summary Results of Particle Size Measurements," AFRPL Two-Phase Flow Conference, AFRPL-TR-67-223, Vol. I, Air Force Rocket Propulsion Laboratory, Edwards, CA. (Mar. 1967).
63. Collins, R. G., "The AFRPL Ballistic Test, Evaluation and Scaling Program," AFRPL-TR-68-198, Air Force Rocket Propulsion Laboratory, Edwards, CA. (May 1965).
64. Stetz, G.A., et al., "The AFRPL Ballistic Test, Evaluation and Scaling Program," AFRPL-TR-68-198, Air Force Rocket Propulsion Laboratory, Edwards, CA. (Nov. 1968).
65. Brown, B., "Oxide Particles in Solid Rocket Exhausts," AFRPL Two-Phase Flow Conference, AFRPL-TR-67-223, Vol. I, Air Force Rocket Propulsion Laboratory, Edwards, CA. (Mar. 1967).
66. Crowe, C. T. and Willoughby, P. G., "A Study of Particle Growth in A Rocket Nozzle," J. AIAA 5, 1300-1304 (July 1967).
67. Thiokol Chemical Corp., Elkton Division, Elkton, Maryland "TE-M-364-4 Extended Delta Rocket Motor" Final Report NASA Contract NAS7-678, 1972.
68. Daines, W. L., Mayberry, J. L., Lund, R. K., and Abel, R., "Prediction of Thrust Losses Occurring in Solid-Propellant Rocket Motors," AIAA/SAE 10th Propulsion Conference, AIAA Paper No. 74-1201, Oct. 1974.
69. Lavery, J.R., Abel, R., Lund, R. K., and Daines, W. L., "Experimental Investigation of the Effects of Internal Nozzle Contouring on Nozzle Performance," AIAA/SAE 10th Propulsion Conference, AIAA Paper No. 74-1202, Oct. 1974.

Appendix A - Reaction Rate Screening

The reaction rate screening done under this contract should by no means be considered complete either from an absolute, or from a relative basis. What was attempted was to develop a preliminary reaction rate set which would allow for the accurate prediction of the losses in performance of a solid rocket motor which are due to finite rate gas phase chemical kinetics.

The criteria by which the reaction rate screening was done was to select the minimum number of species and reactions which would produce an acceptably accurate value of I_{sp} efficiency. Its efficiency is defined as

$$\eta_{KIN} = \frac{I_{sp}^{SPKIN}}{I_{sp}^{SPRE}}$$

where I_{sp}^{SPKIN} = I_{sp} as calculated in the presence of finite rate chemistry as calculated by the ODK module.

I_{sp}^{SPRE} = I_{sp} as calculated by the restricted equilibrium option of the ODE module

However, at the time the reaction set screening was done, the restricted equilibrium option for the ODE module was not completed. This was unfortunate since the difference in I_{sp} as calculated by the two options in the ODE module can exceed 1% and thus influence the number of species and reactions which could be dropped from the reaction set.

The basic steps in developing the master reaction set for aluminized propellants and the screening of that reaction set are outlined below.

1. The reaction set of Reference A1 (AP-PBAN with no Al) was merged with those reactions in Reference A2 (which included aluminized species). This process yielded a initial master reaction rate set of 31 species and 126 reactions.
2. The initial reaction rate set was compared with the results of chemical equilibrium calculations and was found to be deficient.
3. A short literature search was conducted for measured rates concerning aluminized species. No measured rate data was found.
4. Estimates were made for rates involving 6 more species and 30 more reactions using the procedure reported in Reference A1 (the same procedure was used in Reference A2 to estimate the reaction rates of aluminized species).

5. Using the Generalized Kinetics Analysis Program (GKAP) of Reference A3, the total master reaction set was screened. This computer program SCREENED the reaction in an absolute sense. That is, only reactions which had negligible influence on the fluid flow or rate of production of a chemical species everywhere in the nozzle expansion were dropped. The total reaction set was reduced only minimally by this first step in the screening process.
6. The next step in screening procedure was to reduce the number of species and hence the number of reactions by making an ODE run omitting species thought possibly to be unimportant and comparing the results to an ODK calculation using the reduced reaction set. This procedure reduced the reaction set to 28 species and 73 reactions.

While the above screening procedure reduced both the number of species and reactions considered in performance calculations by the SPP code, it is by no means considered adequate. Too many species and reactions were included in this set, which are due to the comparison of two inconsistent physical models of the expansion of a chemically reacting gas through a rocket motor nozzle. Thus, the screening done to date should not be considered accurate until measured data are taken on the reactions considered in this set and/or performance losses due to finite rate gas phase chemical kinetics can be quantified.

The final reaction set selected for conventional aluminized propellants is shown in Table 2-13 of Volume III. The following notes concerning the comment field of this reaction set are intended to help the reader understand where these reactions and rate data came from.

- The first part of each section (third body and binary exchange reactions) is from Reference A1. For example, BAULCH(1968)L1, refers to the measurements made by Baulch in 1968 and reported in LEEDS 1 report.
- The second part is from Reference A2 and refers to the reaction number built into that computer program.
- The third part, always suffixed by the word ESTIMATE, is from reactions and rates estimated by the authors of this document.

APPENDIX REFERENCES

- A1 Coats, D. E., and Nickerson, G. R., "Analysis of a Solid Propellant Gas Generator Using An Ammonium Perchlorate-Polybutadiene Composite Propellant," AFRPL-TR-72-58, May 1972.
- A2 Kliegel, J. R., et al., "One-Dimensional Two-Phase Reacting Gas Non-equilibrium Performance Program," Vol. 1 Engineering Analysis, Report MSC-11780, TRW Systems (August 1967).
- A3 Nickerson, G. R., Frey, H. M., and Coats, D. E., "GKAP-Generalized Kinetics Analysis Program," Dynamic Science Report, June 1971.